



1           **LA-ICPMS U-Pb geochronology of detrital zircon grains from the Coconino,**  
2           **Moenkopi, and Chinle Formations in the Petrified Forest National Park (Arizona)**

3

4

5           George Gehrels<sup>1</sup>, Dominique Giesler<sup>1</sup>, Paul Olsen<sup>2</sup>, Dennis Kent<sup>3</sup>, Adam Marsh<sup>4</sup>, William Parker<sup>4</sup>,  
6           Cornelia Rasmussen<sup>5</sup>, Roland Mundil<sup>5</sup>, Randall Irmis<sup>6</sup>, John Geissman<sup>7</sup>, and Christopher Lepre<sup>3</sup>

7                           <sup>1</sup>Department of Geosciences, University of Arizona, Tucson AZ 85721, USA

8                           <sup>2</sup>Lamont-Doherty Earth Observatory of Columbia University, Palisades, NY 10964, USA

9                           <sup>3</sup>Earth and Planetary Sciences, Rutgers University, Piscataway, NJ 08854, USA

10                           <sup>4</sup>Petrified Forest National Park, Petrified Forest, AZ 86028, USA

11                           <sup>5</sup>Berkeley Geochronology Center, 2455 Ridge Rd., Berkeley CA 94709, USA

12                           <sup>6</sup>Natural History Museum of Utah and Department of Geology & Geophysics,  
13                           University of Utah, Salt Lake City, UT 84108, USA

14                           <sup>7</sup>Department of Geosciences, University of Texas at Dallas, Richardson, TX 75080, USA

15

16

17

18

19

20                           *Correspondence to George Gehrels (ggehrels@gmail.com)*

21

22



## 23 ABSTRACT

24 U-Pb geochronology was conducted by Laser Ablation-Inductively Couple Plasma Mass  
25 Spectrometry (LA-ICPMS) on detrital zircon grains from twenty-nine samples from the Coconino  
26 Sandstone, Moenkopi Formation, and Chinle Formation. These samples were recovered from  
27 ~520 m of drill core that was acquired during the Colorado Plateau Coring Project (CPCP),  
28 located in Petrified Forest National Park (Arizona).

29 A sample from the lower Permian Coconino Sandstone yields a broad distribution of  
30 Proterozoic and Paleozoic ages that are consistent with derivation from the Appalachian and  
31 Ouachita orogens, with little input from local basement or Ancestral Rocky Mountain sources.  
32 Four samples from the Holbrook Member of the Moenkopi Formation yield a different set of  
33 Precambrian and Paleozoic age groups, indicating derivation from the Ouachita orogen, the  
34 East Mexico Arc, and the Permo-Triassic arc built along the Cordilleran margin.

35 Twenty-three samples from the Chinle Formation contain variable proportions of Proterozoic  
36 and Paleozoic zircon grains, but are dominated by Late Triassic grains. LA-ICPMS ages of these  
37 grains belong to five main groups that correspond to the Mesa Redondo Member, Blue Mesa  
38 Member and lower part of the Sonsela Member, upper part of the Sonsela Member, middle  
39 part of the Petrified Forest Member, and upper part of the Petrified Forest Member. The ages  
40 of pre-Triassic grains also correspond to these chronostratigraphic units, and are interpreted to  
41 reflect varying contributions from the Appalachian orogen to the east, Ouachita orogen to the  
42 southeast, Precambrian basement exposed in the Ancestral Mogollon Highlands to the south,  
43 East Mexico arc, and Permian-Triassic arc built along the southern Cordilleran margin. Triassic  
44 grains in each chronostratigraphic unit also have distinct U and Th concentrations, which are  
45 interpreted to reflect temporal changes in the chemistry of arc magmatism.

46 Comparison of our LA-ICPMS ages with available CA-TIMS ages and new magnetostratigraphic  
47 data provides new insights into the depositional history of the Chinle Formation, as well as  
48 methods utilized to determine depositional ages of fluvial strata. For parts of the Chinle  
49 Formation that are dominated by fine-grained clastic strata (e.g. mudstone and siltstone), such  
50 as the Blue Mesa Member and Petrified Forest Member, all three chronometers agree (to  
51 within ~1 m.y.), and robust depositional chronologies have been determined. In contrast, for  
52 stratigraphic intervals dominated by coarse-grained clastic strata (e.g., sandstone), such as  
53 most of the Sonsela Member, the three chronologic records disagree due to recycling of older  
54 zircon grains and variable dilution of syn-depositional-age grains. This results in LA-ICPMS ages  
55 that significantly pre-date deposition, and CA-TIMS ages that range between the other two  
56 chronometers. These complications challenge attempts to establish a well-defined  
57 chronostratigraphic age model for the Chinle Formation, and to evaluate possible connections  
58 among fundamental Late Triassic biotic and climatic changes and a red siliceous horizon  
59 encountered in the CPCP core.





## 60 1. INTRODUCTION

61 Triassic strata of the Colorado Plateau and environs provide rich and geographically extensive  
62 records of environmental and biotic change during a critical period of Earth history, as well as  
63 the transition from passive- to convergent-margin tectonism along the North American  
64 Cordillera (e.g., Parker and Martz, 2011; Olsen et al., 2011). As demonstrated by Riggs et al.  
65 (1996, 2003, 2012, 2013, 2016), Dickinson and Gehrels (2008), Irmis et al. (2011), Ramezani et  
66 al. (2011, 2014), Atchley et al. (2013), Nordt et al. (2015), Kent et al. (2018, 2019), Olsen et al.  
67 (2018, 2019), Marsh et al. (2019), and Rasmussen et al. (2019), Chinle Formation strata have  
68 the potential to record the timing of these changes in great detail given their several-hundred-  
69 meter thickness, abundance of near-depositional-age zircon grains, and recoverable  
70 paleomagnetic reversal stratigraphy.

71 In an effort to further develop this record, ~520 m of continuous core was collected from  
72 Triassic and underlying Permian strata at Petrified Forest National Park (PEFO), which is located  
73 on the southern Colorado Plateau of northern Arizona (Fig. 1). The objectives and primary  
74 findings of this project have been described by Olsen et al. (2018, 2019), Kent et al. (2018,  
75 2019), and Rasmussen et al. (2019), and numerous related studies are currently in progress.  
76 This contribution to the project reports on U-Pb geochronologic analyses of detrital zircon  
77 grains that were extracted from twenty-nine samples from this core (CPCP-PFNP13-1A).  
78 Analyses were conducted by laser ablation-inductively coupled mass spectrometry (LA-ICPMS),  
79 with between 36 and 490 grains analyzed per sample. Grains were chosen for analysis by  
80 random selection in an effort to provide unbiased information about provenance. Fortunately,  
81 a significant number of near-depositional-age grains were recovered from many samples in the  
82 Chinle Formation, which provides opportunities to also determine robust maximum  
83 depositional ages. This report explores variations in both provenance and maximum  
84 depositional age of strata intersected in the CPCP-PFNP13-1A core, and the implications for  
85 Permian-Triassic environmental and biotic transformations and the tectonic evolution of  
86 southwestern North America.

## 87 2. STRATA ENCOUNTERED IN THE PETRIFIED FOREST NATIONAL PARK DRILL CORE

88 The lowest stratigraphic horizon encountered consists of quartz arenite belonging to the  
89 Coconino Sandstone (Fig. 2). This unit belongs to regionally extensive erg deposits of early  
90 Permian (Leonardian) age (Blakey et al., 1988; Lawton et al., 2015; Dickinson, 2018).

91 Overlying strata of the Coconino Sandstone are tabular, thin to thick-bedded, reddish  
92 mudstone, siltstone, and sandstone layers of the Lower-Middle Triassic Moenkopi Formation. In  
93 the PEFO region, the Moenkopi Formation consists of thin-bedded reddish siltstone with  
94 interlayered sandstone and mudstone. Lower, finer-grained strata are assigned to the Wupatki  
95 Member and Moqui Member, and upper sandstone-rich horizons dominate the Holbrook  
96 Member. The base is a regional unconformity, the TR-1 unconformity of Pipiringos and  
97 O'Sullivan (1978), along which strata of the lower Permian Toroweap Formation and Kaibab



98 Formation have been removed. Strata of the Moenkopi Formation are interpreted to have  
99 accumulated on a northwest-sloping coastal plain, with thinner fluvial strata to the southeast  
100 and thicker marginal marine strata to the northwest (Dickinson, 2018). The Moenkopi  
101 Formation basin was bounded by residual uplifts of the Ancestral Rocky Mountains to the  
102 northeast and highlands of the Ouachita orogen to the southeast. Highlands developed within  
103 early phases of the Cordilleran magmatic arc may have existed to the southwest.

104 Strata of the Moenkopi Formation are overlain unconformably [Tr-3 unconformity of Pippingos  
105 and O’Sullivan (1978)] by the Chinle Formation (Fig. 2). The transition is marked in most areas  
106 by the Shinarump Conglomerate, which consists of cobbles of chert, quartzite, limestone and  
107 subordinate felsic volcanic rocks. Riggs et al. (2012) have determined U-Pb ages of 232-224 Ma  
108 on volcanic cobbles in the Shinarump Conglomerate. The Shinarump Conglomerate is  
109 interpreted to correlate with finer-grained strata of the Mesa Redondo Member (Irmis et al.,  
110 2011; Martz et al., 2012, 2017; Riggs et al., 2016). Strata of the Shinarump Conglomerate and  
111 Mesa Redondo Member are interpreted to have accumulated in paleovalleys that were carved  
112 into underlying strata. Strikingly variegated, strongly pedogenically modified, red, purple, and  
113 yellow strata in the core are assigned to the Mesa Redondo Member given the lack of  
114 conglomerate. Strata of the Mesa Redondo Member in outcrop have yielded U-Pb/zircon ages  
115 of ~227.6 Ma (Atchley et al., 2013) and ~225.2 Ma (Ramezani et al., 2011).

116 Gradationally overlying the Mesa Redondo Member are strata of the Blue Mesa Member,  
117 which consist of purplish to gray and red bentonitic mudstone with sandstone beds that are  
118 generally 0.5 m in thickness (Woody, 2006). Blue Mesa Member mudstones are pervasively  
119 pedogenically modified in the core. These strata are interpreted to have accumulated primarily  
120 as overbank deposits within a mixed-load meandering river system (Martz and Parker, 2010).  
121 Previously reported U-Pb (ID-TIMS or CA-TIMS) ages from outcrop of the Blue Mesa Member  
122 range from ~223 Ma to ~218 Ma (Heckert et al., 2009; Ramezani et al., 2011; Irmis et al., 2011;  
123 Atchley et al., 2013; Rasmussen et al., 2019).

124 Strata of the Blue Mesa Member are overlain by sandstone-rich and conglomerate-bearing  
125 strata of the Sonsela Member. Lucas (1993) and Heckert and Lucas (2002) refer to the base of  
126 the Sonsela Member as a regionally significant unconformity, although this interpretation has  
127 been questioned by Woody (2006) and Martz and Parker (2010) given that conglomeratic  
128 sandstone of the Sonsela is interbedded with mudstone of the Blue Mesa Member. Martz and  
129 Parker (2010) suggest that the transition from the Blue Mesa Member to the Sonsela Member  
130 marks a change in depositional regime (from mainly overbank deposits to bedload-dominated  
131 channel deposits) but does not mark a significant hiatus in deposition.

132 The Sonsela Member consists predominantly of sandstone with lesser mudstone and local  
133 conglomerate. Sandstone beds are variable in thickness, have significant lateral extent, and  
134 exhibit cut-and-fill structure (Woody, 2006). Conglomerate (with abundant volcanic clasts) is  
135 common within the sandstone beds. Five units have been recognized, a lower sandstone  
136 interval (Camp Butte beds), a lower-middle unit with abundant mudstone (Lot’s Wife beds), a



137 middle sandstone and conglomerate unit (Jasper Forest/Rainbow Forest bed), a middle-upper  
138 unit with pedogenic carbonate and abundant mudstone (Jim Camp Wash beds), and an upper  
139 sandstone unit (Martha's Butte beds) (Martz and Parker, 2010). The five units are gradational,  
140 with the main variation being the abundance of mudstone in two of the middle units. A reddish  
141 siliceous horizon of uncertain regional extent has been recognized within the middle of the  
142 upper mudstone-rich unit in the CPCP-PFNP13-1A core. Similar horizons within other exposures  
143 of the Sonsela Member are marked by a significant die-off of the conifers that characterize  
144 Petrified Forest National Park (Creber and Ash, 1990), a turn-over of the vertebrate fauna  
145 (Parker and Martz, 2009, 2011), and perhaps a significant change in flora and paleoclimate  
146 (Reichgelt et al., 2013; Nordt et al., 2015; Baranyi et al., 2017). U-Pb (CA-TIMS/zircon) ages from  
147 the Sonsela Member range from ~220 to ~214 Ma (Ramezani et al., 2011; Rasmussen et al.,  
148 2019) from below the siliceous horizon and from ~214 to ~213 Ma (Ramezani et al., 2011;  
149 Nordt et al., 2015; Kent et al., 2018; Rasmussen et al., 2019) from above.

150 Overlying the conglomeratic sandstones of the Sonsela Member is a purplish mudstone that  
151 marks the base of the Petrified Forest Member (Fig. 2). This member consists of red and purple  
152 mudstone with abundant paleosols and pedogenic carbonate nodules, with local conglomeratic  
153 sandstone beds that formed in bedload-dominated streams. Near the top of the unit is the  
154 Black Forest bed, which consists of limestone-pebble conglomerate and reworked andesitic tuff  
155 (Ash, 1992). Zircon grains from the Black Forest bed have yielded U-Pb (ID-TIMS or CA-TIMS)  
156 ages of ~213 Ma to ~210 Ma (Riggs et al., 2003; Heckert et al., 2009; Ramezani et al., 2011; Kent  
157 et al., 2018; Rasmussen et al., 2019).

### 158 **3. SAMPLED HORIZONS**

159 We analyzed detrital zircon grains from twenty-nine samples collected from the Permian and  
160 Triassic strata described above. Samples include one from the Coconino Sandstone, five from  
161 the Moenkopi Formation (one that may be from the Wupatki Member and four from the  
162 Holbrook Member), and twenty-three from the Chinle Formation (one from the Mesa Redondo  
163 Member, three from the Blue Mesa Member, twelve from the Sonsela Member, and seven  
164 from the Petrified Forest Member). Approximate stratigraphic positions of the samples are  
165 shown on Figure 2, lithic characteristics are described in DR Table 1, and images of the sampled  
166 material (both core and thin sections) are presented in Appendix 1. Each sample consisted of 20  
167 cm (for sandstone) to 30 cm (for mudstone-siltstone) of  $\frac{1}{4}$  sections of the core.

### 168 **4. ANALYTICAL AND INTERPRETIVE METHODS**

169 Zircon mineral separation was performed at the Arizona LaserChron Center  
170 ([www.laserchron.org](http://www.laserchron.org)) using methods modified from those outlined by Gehrels (2000), Gehrels  
171 et al. (2008), and Gehrels and Pecha (2014) because of the small size of all samples and the  
172 abundance of clay minerals in many samples. The process included using a hand-crusher to  
173 break the samples apart, a gold pan for initial density separation, and an ultrasonic disruptor  
174 (Hoke et al., 2014) to separate zircon crystals from clay mineral grains. Magnetic separation was



175 performed with a Frantz Isodynamic separator, followed by density separation using methylene  
176 iodide.

177 Zircon grains greater than 60  $\mu\text{m}$  in size were enclosed in 1-inch epoxy mounts along with  
178 fragments of zircon standards SL (primary) and FC-1 and R33 (secondary). Mounts were  
179 polished approximately 5-10  $\mu\text{m}$  deep to expose the internal structure of the grains but retain  
180 as much material as possible for subsequent CA-TIMS analysis. Imaging was performed with a  
181 backscatter electron detector system (BSE) using a Hitachi S3400 scanning electron microscope  
182 (SEM) to ensure analysis of zircon and to avoid inclusions and fractures. Mounts were cleaned  
183 with 1% HCl and 1% HNO<sub>3</sub> prior to isotopic analysis.

184 U-Pb isotopic analyses were conducted by LA-ICPMS using a Teledyne/Photon Machines  
185 Analyte G2 laser connected to a Thermo Element2 mass spectrometer. Analyses utilized a 20  
186  $\mu\text{m}$  diameter laser beam fired at 7 hz for 15 seconds, resulting in 10-12  $\mu\text{m}$  deep pits. Details of  
187 the analytical methods are reported in DR Table 2.

188 U-Pb ages are calculated with an in-house data-reduction routine (E2agecalc) following  
189 methods of Pullen et al. (2018). Analyses of zircon grains from our samples are reported in DR  
190 Table 3, with results filtered for discordance (using cutoffs of 80% and 105% concordance),  
191 precision (10%), and common Pb (>600 cps counts of 204). Following the recommendations of  
192 Horstwood et al. (2016), uncertainties for individual analyses include only internal (random or  
193 measurement) uncertainty contributions, whereas uncertainties of pooled ages contain both  
194 internal and external (systematic) contributions.

195 Detrital age distributions are displayed and analyzed with normalized probability density plots,  
196 which are based on the individual ages and uncertainties from each sample. Provenance  
197 interpretations are based on the main clusters of ages, with less emphasis on ages that do not  
198 belong to clusters given the possibility that they are unreliable due to Pb loss, inheritance,  
199 analysis of inclusions, high common Pb, or unusual Pb/U fractionation due to ablation along  
200 fractures (Gehrels, 2014).

201 Analysis of provenance is conducted by comparison with age distributions from five likely  
202 source regions for Permian-Triassic strata of the Colorado Plateau, which include the  
203 Appalachian orogen, the Ouachita orogen, local basement rocks of southwestern Laurentia, the  
204 East Mexico arc, and the Permian-Triassic magmatic arc developed along the Cordilleran margin  
205 of southwestern North America (Fig. 1; Dickinson, 2018). The age distributions for these regions  
206 include data from: (1) upper Paleozoic strata of the Appalachian foreland basin (Thomas et al.,  
207 2017) and Illinois and Forest City basins (Kissock et al., 2018), (2) upper Paleozoic strata of the  
208 Delaware (Xie et al., 2018), Fort Worth (Absalem et al., 2018), and Marathon (Thomas et al.,  
209 2019) basins, (3) lower Paleozoic strata of the Grand Canyon (Gehrels et al., 2011) and  
210 Cordilleran passive margin strata in southern California and northern Sonora (Gehrels and  
211 Pecha, 2014), (4) Permian and Triassic strata of the Barranca and El Antimonio Formations of  
212 Sonora (Gonzalez-Leon et al., 2009; Gehrels and Pecha, 2014), Jura-Cretaceous strata of the



213 Great Valley (DeGraaff-Surpless et al., 2002; Surpless et al., 2006; Wright and Wyld, 2007),  
214 Permian-Triassic igneous rocks in California (Chen and Moore, 1982; Miller et al., 1995; Tobisch  
215 et al., 2000; Barth and Wooden, 2006, 2011, 2013; Saleeby and Dunne, 2015), and (5) Mesozoic  
216 strata that accumulated adjacent to the East Mexico arc (Ortega-Flores et al., 2014). Age  
217 distributions for these five regions are presented in Figure 3.

218 Comparisons of age distributions are quantified using several different statistical measures that  
219 examine the degree to which age distributions contain similar proportions of similar age  
220 groups. Five metrics used in this study include the cross-correlation coefficient, values of  
221 similarity and likeness, and the Kolmogorov-Smirnov (K-S) D values and Kuiper V values. The  
222 statistical basis as well as strengths and limitations of each of these metrics are summarized by  
223 Saylor and Sundell (2016) and Wissink et al. (2018). Results from these comparisons are  
224 presented in DR Table 4. The interpretations offered below are based on cross-correlation  
225 coefficients, although all five metrics yield similar results. Comparisons are also presented  
226 visually through the use of multidimensional scaling (MDS) diagrams (Vermeesch, 2013; Wissink  
227 et al., 2018), which provide a 2-dimensional representation of the differences between multiple  
228 age distributions. MDS analyses are also based on cross-correlation coefficients.

229 Maximum depositional ages are calculated from the age of the youngest distinct cluster of  
230 three or more overlapping ages (Dickinson and Gehrels, 2009; Gehrels, 2014). The age of this  
231 cluster is estimated using four different methods, as described below.

- 232 • Age of the youngest peak on a probability density plot (PDP). This method is advantageous  
233 because no decisions are made about which analyses are included/excluded, but it has the  
234 disadvantage that no uncertainty is reported for the peak age.
- 235 • Weighted Mean age and uncertainty of the youngest cluster. This method calculates the  
236 average age of a cluster by weighting each analysis according to the inverse-square of its  
237 uncertainty. The reported uncertainty relates to the mean age (e.g., standard error of the  
238 mean), not the age distribution of constituent analyses (e.g., standard deviation). An  
239 advantage of this method is that it also yields a Mean Square of the Weighted Deviates  
240 (MSWD), which is an indication of the degree to which the ages belong to a single  
241 population (values of  $\sim 1$  or less indicate a single population). A disadvantage of this method  
242 is that the investigator must decide which ages are included in the calculation, which leads  
243 to the possibility of subjective bias. In this study, clusters include the main set of continuous  
244 ages, with boundaries selected at the youngest and oldest gap in ages. This calculation is  
245 available from the Weighted Mean function in Isoplot (Ludwig, 2008).
- 246 • Tuffzirc age and uncertainty of the youngest cluster. This method uses the age extractor  
247 function in Isoplot (Ludwig, 2008), which identifies the largest cluster of ages that overlap to  
248 an acceptable degree (probability-of-fit  $> 0.05$ ), reports the median value as the most likely  
249 age, and uses the range of included ages to calculate an asymmetric uncertainty. The  
250 reported uncertainty refers to the median value (not the range of constituent analyses).  
251 Excluded ages are interpreted to pre-date the selected cluster (if older), or to be



252       compromised by Pb loss (if younger). This method is advantageous in that no subjective  
253       decisions are made about including/excluding ages.

254       • Maximum Likelihood age and uncertainty. This method uses a maximum likelihood analysis  
255       to determine the gaussian distribution that best fits the youngest cluster. The reported  
256       uncertainty refers to the most likely value (not the range of constituent analyses). This  
257       method is advantageous in that no subjective decisions are made about including/excluding  
258       ages. It is available from the Unmix function of Isoplot (Ludwig, 2008).  
259

260       The results of these calculations are presented in DR Tables 3 and 6.

261       DR Table 6 also reports the age and uncertainty of the youngest analysis from each sample. This  
262       youngest age does not provide a reliable maximum depositional age given that the youngest  
263       age of a distribution will always be younger than the true age due to analytical uncertainty  
264       (Gehrels, 2014). For example, consider the analytical data from a population of zircon grains  
265       that have exactly the same true age. Because of analytical uncertainty, the measured ages of  
266       half of the analyses will be younger than the true age, and half will be older, and the youngest  
267       age will be significantly younger than the mean (true) age. Ironically, the more grains analyzed,  
268       the greater the inaccuracy of this youngest age!

269       In addition to this statistical bias, the youngest single age will be even farther from the mean  
270       (true) age if it has been compromised by Pb loss. We report these youngest ages because they  
271       provide important information about the possibility that analyses included in the youngest  
272       cluster have also experienced Pb loss. DR Table 6 accordingly reports this youngest age (and  
273       uncertainty), as well as information about its U concentration, the average U concentration of  
274       the youngest cluster of ages, and whether the youngest age belongs to the youngest cluster or  
275       is an outlier. U concentration is important because Pb loss is commonly correlated with the  
276       degree of radiation damage, which is a function of U concentration (and age).

277       A second test of the likelihood that analyses belonging to the youngest cluster have  
278       experienced Pb loss is provided by a plot of U concentration versus age for analyses belonging  
279       to the youngest cluster. Such plots are shown for every sample in DR Table 3, and whether a  
280       correlation exists is indicated in DR Table 6.

281       Also included in DR Table 6 are the preferred age and uncertainty for each sample. The  
282       preferred age is based on the average of the four ages determined by peak age, weighted  
283       mean, Tuffzirc, and Unmix analyses. The uncertainty of this preferred age is based on the  
284       average of the uncertainty from each method, and is shown with both internal-only  
285       uncertainties and with combined internal and external uncertainties.

286       The average precision of individual analyses reported herein is 2.3% ( $2\sigma$ ) for  $^{206}\text{Pb}^*/^{238}\text{U}$  dates  
287       and 2.6% for  $^{206}\text{Pb}^*/^{207}\text{Pb}^*$  dates. For pooled ages, calculated as described above, the average  
288       precision is 0.52% ( $2\sigma$ ) including only internal uncertainties and 0.98% ( $2\sigma$ ) including both  
289       internal and external sources of uncertainty. The accuracy of our analyses can be estimated





290 from the age of the secondary standards that were analyzed with each set of unknowns. As  
291 reported in DR Table 7 and shown on Figure 4, sets of  $^{206}\text{Pb}^*/^{238}\text{U}$  dates for FC-1 are offset  
292 between +0.25% and -0.45% from the reported  $^{206}\text{Pb}^*/^{238}\text{U}$  date of 1099.9 Ma (Paces and  
293 Miller, 1993), with an average offset for all 1,065 analyses of +0.03%. For R33, offsets range  
294 from +0.85% to -0.95% from the assumed age of 419.3 Ma (Black et al., 2004), with an average  
295 offset for all 291 ages of -0.23%. MSWD values for the sets of FC-1 and R33 ages are 0.95 and  
296 0.92 (respectively) – this demonstrates that MSWD values for sets of unknown ages are reliable  
297 indicators of the existence of multiple age components.

298 Interpretation of our ages relative to the Geologic Time Scale is based on the August 2018  
299 version of the International Chronostratigraphic Chart (Cohen et al., 2013).

300 U-Pb geochronology by LA-ICPMS also provides U concentrations and U/Th values for each  
301 analysis, which can be used as a geochemical fingerprint of detrital zircon grains (e.g., Gehrels  
302 et al., 2006, 2008; Riggs et al., 2012, 2016). This information is accordingly reported for each  
303 analysis in DR Table 3, and for each set of analyses in DR Table 6.

## 304 5. U-Pb GEOCHRONOLOGIC RESULTS

305 Results of our U-Pb geochronologic analyses are described below, keyed to the age  
306 distributions for individual samples that are shown on Figures 5, 6, and 7. Figure 8 presents age  
307 distributions for combined sets of samples. Age distributions from all of the samples are  
308 compared statistically in DR Table 4 using the five metrics described above, and MDS plots are  
309 shown in Figure 9.

310 We note that Rasmussen et al. (2019) have reported a subset of the LA-ICPMS ages presented  
311 herein. The ages reported in their study are for the grains selected for CA-TIMS analysis, which  
312 in most cases are among the youngest grains in each of our samples (as documented in  
313 Appendix 2). This strategy was followed assuming that these grains represent the youngest age  
314 components in each sample, and accordingly provide the most useful maximum depositional  
315 ages. The individual dates reported in the two studies are identical, but, given the selection  
316 process noted above, the pooled ages reported by Rasmussen et al. (2019) are consistently  
317 younger than the pooled ages reported herein. A comparison of the results of the two studies is  
318 summarized in Appendix 2. The discussions below are based on the full set of ages from each  
319 sample.

320 Sample numbers are registered to the CPCP core (CPCP-PFNP13-1A) by the number of the core  
321 run and segment (e.g., our sample number 383-2 is from CPCP-PFNP13-1A-383Y-2, which  
322 specifies that the material is from run 383, segment 2). The part of each segment that was  
323 collected for geochronologic analysis is specified in DR Table 1.

### 324 5.1 Coconino Sandstone

325 Our sample from quartz arenite of the lower Permian (Leonardian) Coconino Sandstone  
326 (sample 390-1) yielded 285 acceptable ages (DR Table 3; Figure 4). Most grains belong to two



327 broad age groups of ~2.0-1.0 Ga and ~640-295 Ma. Individual age peaks are at 2712, 1898,  
328 1746, 1646, 1497, 1432, 1347, 1162, 1038, 667, 612, 590, 552, 476, 430, 419, 391, 374, 355,  
329 341, and 300 Ma.

## 330 **5.2 Moenkopi Formation**

331 Five samples from the Lower-Middle Triassic Moenkopi Formation have been analyzed (Fig. 2).  
332 The lowest sample (383-2) is assigned to the Wupatki Member based on the red-brown  
333 laminated mudstone to fine-grained sandstone lithology (Fig. 2; Table DR 1). The age  
334 distribution from this sample is very similar to that found in underlying upper Paleozoic strata,  
335 with two dominant age groups from ~2.2 Ga to 1.0 Ga and from ~680 Ma to 250 Ma (Fig. 5).  
336 Although the preferred interpretation for this sample is that it belongs to the lowest part of the  
337 Moenkopi Formation, an alternative is that the sample is late Paleozoic in age, and perhaps  
338 correlative with fine-grained clastic strata (e.g., the Toroweap Formation) that regionally overlie  
339 the Coconino Sandstone. In an effort to provide a comparison with underlying and overlying  
340 strata, the results from this sample are shown on Figures 5 and 6. Additional studies of the  
341 sampled horizon are needed to resolve whether this sample belongs to the Moenkopi  
342 Formation or underlying upper Paleozoic strata.

343 The upper four samples (349-3, 335-1, 327-2, and 319-2) are all from sandstone, siltstone, and  
344 mudstone of the Holbrook Member. These samples yield generally similar age distributions  
345 (average CCC of 0.24; DR Table 4), with significant proportions of ~1.42 Ga, 650-510 Ma, 290-  
346 270 Ma, and 250-235 Ma ages (Fig. 6). With ages from all four Moenkopi Formation samples  
347 combined, PDP peak ages are 1420, 594, 543, 285, and 250 Ma (Fig. 8). As shown in Figures 9B  
348 and 9C, age distributions from the lower two samples (349-3 and 335-1) and upper two samples  
349 (327-2 and 319-2) form two distinct groups. These clusters are also apparent from CCC values of  
350 0.83 and 0.24 for the lower and upper samples (respectively), in comparison with a low average  
351 value (0.08) for comparison of the two sets with each other (DR Table 4).

## 352 **5.3 Chinle Formation**

353 Twenty-three samples from the Mesa Redondo Member, Blue Mesa Member, Sonsela Member,  
354 and Petrified Forest Member of the Chinle Formation have been analyzed (Fig. 2). Results from  
355 each member are described separately below.

### 356 **5.4 Mesa Redondo Member**

357 One sample of sandstone from the Mesa Redondo Member (305-2) yields dominant age groups  
358 of ~2.0-1.6 Ga, 1.44 Ga, 1.1-1.0 Ga, 750-500 Ma, and 450-300 Ma, and 290-220 Ma (Fig. 7), with  
359 PDP peak ages of 1443, 1036, 618, 412, 323, 248, and 223 Ma. As reported in DR Table 4 and  
360 shown on Figure 9C, the >240 Ma ages in this samples resemble ages in the underlying  
361 Moenkopi Formation and Coconino Sandstone.

### 362 **5.5 Blue Mesa Member**





363 Three samples (297-2, 287-2, 261-1) of siltstone and mudstone from the Blue Mesa Member  
364 yield very similar results, with nearly identical <240 Ma ages and small but varying proportions  
365 of ~1.64 Ga, 1.44 Ga, 1.1-1.0 Ga, 650-500 Ma, and 440-240 Ma ages (Figures 7 and 8). Both  
366 <240 Ma ages (Fig. 9A) and >240 Ma ages (Fig. 9C) differ from those in underlying strata of the  
367 Mesa Redondo Member. Between 56% and 89% of the grains analyzed from these samples  
368 yield ages between 232 and 210 Ma, with PDP peak ages of 221-220 Ma (Fig. 7; DR Table 6).  
369 With all three samples combined, 62% of the ages are <240 Ma, and PDP peak ages are 1630,  
370 1440, and 220 Ma (Fig. 8).

### 371 **5.6 Sonsela Member**

372 Twelve samples (243-3 to 158-2) from the Sonsela Member yield two different sets of age  
373 distributions (Figures 7, 8, and 9; DR Table 3). The lower six samples (243-3 to 196-3), all  
374 consisting of sandstone and subordinate siltstone (DR Table 1), yield small numbers of  
375 Precambrian grains that are mostly ~1.65 and 1.44 Ga, with few ~1.1-1.0 Ga grains. These  
376 samples yield between 53% and 79% ages <240 Ma, with most ages between 234 and 208 Ma,  
377 and PDP peak ages of 221-218 Ma (Fig. 7). With ages from all six samples combined, 68% of the  
378 grains are <240 Ma, and PDP peak ages are 1650, 1445, 1084, and 219 Ma (Fig. 8). Comparison  
379 of age distributions (Figures 7 and 8), CCC values (DR Table 4), and MDS patterns (Fig. 9)  
380 suggests that the <240 Ma ages in these strata are indistinguishable from <240 Ma ages in  
381 underlying Blue Mesa strata, whereas >240 Ma ages in the two sets of samples are less similar  
382 due to the variability of ages from the three Blue Mesa Member samples. Ages that are >240  
383 Ma in these strata have even less similarity to ages from the Mesa Redondo Member,  
384 Moenkopi Formation, and Coconino Sandstone (Fig. 9; DR Table 4).

385 The upper six samples from the Sonsela Member (195-2 to 158-2) consist mainly of sandstone  
386 and subordinate siltstone (DR Table 1). All six samples yield a subordinate but consistent  
387 proportion of Precambrian ages that are mostly ~1.43 and 1.1-1.0 Ga, with few 1.65 Ga grains  
388 (Fig. 7). Grains with ages of <240 Ma comprise between 39% and 77% of the grains analyzed.  
389 These ages are somewhat younger than in lower Sonsela Member samples, with PDP peak ages  
390 of 217-214 Ma. With all six samples combined, 50% of the grains are <240 Ma, and PDP peak  
391 ages are 1643, 1434, 1082, 256, and 215 Ma (Fig. 8).

392 Statistical analysis (MDS patterns in Figure 9 and CCC values in DR Table 4) shows that the <240  
393 Ma ages in upper and lower Sonsela Member strata are significantly different, whereas >240  
394 Ma ages are less distinct. Exceptions to this are >240 Ma ages in sample 243-3 (lower Sonsela  
395 Member), which resemble equivalent ages in strata of the upper Sonsela Member (Fig. 9C), and  
396 <240 Ma ages in sample 196-3, which share characteristics with strata of both the upper and  
397 lower Sonsela Member (Fig. 9A). Ages from strata of the upper Sonsela Member show even less  
398 overlap with ages from strata of the Blue Mesa Member and underlying units (Fig. 9 and DR  
399 Table 4).

### 400 **5.7 Petrified Forest Member**



401 Seven samples (131-2 to 52-2) from the Petrified Forest Member were collected mainly from  
402 claystone, mudstone, siltstone, and fine-grained sandstone, with only the lowest sample (131-  
403 2) consisting of coarse-grained sandstone. The upper six fine-grained samples yield between  
404 17% and 72% <240 Ma ages that are significantly younger than in underlying strata, with PDP  
405 peak ages between 212 and 209 Ma. Ages that are >240 Ma in these samples differ from  
406 equivalent ages in strata of the Blue Mesa Member and Sonsela Member, but overlap to  
407 varying degrees with ages in strata of the Mesa Redondo Member, Moenkopi Formation, and  
408 Coconino Sandstone (Fig. 9C; DR Table 4). With the six samples combined, 35% of the grains are  
409 <240 Ma, and PDP peak ages are 1636, 1430, 1032, 629, 379, 287, and 209 Ma (Fig. 8). The  
410 lowest sample (131-2), consisting of coarse-grained sandstone, differs from the other Petrified  
411 Forest Member samples, with an age peak of 221 Ma, and a greater proportion (68%) of >240  
412 Ma ages (Fig. 7). The <240 Ma ages are very similar to equivalent ages in strata of the lower  
413 Sonsela Member (Fig. 9A; CCC=0.97), whereas >240 Ma ages are more similar to ages in the  
414 upper Sonsela Member (CCC=0.72) than in the lower Sonsela Member (CCC=0.59) (Fig. 9C).

#### 415 **5.8 Summary of Chinle results**

416 The patterns of LA-ICPMS ages described above suggest that the studied part of the Chinle  
417 Formation comprises four different units, each of which has a distinct chronologic signature for  
418 both <240 Ma and >240 Ma ages (Fig. 8). These chronostratigraphic units correspond to the  
419 Mesa Redondo Member, Blue Mesa Member and lower part of the Sonsela Member, upper  
420 part of the Sonsela Member, and Petrified Forest Member.

#### 421 **6. U AND Th GEOCHEMISTRY OF CHINLE ZIRCON GRAINS**

422 In an effort to evaluate whether the Triassic zircon grains from the four chronostratigraphic  
423 units also have distinct chemical signatures [following Riggs et al. (2012, 2016)], Figure 10  
424 summarizes the U concentrations and U/Th values for Triassic zircon grains analyzed from each  
425 unit. The patterns exhibited in these plots suggest that (1) zircon grains from the Mesa  
426 Redondo Member are significantly different from zircon grains in overlying strata, (2) grains in  
427 strata of the Blue Mesa Member and lower Sonsela Member differ from grains in overlying  
428 strata of the upper Sonsela Member and Petrified Forest Member, and (3) grains in strata of the  
429 upper Sonsela Member and Petrified Forest Member have distinctive and slightly different  
430 bimodal patterns. Plots showing U concentrations and U/Th values for individual samples are  
431 included in DR Table 3.

#### 432 **7. PROVENANCE INTERPRETATIONS**

433 Detrital zircon geochronology has previously been used to reconstruct the provenance of  
434 Permian and Triassic strata of the Colorado Plateau by Riggs et al. (1996, 2003, 2012, 2013,  
435 2016), Dickinson and Gehrels (2003, 2008), Gehrels et al. (2011), Lawton et al. (2015), and  
436 Marsh et al. (2019). The results of most of these geochronologic studies, and a large number of  
437 stratigraphically based analyses, have recently been summarized by Dickinson (2018). The  
438 following sections compare our new results with this existing information.



439 The following comparisons are based in part on qualitative comparison of age distributions of  
440 the strata that we have analyzed and of age distributions from five potential source areas  
441 (summarized on Figure 3). As described by Gehrels (2000), such comparisons focus on the  
442 degree to which two age distributions contain similar proportions of similar ages. Comparisons  
443 are also based on the results of statistical analyses (DR Table 4) that compare our results with  
444 the age distributions of possible source areas, and on graphic displays of these comparisons  
445 using MDS plots (Fig. 9).

#### 446 **7.1 Coconino Sandstone**

447 Lawton et al. (2015) and Dickinson (2018) suggest that lower Permian strata of the Colorado  
448 Plateau comprise a regional blanket of eolian strata that was shed predominantly from the  
449 Appalachian and/or Ouachita orogens, with increasing input in northern regions from local  
450 basement rocks exposed in the Uncompahgre or Ute Uplift (Fig. 1). These interpretations are  
451 supported by the age distributions shown on Figures 5 and 11, with southern strata (Coconino,  
452 Cedar Mesa, and White Rim sandstones) forming a distinct group dominated by  
453 Appalachian/Ouachita detritus, and northern strata (Castle Valley and Cutler strata) forming a  
454 separate group with increasing proportions of ca 1.44 Ga grains. The age distribution from our  
455 Coconino Sandstone sample (390-1) fits well with other strata from the southern Colorado  
456 Plateau in having abundant 1.2-1.0 and 670-300 Ma grains and a low proportion of ~1.44 Ga  
457 grains (Figures 5 and 11; DR Table 4).

#### 458 **7.2 Moenkopi Formation**

459 As summarized on Figure 6, the detrital zircon ages from our four Holbrook Member samples  
460 are generally similar to ages from a Holbrook Member sandstone reported by Dickinson and  
461 Gehrels (2008). Dominant >300 Ma age groups and interpreted source terranes include ~1.44  
462 Ga and subordinate ~2.0-1.6 Ga grains derived from Laurentian Precambrian basement and  
463 ~670-300 Ma grains derived from Ouachita/Gondwana sources. Based on comparison with  
464 detrital zircon ages from strata that accumulated in proximity to the East Mexico and southern  
465 Cordilleran arcs (Fig. 3), 300-260 Ma grains (PDP peak ages of 285, 284, 265, 260, and 279) are  
466 interpreted to have been shed from the East Mexico arc (peak age of 284 Ma), whereas 260-  
467 230 Ma grains (peak ages of 250, 248, 228, 245, and 239 Ma) were likely shed from Early-  
468 Middle Triassic parts of the Cordilleran magmatic arc in California and northwestern Mexico  
469 (peak ages of 243, 236, and 226 Ma) (Fig. 3). Statistical analyses (DR Table 4) suggest nearly  
470 equal contributions from the Ouachita orogen, local basement rocks, and the East Mexico arc.

471 More detailed analysis of the age distributions (Fig. 6) and MDS patterns (Fig. 9) suggest that  
472 the lower two samples (349-3 and 335-1) [plus sample CP8 of Dickinson and Gehrels (2008)] are  
473 dominated by ~1.44 Ga and ~285 Ma grains, whereas the upper two samples (327-2 and 319-2)  
474 are dominated by ~620-590 Ma and ~250-230 Ma grains. The age distributions (Fig. 6) and  
475 comparison metrics (Fig. 9; DR Table 4) suggest that the lower samples were shed mainly from



476 local basement rocks (CCC=0.30) and the East Mexico arc (CCC=0.22), whereas the upper  
477 samples were shed largely from the Ouachita orogen (CCC=0.23).

### 478 **7.3 Chinle Formation**

479 Our results from detrital zircon grains recovered from strata of the Chinle Formation are  
480 consistent with the provenance and paleogeographic reconstructions offered by Riggs et al.  
481 (1996, 2003, 2012, 2013, 2016), Dickinson (2018), and Marsh et al. (2019). Given the observed  
482 age distributions (Fig. 7) and the location of our study site relative to Late Triassic  
483 paleogeographic and paleotectonic features of southwestern North America (Fig. 12), likely  
484 sources for pre-Triassic grains include rocks exposed in the Ouachita orogen to the southeast  
485 and the Ancestral Mogollon highlands to the south and southwest. Given the abundance of ash  
486 layers, bentonitic mudstone, and near-depositional-age zircon grains in strata of the Chinle  
487 Formation, and the existence of arc-related plutons and volcanic rocks of Triassic age in Sonora  
488 and southern California (Barth and Wooden, 2006, 2011, 2013; Saleeby and Dunne, 2015; Riggs  
489 et al., 2016), Stewart et al. (1986), Riggs et al. (2012, 2016), Dickinson (2018), Marsh et al.  
490 (2016), and many other researchers conclude that Triassic grains in Chinle strata were derived  
491 from the active arc built along the southern Cordilleran margin. The occurrence in fore-arc and  
492 back-arc strata of very similar distributions of ages (Fig. 3) is inconsistent with interpretations  
493 (e.g., Hildebrand, 2009, 2013) that the early Mesozoic arc was located far from southwestern  
494 North America.

495 Although our data are entirely consistent with the provenance interpretations outlined above,  
496 the density of our sampling and the large number of analyses from most samples provide  
497 opportunities to reconstruct temporal changes in Triassic provenance in greater detail, and with  
498 the benefit of statistical analyses to quantify conclusions. Following are interpretations based  
499 on strata belonging to each of the different members of the Chinle Formation.

### 500 **7.4 Mesa Redondo Member**

501 The provenance of strata belonging to the Mesa Redondo Member is similar to that of the  
502 underlying Moenkopi Formation, with our sample (305-2) containing abundant ~640-300 Ma  
503 grains derived from Ouachita/Gondwana sources as well as ~290-260 Ma grains derived from  
504 the East Mexico arc (Fig. 8). Statistical analysis confirms higher similarity of >240 Ma grains with  
505 Ouachita sources (0.58) than with Appalachian (0.35) or local basement (0.15) sources (DR  
506 Table 4). This sample also yields a significant proportion of Triassic ages that approximate the  
507 depositional age for these strata (Fig. 7). These young grains, with a PDP age peak of 223 Ma,  
508 are interpreted to have been transported primarily by aeolian processes from the active  
509 magmatic arc to the west (Fig. 12). Statistical analysis demonstrates that the Triassic ages in  
510 these samples are significantly different from ages in overlying strata (Fig. 9A) and that the  
511 >240 Ma ages are similar to those in strata of the Petrified Forest Member (Fig. 9C).

### 512 **7.5 Blue Mesa Member**



513 Our three samples from strata of the Blue Mesa Member yield a large proportion of Triassic  
514 zircon grains (Figures 7 and 8) that were derived from the active Cordilleran magmatic arc to  
515 the west (Fig. 12), and a small proportion of pre-240 Ma grains that were shed from local  
516 basement rocks and the Ouachita and/or Appalachian orogens (Fig. 8). Statistical analysis  
517 confirms that the Triassic ages in all these samples are quite similar (Fig. 9A), whereas the age  
518 distributions of >240 Ma grains in the three samples are more variable (Fig. 9C; DR Table 4).

#### 519 **7.6 Lower Sonsela member**

520 The lower six samples from the Sonsela Member yield a large proportion of Triassic grains  
521 derived from the Cordilleran magmatic arc, and fewer ages derived from local basement rocks  
522 and Ouachita/Gondwana sources (Figures 7 and 8). Distinctive among the older grains is a  
523 significant proportion of ~1.44 Ga grains that may have been incorporated during transport  
524 from the Ouachita orogenic highlands, or may signal increased input from the Ancestral  
525 Mogollon highlands to the southwest (Marsh et al., 2019) (Fig. 12). MDS analysis demonstrates  
526 that the <240 Ma and >240 Ma ages in these samples are quite similar, with the only significant  
527 difference being the larger number of ~1.1 Ga grains in sample 243-3 (Figures 7 and 9C).

#### 528 **7.7 Upper Sonsela Member**

529 The upper six samples from the Sonsela Member reveal a continued low contribution from the  
530 Ouachita orogen, and a significant increase in the proportion of ~1.08 Ga and 260-240 Ma  
531 grains (Figures 7 and 8). The ~260-240 Ma grains were likely derived from Permian-Early Triassic  
532 igneous rocks along the southern Cordilleran margin (Saleeby and Dunne, 2015; Riggs et al.,  
533 2016), exposed in the Ancestral Mogollon Highlands (Fig. 12). The prominent ~1.44 and 1.08 Ga  
534 grains in these samples may also have been shed from highland sources to the south and  
535 southwest. Triassic grains in these samples record a slightly younger (230 to 204 Ma, peak age  
536 of 215 Ma) phase of magmatism along the Cordilleran margin. Significant changes in both <240  
537 Ma and >240 Ma ages occur between samples 196-3 and 195-2 (Figure 7). MDS analysis  
538 demonstrates that patterns of both <240 Ma and >240 Ma ages are consistent among the six  
539 upper Sonsela Member samples, but are distinct from ages in all other parts of the Chinle  
540 Formation (Figures 7 and 9).

#### 541 **7.8 Petrified Forest Member**

542 Strata of the Petrified Forest Member record an important shift in provenance, with  
543 significantly greater detrital input from the East Mexico arc (~287 Ma) and the Ouachita orogen  
544 (~640-300 Ma), and a broader range of >1.0 Ga basement sources (Figures 7 and 8). Triassic  
545 grains in these strata are also significantly younger, with ages of 228 to 200 Ma (peak age of  
546 209 Ma).

547 An exception to these patterns is recorded by ages from the coarse-grained sandstone of  
548 sample 131-2, which has Precambrian grains that are mainly ~1.1-1.0 and 1.44 Ga (like upper  
549 Sonsela Member; Fig. 9B), and Triassic grains that are ~221 Ma (like strata of the lower Sonsela



550 Member and Blue Mesa Member; Fig. 9A). This lower Petrified Forest Member sample is  
551 interpreted to have been reworked mainly from lateral equivalents of underlying strata of the  
552 Sonsela Member and Blue Mesa Member, with little or no input from the active arc to the west.  
553 MDS analysis shows that sample 116-1 contains a mix of these older reworked grains and the  
554 younger grains present in overlying strata (Fig. 9A).

## 555 **8. MAXIMUM DEPOSITIONAL AGES**

556 The depositional age of Triassic strata on the Colorado Plateau is of considerable interest  
557 because of the rich faunal and paleoclimatic records preserved within the Moenkopi Formation  
558 and Chinle Formation, and as the zircon-based geochronological framework for the early  
559 Mesozoic when coupled with paleomagnetic polarity stratigraphy and astrochronology (Olsen  
560 et al., 2018, 2019; Kent et al., 2018, 2019; Rasmussen et al., 2019). There accordingly have been  
561 many prior attempts to determine the depositional age of these strata by dating igneous zircon  
562 grains in ash beds or volcanic cobbles and detrital zircon grains in clastic strata (e.g., Riggs et al.,  
563 1996, 2003, 2012, 2013, 2016; Heckert et al., 2009; Dickinson and Gehrels, 2009; Irmis et al.,  
564 2011; Ramezani et al., 2011, 2014; Atchley et al., 2013; Nordt et al., 2015). As part the Colorado  
565 Plateau Coring Project, Kent et al. (2018) and Rasmussen et al. (2019) report the results of CA-  
566 TIMS analyses on many of the same samples reported herein. All of the available CA-TIMS ages,  
567 and the preferred age models of Kent et al. (2019) and Rasmussen et al. (2019), are shown on  
568 Figure 13.

569 Maximum depositional ages (MDA's) have been calculated from the LA-ICPMS ages using four  
570 different methods (described above), with results presented in DR Tables 3 and 6 and shown  
571 graphically on Figure 13. In the following discussion we assume that the average of the ages  
572 and uncertainties calculated using these four different methods yields the most reliable  
573 maximum depositional age available from our LA-ICPMS data. These preferred ages are  
574 reported in DR Table 6, shown on Figure 13, and described below with  $2\sigma$  uncertainties  
575 incorporating only internal contributions (for inter-sample comparison) and incorporating both  
576 internal and external uncertainty contributions (for comparison with ages from other studies)  
577 (e.g.,  $224.4 \pm 2.0/2.7$  Ma).

578 The possibility that a maximum depositional age has been compromised by Pb loss is evaluated  
579 by determining whether there is a correlation between U concentration and age. One criterion  
580 is whether the youngest single age has higher U concentration than the average of the  
581 youngest cluster – if yes than the youngest analysis (and perhaps other analyses within the  
582 youngest cluster) may have experienced Pb loss. A second criterion is whether analyses within  
583 the youngest cluster display an inverse correlation between U concentration and age – if yes,  
584 then the higher U and younger analyses within the cluster may have experienced Pb loss.  
585 Rasmussen et al. (2019) document Pb loss in zircon grains from several of our samples by  
586 showing that CA-TIMS ages are commonly older than LA-ICPMS ages from the same crystals.

### 587 **8.1 Coconino Sandstone**





588 Our analyses do not provide a useful maximum depositional age for strata of the Coconino  
589 Sandstone (sample 390-1) because few late Paleozoic ages were recovered from this sample.

### 590 **8.2 Holbrook Formation of the Moenkopi Formation**

591 Of our four samples from the Holbrook Member of the Moenkopi Formation, three yield  
592 preferred MDA's that young upward from 249.5 ( $\pm 1.6/2.5$ ) Ma to 248.4 ( $\pm 2.0/2.8$ ) Ma to 245.7  
593 ( $\pm 1.9/2.7$ ) Ma (DR Table 6). These MDA's are consistent with the inferred Early-Middle Triassic  
594 age of the strata and the corresponding  $\sim 251$ -237 Ma range for Early and Middle Triassic time  
595 on the Geologic Time Scale (Cohen et al., 2013). All three samples show patterns of U  
596 concentration that suggest the possibility of Pb loss (DR Table 6).

### 597 **8.3 Mesa Redondo Member of the Chinle Formation**

598 Our one sample (305-2) from strata of the Mesa Redondo Member yields a preferred MDA of  
599  $223.3 \pm 1.3/2.2$  Ma (DR Table 6). A low MSWD value (0.5) suggests that all ages belong to the  
600 same age population, and patterns of U concentration do not indicate the presence of Pb loss.  
601 This MDA overlaps with CA-TIMS ages of  $\sim 224.7$ -221.7 Ma from the same sample but is older  
602 than the preferred single-grain age of  $\sim 221.7$  Ma (Rasmussen et al., 2019). The LA-ICPMS MDA  
603 of  $223.3 \pm 1.3/2.2$  is significantly younger than CA-TIMS ages of  $\sim 225.2$  Ma (Ramezani et al.,  
604 2011) and  $\sim 227.6$  (Atchley et al., 2013) from outcrop samples of the Mesa Redondo Member.

### 605 **8.4 Blue Mesa Member of the Chinle Formation**

606 Our three samples (297-2, 287-2, 261-1) from strata of the Blue Mesa Member yield preferred  
607 MDA's of  $220.6 \pm 0.6/2.1$ ,  $220.2 \pm 1.3/2.2$ , and  $220.7 \pm 1.3/1.9$  Ma (DR Table 6). All samples  
608 yield MSWD values  $>1.0$  (average of 2.4), which documents the presence of multiple age  
609 populations. Patterns of U concentration suggest the presence of Pb loss in all three samples.  
610 As shown on Figure 13, these ages are similar to most CA-TIMS ages from strata of the Blue  
611 Mesa Member. From lower strata, our ages are slightly younger than a CA-TIMS age of  $\sim 221.8$   
612 Ma [from sample 297-2; Rasmussen et al. (2019)], indistinguishable from a CA-TIMS age of  
613  $\sim 220.5$  Ma [from sample 287-2; Rasmussen et al. (2019)], and similar to an ID-TIMS age of  
614  $\sim 220.9$  Ma [from outcrop; Heckert et al. (2009)]. From upper strata, our age is similar to a CA-  
615 TIMS age from outcrop of  $\sim 220.1$  Ma (Atchley et al., 2013) but significantly younger than a CA-  
616 TIMS age of  $\sim 223.0$  Ma (Ramezani et al., 2011), also from outcrop.

### 617 **8.5 Lower part of the Sonsela Member**

618 Our six samples from the lower part of the Sonsela Member (243-3 to 196-3) yield preferred  
619 MDA's of  $220.3 \pm 0.9/1.8$  Ma (sample 243-3),  $220.6 \pm 0.5/1.8$  Ma (sample 227-3),  $220.5 \pm$   
620  $0.6/1.6$  Ma (sample 215-2),  $220.9 \pm 0.7/2.3$  Ma (sample 210-1), and  $220.6 \pm 0.6/1.7$  Ma (sample  
621 201-1). The sixth, uppermost sample (196-3) yields younger ages with a preferred MDA of  $218.2$   
622  $\pm 0.7/1.6$  Ma. MSWD values for these samples are all high (average of 2.6), which demonstrates  
623 the presence of multiple age components.



624 As shown on Figure 13, these MDA's are 1-3 m.y. older than most CA-TIMS ages from  
625 equivalent strata. From oldest to youngest, the CA-TIMS ages include ~220.1 Ma [from outcrop;  
626 Atchley et al. (2013)] from near the base, through ~218.8 Ma [sample 243-3; Rasmussen et al.  
627 (2019)], ~217.7 Ma [sample 227-3; Rasmussen et al. (2019)], ~219.3 Ma [from outcrop;  
628 Ramezani et al. (2011)], ~217.8 Ma [sample 215-2; Rasmussen et al. (2019)], ~218.0 Ma [from  
629 outcrop; Ramezani et al. (2011)], and ~215.7 Ma and 214.4 Ma [samples 201-1 and 196-3;  
630 Rasmussen et al. (2019)] at the top. The LA-ICPMS-based MDA's ages are also older than a  
631 ~216.6 Ma MDA determined on LA-ICPMS ages from an outcrop sample of sandstone in the  
632 middle part of the lower Sonsela Member, exposed ~132 km north of the CPCP core site (Marsh  
633 et al., 2019).

#### 634 **8.6 Upper part of the Sonsela Member**

635 The lower five samples from the upper Sonsela Member yield similar preferred MDA's of 215.4  
636  $\pm 1.1/2.2$  Ma (sample 195-2), 216.5  $\pm 0.7/1.9$  Ma (sample 188-2), 216.1  $\pm 0.9/2.1$  Ma (sample  
637 182-1), 215.1  $\pm 0.8/1.9$  Ma (sample 177-1), and 216.6  $\pm 1.0/2.0$  Ma (sample 169-1). An upper  
638 sample yields a younger MDA of 213.8  $\pm 0.6/2.1$  Ma (sample 158-2). All samples yield MSWD  
639 values greater than 1.0 (average of 2.6), demonstrating the presence of multiple age  
640 components. Most samples have patterns of U concentration that suggest the possibility of Pb  
641 loss. The lower five MDA's are 2-3 m.y. older than CA-TIMS ages from equivalent strata, which  
642 include outcrop ages of ~213.9 (Ramezani et al., 2011), ~213.6 Ma (Nordt et al., 2015), and  
643 ~213.1 Ma (Ramezani et al., 2011), and CPCP core ages of ~214.0 Ma [samples 182-1 and 177-1;  
644 Rasmussen et al. (2019)]. A CA-TIMS age of ~213.5 Ma for the upper sample [158-2; Rasmussen  
645 et al. (2019)] is nearly identical to our age determination.

#### 646 **8.7 Petrified Forest Member**

647 Our seven samples from the Petrified Forest Member yield three sets of preferred MDA's. The  
648 lowest unit (sample 131-2) yields an MDA of 221.5  $\pm 0.6/2.1$  Ma, which is significantly older  
649 than MDA's in adjacent strata. Four samples near the middle of the unit yield similar preferred  
650 MDA's of 211.5  $\pm 3.1/3.4$  Ma (sample 116-1), 211.6  $\pm 1.7/2.5$  Ma (sample 104-3), 211.2  $\pm$   
651 1.2/1.9 Ma (sample 92-2), and 211.7  $\pm 1.0/2.0$  Ma (sample 84-2). These MDA's are very similar  
652 to an ID-TIMS age of ~211.9 Ma (Irmis et al., 2011) from equivalent strata in outcrop. Two  
653 upper samples, from the Black Forest bed, yield preferred MDA's of 209.6  $\pm 3.0/3.4$  Ma (sample  
654 66-1) and 209.8  $\pm 0.5/1.6$  Ma (sample 52-2). These MDA's are similar to CA-TIMS ages of ~210.2  
655 Ma from core [sample 52-2; Rasmussen et al. (2019)] and ~209.9 Ma from outcrop (Ramezani  
656 et al., 2011), but are significantly younger than outcrop-based ID-TIMS ages of ~211.0 Ma  
657 (Heckert et al., 2009) and ~213.0 Ma (Riggs et al., 2003). Most of our samples yield MSWD  
658 values greater than 1.0 (average of 1.5), suggesting the presence of multiple age components,  
659 and have patterns of U concentration that suggest the presence of Pb loss.

#### 660 **9. COMPARISON OF LA-ICPMS, CA-TIMS, AND MAGNETOSTRATIGRAPHIC CONSTRAINTS ON** 661 **DEPOSITIONAL AGE OF CHINLE FORMATION STRATA**





662 Our preferred maximum depositional ages for strata of the Chinle Formation range from ~223.3  
663 to ~209.6 Ma, which is similar to the ~227.6 to ~209.9 Ma range of CA-TIMS ages (Fig. 13). All  
664 available U-Pb data therefore suggest that the analyzed Chinle Formation strata are Late  
665 Triassic, and probably Norian in age (Dickinson, 2018), given the assigned ages of ~237 to  
666 ~201.3 for Late Triassic time (Cohen et al., 2013) and ~227 to ~208.5 Ma (Cohen et al., 2013) or  
667 ~205.7 Ma (Kent et al., 2017) for Norian time.

668 Figure 13 presents a comparison of our preferred maximum depositional ages, all available ID-  
669 and CA-TIMS ages [from Riggs et al. (2003), Heckert et al. (2009), Ramezani et al. (2011), Irmis  
670 et al. (2011), Atchley et al. (2013), Nordt et al., (2015), Kent et al. (2018), and Rasmussen et al.  
671 (2019)], and two age models that are based on magnetostratigraphic and CA-TIMS  
672 geochronologic information (Kent et al., 2019; Rasmussen et al., 2019). As shown on this figure,  
673 our LA-ICPMS MDA's overlap with most CA-TIMS ages and both age models for most strata  
674 belonging to the Blue Mesa Member and Petrified Forest Member, but are significantly older  
675 for strata of the Sonsela Member. The following discussion explores this pattern of  
676 convergence/divergence of the three chronometers – details of the magnetostratigraphic  
677 information, CA-TIMS data, and age models are discussed by Kent et al. (2018, 2019) and  
678 Rasmussen et al. (2019).

679 Our preferred interpretation of the chronostratigraphic patterns is that U-Pb ages agree with  
680 magnetostratigraphic ages for strata containing abundant zircon crystals which are air-fall in  
681 origin, whereas U-Pb ages tend to predate deposition for strata that are dominated by zircon  
682 grains recycled from older units. The difference in proportion of air-fall (near depositional age)  
683 versus recycled (older) ages is interpreted to be controlled mainly by the grain size of the  
684 sedimentary host, which is important because only >60  $\mu\text{m}$  zircon grains were analyzed in this  
685 study. Given that most detrital zircon grains transported with mud and silt are less than 60  $\mu\text{m}$   
686 in diameter, zircon grains analyzed from mudstone-siltstone samples (and sequences) are  
687 interpreted to be dominated by air-fall crystals rather than older recycled components. In  
688 contrast, because coarser grained sediment is able to transport >60  $\mu\text{m}$  zircon grains,  
689 sandstone samples (and sequences) contain abundant recycled (older) zircon grains and a lower  
690 proportion of air-fall (near depositional-age) zircon grains.

691 Our LA-ICPMS ages from sandstones are significantly impacted by this difference because zircon  
692 grains were selected for analysis at random in an effort to generate an unbiased age  
693 distribution. CA-TIMS analyses from Chinle Formation sandstones have a higher yield of syn-  
694 depositional ages because zircon grains were selected for analysis on the basis of their juvenile  
695 appearance [e.g., acicular and prismatic crystals; Ramezani et al. (2011)] or from the youngest  
696 grains in an LA-ICPMS data set (e.g., Rasmussen et al., 2019; Appendix 2).

697 These interpreted connections between stratigraphy, grain size, and proportions of air-fall  
698 versus recycled zircon grains lead to the interpretation that the three chronometric records  
699 agree (to within ~1 m.y.) for strata of the lower Blue Mesa Member and middle-upper Petrified  
700 Forest Member because these units are dominated by mudstone and siltstone, resulting in U-



701 Pb ages mainly from air-fall (or slightly reworked) zircon grains. In contrast, LA-ICPMS ages from  
702 the Sonsela Member significantly pre-date deposition because the dominant sandstones  
703 contain abundant zircon grains recycled from slightly older units. For strata of the upper  
704 Sonsela Member, CA-TIMS ages approximate the true depositional age because the methods of  
705 grain selection were successful in identifying populations of air-fall zircon grains. For strata of  
706 the lower Sonsela Member, however, these methods were unsuccessful in identifying a  
707 sufficient number of air-fall zircon grains to determine a reliable depositional age, presumably  
708 because of their low abundance relative to recycled grains.

#### 709 **10. IMPLICATIONS FOR THE STRATIGRAPHY OF THE CHINLE FORMATION**

710 The interpreted connections between the three geochronologic records and Chinle stratigraphy  
711 provide an opportunity to reconstruct the depositional history of the Chinle Formation.  
712 Fundamental assumptions in reconstructing this history are that:

713 (1) Chinle Formation strata encountered in the CPCP core record nearly continuous deposition  
714 as described in the age model of Kent et al. (2019), perhaps with a period of erosion or very  
715 slow deposition in the middle part of the Sonsela Member (Rasmussen et al., 2019).

716 (2) LA-ICPMS ages recovered from strata of the Chinle Formation belong to five separate groups  
717 (red vertical bars of Figure 13) due to the hypothesized connections between stratigraphy, grain  
718 size, and proportions of near-depositional-age (air-fall) versus older (recycled) zircon ages.

719 (3) Late Triassic igneous activity in the Cordilleran magmatic arc provided a nearly continuous  
720 supply of zircon grains of air-fall origin to the Chinle deposystem. This assumption is supported  
721 by the relatively continuous distribution of U-Pb ages within the Cordilleran magmatic arc and  
722 back-arc (upper curves of Figure 13). This view is in contrast to the hypothesis of Kent et al.  
723 (2019) that variations in the proportions of depositional-age versus older zircon grains result  
724 mainly from temporal changes in magmatic flux.

725 The interpreted stratigraphic evolution is summarized below and shown schematically on  
726 Figure 14. Important phases in this evolution are as follows:

727 A: An LA-ICPMS MDA of  $\sim 223.3$  Ma from our one sample from the Mesa Redondo Member  
728 (305-2) agrees with the magnetostratigraphic information, the two age models, and the set of  
729 CA-TIMS ages from this sample, presumably because these fine-grained strata are dominated  
730 by zircon grains of air-fall origin. Older CA-TIMS ages of  $\sim 225.2$  Ma (Ramezani et al., 2011) and  
731  $\sim 227.6$  (Atchley et al., 2013) from outcrops of the Mesa Redondo Member may be  
732 compromised by an abundance of recycled zircon grains.

733 B: LA-ICPMS ages of  $\sim 221$  Ma from fine-grained strata in the lower part of the Blue Mesa  
734 Member are also near depositional age, presumably because the  $>60$   $\mu\text{m}$  zircon grains in these  
735 fine-grained strata are dominated by air-fall (or slightly reworked) components.



736 C: LA-ICPMS ages from strata of the upper Blue Mesa Member significantly pre-date deposition,  
737 presumably because these strata are dominated by recycled zircons. The predominance of ~221  
738 Ma LA-ICPMS MDA's suggests that most zircon grains were recycled from lateral equivalents of  
739 underlying strata in the lower part of the Blue Mesa Member. CA-TIMS ages also pre-date  
740 deposition, presumably because of the difficulty of isolating near-depositional-age grains of air-  
741 fall origin.

742 D: This pattern continues up through most of the lower Sonsela Member, with LA-ICPMS MDA's  
743 remaining at ~221 due to recycling of strata from lateral equivalents of the lower Blue Mesa  
744 Member. Most CA-TIMS ages predate the age of deposition because depositional-age (air fall)  
745 grains were diluted by recycled components.

746 E: The age patterns from sandstones of the upper Sonsela Member are somewhat puzzling  
747 given that the dominant ~217-215 Ma LA-ICPMS MDA's pre-date deposition, but fine-grained  
748 strata that could have sourced grains of these ages are not present in the lower Sonsela  
749 Member (Fig. 13). One possibility, as described above, is that the ~217-215 Ma grains were  
750 eroded from fine-grained strata exposed elsewhere (perhaps near Sonsela Buttes; Marsh et al.,  
751 2019) that are dominated by grains of this age. A second possibility is that fine-grained strata  
752 dominated by ~217-215 Ma ages were originally present in the underlying lower Sonsela  
753 Member, but were removed by erosion and recycled into strata of the upper Sonsela Member.  
754 An erosional event of the appropriate age and stratigraphic position has been described by  
755 Rasmussen et al. (2019), as shown by their age model on Figure 13. The occurrence of very  
756 different <240 Ma ages, >240 Ma ages, and U/Th values in samples 196-3 and 195-2 suggests  
757 that this unconformity most likely coincides with the boundary between lower and upper  
758 Sonsela Member strata, and perhaps with the red siliceous horizon recognized in the CPCP core.  
759 As discussed by Rasmussen et al. (2019), the possibility of an unconformity or condensed  
760 section near this stratigraphic position has important implications for Chinle stratigraphy and  
761 fundamental Late Triassic biotic and climatic changes.

762 F: The dominance of pre-depositional-age grains in sample 131-2 provides strong evidence for  
763 recycling of detrital zircons from lateral equivalents of underlying strata of the Blue Mesa  
764 Member or lower Sonsela Member.

765 G: All chronometers agree for strata of sample 116-1, presumably because these fine-grained  
766 strata are dominated by air-fall (or slightly reworked) detrital zircons.

767 H: LA-ICPMS MDA's from sandstones of the middle Petrified Forest Member (samples 104-3,  
768 92-2, and 84-2) slightly predate deposition because they were recycled from lateral equivalents  
769 of immediately underlying fine-grained strata (e.g., sample 116-1).

770 I: All chronometers agree for strata of the Black Forest bed because this unit is dominated by  
771 air-fall (or slightly reworked) detrital zircon grains.

## 772 11. CONCLUSIONS



773 First-order conclusions that result from our U-Pb geochronologic analyses of detrital zircon  
774 grains from the Coconino Sandstone, Moenkopi Formation, and Chinle Formation are as  
775 follows:

776 1. The provenance of strata belonging to the Coconino Sandstone and Moenkopi Formation can  
777 be reconstructed by comparison of our LA-ICPMS ages (Figures 5 and 6) with age distributions  
778 that characterize potential source regions (Figure 3). As shown on Figures 5 and 11, data from  
779 our sample of the Coconino Sandstone and equivalent sandstones of the southern Colorado  
780 Plateau suggest that these strata belong to an eolian blanket that was derived largely from the  
781 Ouachita and/or Appalachian orogens, whereas strata from the northern Colorado Plateau  
782 consist mainly of sediment derived from local basement uplifts (Fig. 1; Dickinson and Gehrels,  
783 2003; Gehrels et al., 2011; Lawton et al. (2015). Lower-Middle Triassic strata of the Moenkopi  
784 Formation record a very different dispersal system, with most detritus derived from the  
785 Ouachita orogen, the East Mexico arc, and early phases of the Cordilleran magmatic arc (Figures  
786 6 and 9).

787 2. LA-ICPMS ages from strata of the Chinle Formation belong to five groups that generally  
788 correspond to the main stratigraphic units (Figures 7, 8, and 13). Maximum depositional ages  
789 calculated from <240 Ma ages and provenance interpretations derived from >240 Ma ages are  
790 as follows:

791 -- Strata of the Mesa Redondo Member yield a preferred MDA of ~223.3 Ma, and were derived  
792 mainly from the Ouachita orogen.

793 -- Strata of the Blue Mesa Member yield MDA's of ~220.7 to ~220.2 Ma, and were derived from  
794 local basement and Ouachita sources.

795 -- Strata in the lower part of the Sonsela Member yield similar MDA's of ~220.9 to ~220.3 Ma  
796 (plus an uppermost sample with an MDA of ~218.2 Ma). Detritus was derived mainly from local  
797 basement (especially ~1.44 Ga) sources, perhaps located in the ancestral Mogollon highlands to  
798 the south.

799 -- Strata in the upper part of the Sonsela Member yield younger MDA's of ~216.6 to ~215.1 Ma,  
800 plus an uppermost sample with an MDA of ~213.8 Ma. Grains with >240 Ma ages were derived  
801 mainly from Precambrian basement (mainly ~1.44 Ga) and Grenville-age rocks to south, as well  
802 as the East Mexico arc.

803 -- Strata of the Petrified Forest Member yield ages that belong to three separate groups. The  
804 lowest sample yields an MDA of ~221.5, which is significantly older than ages from adjacent  
805 strata. The middle four samples yield MDA's of ~211.7 to ~211.2 Ma, whereas the upper two  
806 samples yield MDA's of ~209.8 and ~209.6 Ma. All six upper samples contain abundant >240 Ma  
807 grains that were shed from a broad range of Ouachita, local basement, and East Mexico arc  
808 sources.



809 3. Patterns of U and Th concentration in Triassic zircon grains from the Chinle Formation belong  
810 to four distinct groups that generally coincide with the chronostratigraphic units described  
811 above. Changes in U and Th concentrations are interpreted to record variations in the chemistry  
812 of arc magmatism through time, as has been documented previously by Barth and Wooden  
813 (2006, 2011, 2013) and Riggs et al. (2010, 2012, 2016).

814 4. Comparison of the Chinle Formation MDA's with magnetostratigraphic information (Kent et  
815 al., 2018, 2019) and CA-TIMS geochronologic information (Rasmussen et al., 2019) from the  
816 CPCP core, plus CA-TIMS ages reported from outcrop samples, indicates that LA-ICPMS MDA's  
817 approximate depositional ages for most strata of the Mesa Redondo Member, Blue Mesa  
818 Member, and Petrified Forest Member, but significantly pre-date deposition for strata of the  
819 Sonsela Member (Fig. 13). The correlation of age patterns with stratigraphy is interpreted to  
820 reflect the proportions of air-fall (or slightly reworked) versus recycled (older) zircon grains:  
821 fine-grained strata are dominated by near-depositional ages because most zircon grains are air-  
822 fall (or slightly reworked) in origin, whereas coarse-grained strata are dominated by pre-  
823 depositional ages because recycled zircon grains dilute the abundance of air-fall crystals.

824 5. This hypothesized connection between stratigraphy and the three geochronologic records  
825 supports the following depositional history for Chinle Formation strata encountered in the CPCP  
826 core (Figures 13 and 14):

827 -- LA-ICPMS ages and magnetostratigraphic information (Kent et al., 2019) indicate that the  
828 sampled part of the Mesa Redondo Formation was deposited at ~223.3 Ma. CA-TIMS ages of  
829 ~225.2 Ma (Ramezani et al., 2011) and ~227.6 (Atchley et al., 2013) from outcrop samples  
830 suggest that strata of the Mesa Redondo Member in other areas are dominated by older  
831 recycled components.

832 -- Magnetostratigraphic information (Kent et al., 2019) suggests that strata of the Blue Mesa  
833 Member and lower Sonsela Member accumulated between ~222 Ma and ~214 Ma, whereas  
834 LA-ICPMS MDA's are consistently ~221 Ma for the same strata (except for the uppermost  
835 sample of ~217 Ma). This suggests that most zircons in strata of the upper Blue Mesa Member  
836 and lower Sonsela Member were recycled from lateral equivalents of strata of the lower Blue  
837 Mesa Member. The observation that most CA-TIMS ages from these strata also pre-date  
838 deposition is interpreted to result from the dilution of air-fall zircon crystals by older recycled  
839 zircon grains.

840 -- Strata of the upper Sonsela Member accumulated between ~215 and ~213 Ma, as  
841 constrained by magnetostratigraphic information and CA-TIMS ages. LA-ICPMS MDAs from  
842 these strata are ~217-215 Ma, which indicates that they are dominated by zircons recycled  
843 from older units. The lack of samples in the lower Sonsela Member that are dominated by  
844 ~217-215 Ma grains suggests that zircon grains of this age in upper Sonsela Member strata may  
845 have been transported from sections of the Chinle Formation exposed outside of the PEFO  
846 area. It is also possible that such strata were exposed in the PEFO area, but were removed



847 during an erosional event inferred by Rasmussen et al. (2019) from the pattern of CA-TIMS ages  
848 in the upper Sonsela Member (Fig. 3). Significant changes in <240 Ma ages, >240 Ma ages, and  
849 U-Th values suggest that this unconformity, if present, occurs between samples 196-3 and 195-  
850 2, and may coincide with the red siliceous horizon recognized in the CPCP core.

851 -- All available evidence suggests that mudstone and subordinate sandstone of the middle  
852 Petrified Forest Member accumulated at ~212-211 Ma, and the Black Forest bed in the upper  
853 part of the unit accumulated at ~210 Ma. In contrast, LA-ICPMS ages recovered from sample  
854 131-2, from the lower part of the Petrified Forest Member, are dominantly ~221 Ma, suggestive  
855 of recycling from lateral equivalents of strata of the Blue Mesa Member and lower Sonsela  
856 Member.

857 6. Comparisons of our LA-ICPMS ages, the available CA-TIMS data, and magnetostratigraphic  
858 information provide insights into methods for determining the depositional age of fluvial strata.  
859 Our results show that the most reliable information comes from sequences dominated by fine-  
860 grained clastic strata (mudstone and siltstone) given that these strata have a low abundance of  
861 pre-depositional-age zircon grains of the appropriate size (>60  $\mu\text{m}$  diameter) for routine  
862 analysis by LA-ICPMS. Mudstone-siltstone samples may accordingly have a high proportion of  
863 zircon grains that are air-fall in origin (or only slightly reworked) and thereby record the age of  
864 deposition. In contrast, sedimentary sequences dominated by sandstone commonly yield zircon  
865 grains that have been recycled from older sediments, thereby diluting syn-depositional-age  
866 zircon grains. Future attempts to determine depositional ages from fluvial strata should  
867 accordingly focus on fine-grained strata, rather than sandstones, in spite of the challenges of  
868 extracting and analyzing the smaller zircon crystals.

## 869 **12. AUTHOR CONTRIBUTION**

870 NG and GG generated the LA-ICPMS data reported in this paper. All coauthors were involved in  
871 acquiring the samples that were analyzed and/or interpreting the data. GG prepared this  
872 manuscript with input from all co-authors.

## 873 **13. COMPETING INTERESTS**

874 The authors declare that they have no conflict of interest.

## 875 **14. ACKNOWLEDGEMENTS**

876 Geochronologic analyses were conducted with support from NSF EAR-0959107 and EAR-  
877 1649254 (to Gehrels). Laboratory analyses were performed primarily by N. Giesler.  
878 Collaborative aspects of the project were supported by NSF EAR 0958976 (PEO & JWG),  
879 0958723 (RM), 0958915 (RBI), and 0958859 (DVK). Funding for coring and much logistical  
880 support was provided by ICDP (International Scientific Continental Drilling Program grant 05-  
881 2010: JWG, PEO, Jingeng Sha, Roberto Molina-Garza, Wolfram Kürschner, and Gerhard  
882 Bachmann). Additional funding was supplied by grants from the Lamont Climate Center (PEO).  
883 Field support was provided by LacCore personnel (Anders Noren, Kristina Brady, and Ryan



884 O’Grady), drilling manager Doug Schnurrenberger, and core-handling volunteers (Justin Clifton,  
885 Bob Graves, Ed Lamb, Max Schnurrenberger, and Riley Black). Superintendent Brad Traver of  
886 the National Park Service arranged for permission to core in the PEFO and provided logistical  
887 support during site selection and drilling. This is Petrified Forest Paleontological Contribution 67.  
888 The conclusions presented here are those of the authors and do not represent the views of the  
889 United States Government.





890 **REFERENCES CITED**

- 891 Alsalem, O.B., Fan, M., Zamora, J., Xie, X., and Griffin, W.R.: Paleozoic sediment dispersal before  
892 and during the collision between Laurentia and Gondwana in the Fort Worth Basin, USA:  
893 *Geosphere*, v. 14, no. 1, p. 1–18, doi: 10.1130/GES01480.1, 2018.
- 894 Ash, S.R.: The Black Forest Bed, a distinctive unit in the Upper Triassic Chinle Formation, north-  
895 eastern Arizona: *Journal of the Arizona-Nevada Academy of Science*, v. 24–25, p. 59–73, 1992.
- 896 Atchley, S.C., Nordt, L.C., Dworkin, S.I., Ramezani, J., Parker, W.G., Ash, S.R., and Bowring, S.A.:  
897 A linkage among Pangean tectonism, cyclic alluviation, climate change, and biologic turnover in  
898 the Late Triassic: The Record from the Chinle Formation, Southwestern United States: *Journal of*  
899 *Sedimentary Research*, v. 83, p. 1147–1161, 2013.
- 900 Baranyi, V., Reichgelt, T., Olsen, P.E., Parker, W.G., Kürschner, W.M.: Norian vegetation history  
901 and related environmental changes: new data from the Chinle Formation, Petrified Forest  
902 National Park (Arizona, SW USA): *Geological Society of America Bulletin*, v. 130, p. 775–795,  
903 doi.org/10.1130/B31673.1, 2017.
- 904 Barth, A.P. and Wooden, J.L.: Timing of magmatism following initial convergence at a passive  
905 margin, southwestern US Cordillera, and ages of lower crustal magma sources: *Journal of*  
906 *Geology*, v. 114, p. 231–245, 2006.
- 907 Barth, A.P., Walker, J.D., Wooden, J.L., Riggs, N.R., and Schweickert, R.A.: Birth of the Sierra  
908 Nevada magmatic arc: Early Mesozoic plutonism and volcanism in the east-central Sierra  
909 Nevada of California: *Geosphere*, v. 7, p. 877–897, 2011.
- 910 Barth, A.P., Wooden, J.L., Jacobson, C.E., and Economos, R.C.: Detrital zircon as a proxy for  
911 tracking the magmatic arc system: The California arc example: *Geology*, v. 41, p. 223–226, 2013.
- 912 Black, L., Kamo, S., Allen, C., Davis, D., Aleinikoff, J., Valley, J., Mundil, R., Campbell, I., Korsch,  
913 R., Williams, I., and Foudoulis, C.: Improved  $^{206}\text{Pb}/^{238}\text{U}$  microprobe geochronology by the  
914 monitoring of a trace-element-related matrix effect; SHRIMP, ID–TIMS, ELA–ICP–MS and  
915 oxygen isotope documentation for a series of zircon standards: *Chemical Geology*, v. 205, p.  
916 115–140, 2004.
- 917 Blakey, R.C., Peterson, F., and Kocurek, G.: Synthesis of late Paleozoic and Mesozoic eolian  
918 deposits of the western interior of the United States: *Sedimentary Geology*, v. 56, p. 3–125,  
919 1988.
- 920 Chen, J.H., and Moore, J.G.: Uranium-lead isotopic ages from the Sierra Nevada batholith:  
921 *Journal of Geophysical Research*, v. 87, p. 4761–4784, 1982.
- 922 Cohen, K.M., Finney, S.C., Gibbard, P.L., and Fan, J.-X.: The ICS International Chronostratigraphic  
923 Chart: *Episodes* v. 36, p. 199–204 (updated 2018), 2013.





- 924 Creber, G.T., and Ash, S.R.: Evidence of widespread fungal attack on Upper Triassic trees in the  
925 southwestern U.S.A.: Review of Palaeobotany and Palynology, v. 63, p. 189-195, 1990.
- 926 DeGraaff-Surpless, K., Graham, S.A., Wooden, J.L., and McWilliams, M.O.: Detrital zircon  
927 provenance analysis of the Great Valley Group, California: Evolution of an arc-forearc system:  
928 Geological Society of America Bulletin, v. 114 (12), p. 1564–1580, 2002.
- 929 Dickinson, W.R.: Tectonosedimentary Relations of Pennsylvanian to Jurassic strata on the  
930 Colorado Plateau, Geological Society of America Special Paper 533, 184 p., 2018.
- 931 Dickinson, W.R., and Gehrels, G.E.: U-Pb ages of detrital zircon grains from Permian and Jurassic  
932 eolian sandstones of the Colorado Plateau, USA: Paleogeographic implications: Sedimentary  
933 Geology, v. 163, p. 29–66, 2003.
- 934 Dickinson, W.R. and Gehrels, G.E.: U-Pb ages of detrital zircon grains in relation to  
935 paleogeography: Triassic paleodrainage networks and sediment dispersal across southwest  
936 Laurentia: Journal of Sedimentary Research, v. 78, p. 745–764, 2008.
- 937 Dickinson, W.R. and Gehrels, G.E.: Use of U–Pb ages of detrital zircon grains to infer maximum  
938 depositional ages of strata: a test against a Colorado Plateau Mesozoic database: Earth and  
939 Planetary Science Letters, v. 288, p. 115–125, 2009.
- 940 Gehrels, G.E.: Introduction to detrital zircon studies of Paleozoic and Triassic strata in western  
941 Nevada and northern California, in Soreghan, M.J. and Gehrels, G.E., eds., Paleozoic and Triassic  
942 paleogeography and tectonics of western Nevada and northern California: Geological Society of  
943 America Special Paper 347, p. 1-18, 2000.
- 944 Gehrels, G.E.: Detrital zircon U-Pb geochronology applied to tectonics: Annual Review of Earth  
945 and Planetary Sciences, v. 42, p. 127-149, 2014.
- 946 Gehrels, G. and Pecha, M.: Detrital zircon U-Pb geochronology and Hf isotope geochemistry of  
947 Paleozoic and Triassic passive margin strata of western North America: Geosphere, v. 10 (1), p.  
948 49-65, 2014.
- 949 Gehrels, G.E., Valencia, V., Pullen, A.: Detrital zircon geochronology by Laser-Ablation  
950 Multicollector ICPMS at the Arizona LaserChron Center, in Loszewski, T., and Huff, W., eds.,  
951 Geochronology: Emerging Opportunities, Paleontology Society Short Course: Paleontology  
952 Society Papers, v. 11, 10 p., 2006.
- 953 Gehrels, G.E., Valencia, V., Ruiz, J.: Enhanced precision, accuracy, efficiency, and spatial  
954 resolution of U-Pb ages by laser ablation–multicollector–inductively coupled plasma–mass  
955 spectrometry: Geochemistry, Geophysics, Geosystems, v. 9, Q03017,  
956 doi:10.1029/2007GC001805, 2008.



- 957 Gehrels, G., Blakey, R., Karlstrom, K., Timmons, M., Dickinson, W., and Pecha, M.: Detrital zircon  
958 U-Pb geochronology of Paleozoic strata in the Grand Canyon: *Lithosphere*, v. 3 (3), p. 183-200,  
959 2011.
- 960 González-León, C.M., Valencia, V.A., Lawton, T.F., Amato, J.M., Gehrels, G.E., Leggett, W.J.,  
961 Montijo-Contreras, O., Fernández, M.A.: The lower Mesozoic record of detrital zircon U-Pb  
962 geochronology of Sonora, México, and its paleogeographic implications: *Revista Mexicana de*  
963 *Ciencias Geológicas*, v. 26 (2), p. 301-314, 2009.
- 964 Heckert, A.B. and Lucas, S.G.: Revised Upper Triassic stratigraphy of the Petrified Forest  
965 National Park, Arizona, USA: *New Mexico Museum of Natural History Science Bulletin*, v. 21, p.  
966 1–36, 2002.
- 967 Heckert, A.B., Lucas, S.G., Dickinson, W.R., and Mortensen, J.K.: New ID-TIMS U-Pb ages for  
968 Chinle Group strata (Upper Triassic) in New Mexico and Arizona, correlation to the Newark  
969 Supergroup, and implications for the “long Norian”: *Geological Society of America Abstracts*  
970 *with Programs*, v. 41, p. 123, 2009.
- 971 Hildebrand, R.S.: Did westward subduction cause Cretaceous-Tertiary orogeny in the North  
972 American Cordillera?: *Geological Society of America Special paper* 457, 71 p., 2009.
- 973 Hildebrand, R.S.: Mesozoic assembly of the North American cordillera: *Geological Society of*  
974 *America Special paper* 495, 169 p., 2013.
- 975 Hoke, G., Schmitz, M., and Bowring, S.: An ultrasonic method for isolating nonclay components  
976 from clay-rich material: *Geochemistry Geophysics Geosystems*, v. 15, p. 492–498, 2014.
- 977 Horstwood, M., Kosler, J., Gehrels, G., Jackson, S., McLean, N., Paton, C., Pearson, N., Sircombe,  
978 K., Sylvester, P., Vermeesch, P., Bowring, J., Condon, D., and Schoene, B.: Community-Derived  
979 Standards for LA-ICP-MS U-Th-Pb Geochronology – Uncertainty Propagation, Age Interpretation  
980 and Data Reporting: *Geostandards and Geoanalytical Research*, v. 40 (3), p. 311-332, 2016.
- 981 Irmis, R.B., Mundil, R., Martz, J.W., and Parker, W.G.: High-resolution U-Pb ages from the Upper  
982 Triassic Chinle Formation (New Mexico, USA) support a diachronous rise of dinosaurs: *Earth and*  
983 *Planetary Science Letters*, v. 309, p. 258–267, 2011.
- 984 Kent, D.V., Olsen, P.E., and Muttoni, G.: Astrochronostratigraphic polarity time scale (APTS) for  
985 the Late Triassic and Early Jurassic from continental sediments and correlation with standard  
986 marine stages: *Earth-Science Reviews*, v. 166, p. 153–180, 2017.
- 987 Kent, D.V., Olsen, P.E., Rasmussen, C., Lepre, C.J., Mundil, R., Irmis, R.B., Gehrels, G.E., Giesler,  
988 D., Geissman, J.W., and Parker, W.G.: Empirical evidence for stability of the 405 kyr Jupiter-  
989 Venus eccentricity cycle over hundreds of millions of years: *Proceedings of the National*  
990 *Academy of Sciences*, v. 115, p. 6153–6158, 2018.



- 991 Kent, D.V., Olsen, P.E., Lepre, C. Mundil, R., Rasmussen, C., Irmis, R.B., Gehrels, G.E., Giesler, D.,  
992 Geissman, J.W., Parker, W.G.: Magnetostratigraphy of the entire Chinle Formation (Norian age)  
993 in scientific drill core PFNP-1A from the Petrified Forest National Park (Arizona, USA) and  
994 implications for global correlations in the Late Triassic: Geophysics, Geochemistry, Geosystems  
995 (in review), 2019.
- 996 Kissock, J.K., Finzel, E.S., Malone, D.H., and Craddock, J.P.: Lower–Middle Pennsylvanian strata  
997 in the North American midcontinent record the interplay between erosional unroofing of the  
998 Appalachians and eustatic sea-level rise: *Geosphere*, v. 14 (1), p. 141–161, 2018.
- 999 Lawton, T.F., Buller, C.D., and Parr, T.R.: Provenance of a Permian erg on the western margin of  
1000 Pangea: Depositional system of the Kungurian (late Leonardian) Castle Valley and White Rim  
1001 sandstones and subjacent Cutler Group, Paradox Basin, Utah, USA: *Geosphere*, v. 11 (5), p. 1–  
1002 32, 2015.
- 1003 Lucas, S.G.: The Chinle Group: revised stratigraphy and biochronology of Upper Triassic  
1004 nonmarine strata in the western United States, in: *Aspects of Mesozoic Geology and  
1005 Paleontology of the Colorado Plateau*, edited by: Morales, M., Museum of Northern Arizona  
1006 Bulletin 59, Flagstaff: Museum of Northern Arizona Press, p. 27–50., 1993.
- 1007 Ludwig, K.R.: Isoplot 3.6: Berkeley Geochronology Center Special Publication 4, 77 p., 2008.
- 1008 Marsh, A.D., Parker, W.G., Stockli, D.F., and Martz, J.W.: Regional correlation of the Sonsela  
1009 Member (Upper Triassic Chinle Formation) and detrital U-Pb zircon data from the Sonsela  
1010 Sandstone bed near the Sonsela Buttes, northeastern Arizona, USA, support the presence of a  
1011 distributive fluvial system: *Geosphere*, v. 15, <https://doi.org/10.1130/GES02004.1>, 2019.
- 1012 Martz, J.W. and Parker, W.G.: Revised lithostratigraphy of the Sonsela Member (Chinle  
1013 Formation, Upper Triassic) in the southwestern part of Petrified Forest National Park, Arizona:  
1014 *PLoS ONE* 5(2): e9329. doi:10.1371/journal.pone.0009329, 2010.
- 1015 Martz, J.W., Parker, W.G., Skinner, L., Raucci, J.J., Umhoefer, P., and Blakey, R.C.: Geologic map  
1016 of Petrified Forest National Park, Arizona: Arizona Geological Survey Contributed Map CM-12-A,  
1017 1 map sheet, scale 1:50,000, 18 p., [http://repository.azgs.gov/uri\\_gin/azgs/dlio/1487](http://repository.azgs.gov/uri_gin/azgs/dlio/1487), 2012.
- 1018 Martz, J.W., Kirkland, J.I., Milner, A.R.C., Parker, W.G., Santucci, V.L.: Upper Triassic  
1019 lithostratigraphy, depositional systems, and vertebrate paleontology across southern Utah:  
1020 *Geology of the Intermountain West*, v. 4, p. 99–180, [https://www.utahgeology.org/wp-  
1021 content/uploads/2018/05/GIW2017-v04-pp099-180-Martz.pdf](https://www.utahgeology.org/wp-content/uploads/2018/05/GIW2017-v04-pp099-180-Martz.pdf), 2017.
- 1022 Miller, J.S., Glazner, A.F., Walker, J.D., and Martin, M.W.: Geochronologic and isotopic evidence  
1023 for Triassic–Jurassic emplacement of the eugeoclinal allochthon in the Mojave Desert region,  
1024 California: *Geological Society of America Bulletin*, v. 107, p. 1441–1457, 1995.



- 1025 Nordt, L., Atchley, S., Dworkin, S.: Collapse of the Late Triassic megamonsoon in western  
1026 equatorial Pangea, present-day American southwest: *Geological Society of America Bulletin*, v.  
1027 127 (11/12), p. 1798–1815, 2015.
- 1028 Olsen, P. E., Kent, D.V., and Whiteside, H.: Implications of the Newark Supergroup-based  
1029 astrochronology and geomagnetic polarity time scale (Newark-APTS) for the tempo and mode  
1030 of the early diversification of the Dinosauria: *Earth and Environmental Science Transactions of*  
1031 *the Royal Society of Edinburgh*, v. 101, p. 201–229, 2011.
- 1032 Olsen, P., Geissman, J., Kent, D., Gehrels, G., and 23 others: Colorado Plateau Coring Project,  
1033 Phase I (CPCP-I): a continuously cored, globally exportable chronology of Triassic continental  
1034 environmental change from western North America: *Scientific Drilling*, v. 24, p. 15–40, 2018.
- 1035 Olsen, P.E., Laskar, J., Kent, D.V., Kinney, S.T., Reynolds, D.J., Sha, J. and Whiteside, J.H.:  
1036 Mapping Solar System chaos with the Geological Orrery: *Proceedings of the National Academy*  
1037 *of Sciences*, v. 116 (22), p. 10664-10673, 2019.
- 1038 Ortega-Flores, B., Solari, L., Lawton, T.F., and Ortega-Obregón, C.: Detrital-zircon record of  
1039 major Middle Triassic–Early Cretaceous provenance shift, central Mexico: demise of  
1040 Gondwanan continental fluvial systems and onset of backarc volcanism and sedimentation:  
1041 *International Geology Review*, v. 56 (2), p. 237-261, 2014.
- 1042 Paces, J.B., & Miller, J.D.: Precise U-Pb ages of Duluth Complex and related mafic intrusions,  
1043 northeastern Minnesota: Geochronological insights to physical, petrogenetic, paleomagnetic,  
1044 and tectonomagmatic processes associated with the 1.1 Ga midcontinent rift system: *Journal of*  
1045 *Geophysical Research*, v. 98 (B8), p. 13997–14013. <https://doi.org/10.1029/93JB01159>, 1993.
- 1046 Parker, W., and Martz, J.: Constraining the stratigraphic position of the Late Triassic (Norian)  
1047 Adamanian–Revueltian faunal transition in the Chinle Formation of Petrified Forest National  
1048 Park, Arizona: *Journal of Vertebrate Paleontology*, v. 29 (suppl. to 3), p. 162A, 2009.
- 1049 Parker, W.G., and Martz, J.W.: The Late Triassic (Norian) Adamanian–Revueltian tetrapod faunal  
1050 transition in the Chinle Formation of Petrified Forest National Park, Arizona, *Earth and*  
1051 *Environmental Science Transactions of the Royal Society of Edinburgh*: v. 101, p. 231–260,  
1052 2011.
- 1053 Pipiringos, G.N., O’Sullivan, R.B.: Principal unconformities in Triassic and Jurassic rocks, Western  
1054 Interior United States – a preliminary survey: *Geological Survey Professional Paper 1035-A*, 29  
1055 p., 1978.
- 1056 Pullen, A., Ibanez-Mejia, M., Gehrels, G., Giesler, D., and Pecha, M.: Optimization of a Laser  
1057 Ablation-Single Collector-Inductively Coupled Plasma-Mass Spectrometer (Thermo Element 2)  
1058 for Accurate, Precise, and Efficient Zircon U-Th-Pb Geochronology: *Geochemistry, Geophysics,*  
1059 *Geosystems*, v. 19. <https://doi.org/10.1029/2018GC007889>, 2018.



- 1060 Ramezani, J., Hoke, G.D., Fastovsky, D.E., Bowring, S.A., Therrien, F., Dworkin, S.I., Atchley, S.C.,  
1061 and Nordt, L.C.: High precision U-Pb zircon geochronology of the Late Triassic Chinle Formation,  
1062 Petrified Forest National Park (Arizona, USA): Temporal constraints on the early evolution of  
1063 dinosaurs: *Geological Society of America Bulletin*, v. 123, p. 2142–2159, 2011.
- 1064 Ramezani, J., Fastovsky, D.E., and Bowring, S.A.: Revised chronostratigraphy of the lower Chinle  
1065 Formation strata in Arizona and New Mexico (USA): high-precision U-Pb  
1066 geochronological constraints on the Late Triassic evolution of dinosaurs: *American Journal of  
1067 Science*, v. 314, p. 981–1008, 2014.
- 1068 Rasmussen, C., Mundil, R., Irmis, R.B., Geisler, D., Gehrels, G.E., Olsen, P.E., Kent, D.V., Lepre, C.,  
1069 Geissmann, J.W., and Parker, W.G.: A high-resolution age model for the Upper Triassic Chinle  
1070 Formation (Petrified Forest National Park, Arizona, USA) constrained by U-Pb geochronology  
1071 and magnetostratigraphy: implications for Late Triassic paleoecological and  
1072 paleoenvironmental change: *Geological Society of America Bulletin* (in review), 2019.
- 1073 Reichgelt, T., Parker, W.G., Martz, J.W., Conran, J.G., Cittert, J.H.A.K., Kürschner, W.M.: The  
1074 palynology of the Sonsela Member (Late Triassic, Norian) at Petrified Forest National Park,  
1075 Arizona, USA: *Review of Palaeobotany and Palynology*, v. 189, p. 18–28,  
1076 doi.org/10.1016/j.revpalbo.2012.11.001, 2013.
- 1077 Riggs, N.R., Lehman, T.M., Gehrels, G.E., and Dickinson, W.R.: Detrital zircon link between  
1078 headwaters and terminus of the Upper Triassic Chinle–Dockum paleoriver system: *Science*, v.  
1079 273, p. 97–100, 1996.
- 1080 Riggs, N.R., Ash, S.R., Barth, A.P., Gehrels, G.E., and Wooden, J.L.: Isotopic age of the Black  
1081 Forest Bed, Petrified Forest Member, Chinle Formation, Arizona: an example of dating a  
1082 continental sandstone: *Geological Society of America Bulletin*, v. 115, p. 1315–1323, 2003.
- 1083 Riggs, N.R., Barth, A.P., González-León, C., Jacobson, C.E., Howell, E., Wooden, J.E., and Walker,  
1084 J.D.: Provenance of Upper Triassic strata in southwestern North America as suggested by  
1085 isotopic analysis and chemistry of zircon crystals, in Rasbury, E.T., Hemming, S., and Riggs, N.,  
1086 eds., *Mineralogical and Geochemical Approaches to Provenance: Geological Society of America  
1087 Special Paper 487*, p. 13–36, doi: 10.1130/2012.2487(02), 2012.
- 1088 Riggs, N.R., Reynolds, S.J., Lindner, P.J., Howell, E.R., Barth, A.P., Parker, W.G., and Walker, J.D.:  
1089 The Early Mesozoic Cordilleran arc and Late Triassic paleotopography: The detrital record in  
1090 Upper Triassic sedimentary successions on and off the Colorado Plateau: *Geosphere*, v. 9, p.  
1091 602–613, 2013.
- 1092 Riggs, N.R., Oberling, Z.A., Howell, E.R., Parker, W.G., Barth, A.P., Cecil, M.R., and Martz, J.W.:  
1093 Sources of volcanic detritus in the basal Chinle Formation, southwestern Laurentia, and  
1094 implications for the Early Mesozoic magmatic arc: *Geosphere*, v. 12, p. 439–463, 2016.



- 1095 Saleeby, J., and Dunne, G.: Temporal and tectonic relations of early Mesozoic arc magmatism,  
1096 southern Sierra Nevada, California, in Anderson, T.H., Didenko, A.N., Johnson, C.L., Khanchuk,  
1097 A.I., and MacDonald, J.H., Jr., eds., Late Jurassic Margin of Laurasia—A Record of Faulting  
1098 Accommodating Plate Rotation: Geological Society of America Special Paper 513, p. 223–268,  
1099 2015.
- 1100 Saylor, J.E., and Sundell, K.E.: Quantifying comparison of large detrital geochronology data sets.  
1101 *Geosphere*12, 203–220, 2016.
- 1102 Saylor, J.E., Jordan, J.C., Sundell, K.E., Wang, X., Wang, S., and Deng, T.: Topographic growth of  
1103 the Jishi Shan and its impact on basin and hydrology evolution, NE Tibetan Plateau: *Basin  
1104 Research*, v. 30(3), p. 544–563, 2018.
- 1105 Stewart, J.H., Anderson, T.H., Haxel, G.B., Silver, L.T., and Wright, J.E.: Late Triassic  
1106 paleogeography of the southern Cordillera: The problem of a source for the voluminous  
1107 volcanic detritus in the Chinle Formation of the Colorado Plateau region: *Geology*, v. 14, p. 567–  
1108 570, 1986.
- 1109 Sundell, K.E., Saylor, J.E., and Pecha, M.: Sediment provenance and recycling of detrital zircons  
1110 from Cenozoic Altiplano strata in southern Peru and implications for the crustal evolution of  
1111 west-central South America: *Journal of South American Earth Sciences*, (in review), 2019.
- 1112 Surpless, K.D., Graham, S.A., Covault, J.A., and Wooden, J.L.: Does the Great Valley Group  
1113 contain Jurassic strata? Reevaluation of the age and early evolution of a classic forearc basin:  
1114 *Geology*, v. 34 (1), p. 21–24, 2006.
- 1115 Thomas, W.A., Gehrels, G.E., Greb, S.F., Nadon, G.C., Satkoski, A.M., and Romero, M.C.: Detrital  
1116 zircon grains and sediment dispersal in the Appalachian foreland: *Geosphere*, v. 13 (6), p. 2206–  
1117 2230, 2017.
- 1118 Thomas, W.A., Gehrels, G.E., Lawton, T., Satterfield, J., Romero, M., and Sundell, K.: Detrital  
1119 zircon grains and sediment dispersal from the Coahuila terrane of northern Mexico into the  
1120 Marathon foreland of the southern Midcontinent: *Geosphere*, v. 16 (in press), 2019.
- 1121 Tobisch, O.T., Fiske, R.S., Saleeby, J.B., Holt, E., and Sorensen, S.S.: Steep tilting of metavolcanic  
1122 rocks by multiple mechanisms, central Sierra Nevada, California: *Geological Society of America  
1123 Bulletin*, v. 112 (7), p. 1043–1058, 2000.
- 1124 Vermeesch, P.: Multi-sample comparison of detrital age distributions: *Chemical Geology*, v. 341,  
1125 p. 140–146, 2013.
- 1126 Wissink, G.K., Wilkinson, B.H., and Hoke, G.D.: Pairwise sample comparisons and  
1127 multidimensional scaling of detrital zircon ages with examples from the North American  
1128 platform, basin, and passive margin settings: *Lithosphere*, <https://doi.org/10.1130/L700.1>,  
1129 2018.



- 1130 Woody, D.T.: Revised stratigraphy of the lower Chinle Formation (Upper Triassic) of Petrified  
1131 Forest National Park, Arizona: Museum of Northern Arizona Bulletin, v. 62, p. 17–45, 2006.
- 1132 Wright, J.E., and Wyld, S.J.: Alternative tectonic model for Late Jurassic through Early  
1133 Cretaceous evolution of the Great Valley Group, California, in Cloos, M., Carlson, W.D., Gilbert,  
1134 M.C., Liou, J.G., and Sorensen, S.S., eds., Convergent Margin Terranes and Associated Regions:  
1135 A Tribute to W.G. Ernst: Geological Society of America Special Paper 419, p. 1-15, 2007.
- 1136 Xie, X., Anthony, J.M., and Busbey, A.B.: Provenance of Permian Delaware Mountain Group,  
1137 central and southern Delaware basin, and implications of sediment dispersal pathway near the  
1138 southwestern terminus of Pangea: International Geology Review, DOI:  
1139 10.1080/00206814.2018.1425925, 2018.





1140 **FIGURE CAPTIONS**

1141 **Figure 1.** Map showing the main basement provinces of southern North America and Mexico.  
1142 Also shown are locations of the study area within the Colorado Plateau, outlines of Ancestral  
1143 Rocky Mountains uplifts, and the Permian-Triassic magmatic arc along the continental margin  
1144 of southwestern North America. Modified from Gehrels et al. (2011).

1145 **Figure 2.** Strata encountered in the Colorado Plateau Coring Project (adapted from Olsen et al.,  
1146 2018). Sampled horizons are shown relative to core depth, stratigraphic depth, and  
1147 stratigraphic nomenclature relevant for the Petrified Forest region. Detailed descriptions of  
1148 samples are provided in DR Table 1; images of the sampled material are presented in Appendix  
1149 1.

1150 **Figure 3.** Normalized probability density plots of U-Pb (zircon) ages from source terranes.  
1151 Distinctive age groups include 1750-1620 Ma and 1520-1360 Ma ages from southwest Laurentia  
1152 basement provinces, 1240-960 Ma ages from Grenville-age provinces exposed in the  
1153 Appalachian and Ouachita orogens, 640-570 Ma and 480-370 Ma ages characteristic of the  
1154 Appalachian orogen, 670-300 Ma ages from the Ouachita orogen, 300-260 Ma ages from the  
1155 East Mexico arc, and 260-200 Ma ages belonging to the Cordilleran magmatic arc of  
1156 southwestern North America. See text for sources of information.

1157 **Figure 4.** Plot showing the accuracy of  $^{206}\text{Pb}^*/^{238}\text{U}$  dates of secondary standards analyzed  
1158 during the current study. Each pair of symbols represents the weighted mean age and  $2\sigma$   
1159 uncertainty of R33 and FC-1 analyses conducted with each sample, expressed as % offset from  
1160 reported ID-TIMS dates of 1099.9 Ma for FC-1 (Paces and Miller, 1993) and 419.26 Ma for R33  
1161 (Black et al., 2004). For FC-1, 1065 analyses are reported, with MSWD = 0.95 for all analyses. For  
1162 R33, 295 analyses are reported, with MSWD = 0.92 for all analyses. Data are reported in DR  
1163 Table 7.

1164 **Figure 5.** Normalized probability density plots of detrital zircon ages from our sample of the  
1165 Coconino Sandstone and from other lower Permian sandstones of the Colorado Plateau.  
1166 Numbers of constituent analyses are shown for each sample. Data are from <sup>1</sup>Dickinson and  
1167 Gehrels (2003), <sup>2</sup>Gehrels et al. (2011), <sup>3</sup>Lawton et al. (2015), and <sup>4</sup>this study. Shown for  
1168 reference are age ranges from the Appalachian orogen (purple bands) and from local basement  
1169 rocks (blue bands) (from Figure 3), which are interpreted by previous researchers to have  
1170 sourced most of the detritus in these units. Also shown is our sample 383-2, which is  
1171 interpreted to belong to the Wupatki Member of the Moenkopi Formation, but has an age  
1172 signature characteristic of lower Permian strata of the Colorado Plateau.

1173 **Figure 6.** Probability density plots of detrital zircon ages from four samples from the Moenkopi  
1174 Formation (lower four curves) as well as a Moenkopi sample from Dickinson and Gehrels  
1175 (2008). Numbers of constituent analyses are shown for each sample. Samples 349-3, 335-1,  
1176 327-2, and 319-2, plus the sample from Dickinson and Gehrels (2008), are all from the Holbrook





1177 Member. Sample 383-2 is interpreted to belong to the Wupatki Member, but has an age  
1178 distribution that resembles lower Permian strata. Source regions are interpreted to include  
1179 local basement rocks (blue bands), the Ouachita orogen (green bands), the East Mexico arc (red  
1180 band), and the Late Permian-Triassic arc built along the Cordilleran margin (orange band).

1181 **Figure 7.** Normalized probability density plots of detrital zircon ages from twenty-four samples  
1182 from the Mesa Redondo, Blue Mesa, Sonsela, and Petrified Forest Members of the Chinle  
1183 Formation. Numbers of constituent analyses are shown for each sample. Age distributions older  
1184 than 240 Ma are exaggerated by 10x. Tick marks indicate the preferred maximum depositional  
1185 age for each sample (from DR Table 6). Source regions are interpreted to include local  
1186 basement rocks (blue bands), the Ouachita orogen (green bands), the East Mexico arc (red  
1187 band), and the Late Permian-Triassic arc built along the Cordilleran margin (orange band).  
1188 Percent of all grains that are <240 Ma in age are shown for each sample on the left.

1189 **Figure 8.** Normalized probability density plots of detrital zircon ages from each set of samples  
1190 analyzed in this study. Numbers of constituent analyses are shown for each sample. Age  
1191 distributions older than 240 Ma for Chinle strata are exaggerated by 10x relative to <240 Ma  
1192 ages. Age distributions for Moenkopi and Coconino Sandstones are exaggerated by 5x relative  
1193 to Chinle ages. Source regions are interpreted to include local basement rocks (blue bands), the  
1194 Ouachita orogen (green bands), the East Mexico arc (red band), and the Late Permian-Triassic  
1195 arc built along the Cordilleran margin (orange band). Results from sample 383-2 are not  
1196 included in this plot because of its uncertain stratigraphic position. Data from sample 131-2 are  
1197 omitted because they differ from ages present in other samples from the Petrified Forest  
1198 Member. Percent of all grains that are <240 Ma in age are shown for each sample on the left.

1199 **Figure 9.** MDS plot comparing age distributions of samples analyzed herein with each other and  
1200 with possible source areas. MDS (metric) analyses are based on the cross-correlation  
1201 coefficient, and were conducted using the software of Saylor et al. (2018). Data from samples  
1202 analyzed herein are in DR Table 3. Ages for source regions are from the sources cited in the  
1203 text. Stars represent MDS values for sets of examples. Samples 383-2 with the exception that  
1204 sample 131 is not included with other Petrified Forest samples.

1205 **Figure 10.** Density distributions of U concentration versus U/Th for Triassic grains in the four  
1206 chronostratigraphic units recognized in this study. Plots made with Hf density plotter software  
1207 of Sundell et al. (2019).

1208 **Figure 11.** MDS plot comparing age distributions of Permian strata of the Colorado Plateau with  
1209 each other and with potential source regions including the Appalachian orogen, Ouachita  
1210 orogen, and basement rocks of southwestern North America. Data sources are described in  
1211 Figures 3 and 4. The data support the interpretation of Lawton et al. (2015) that the Coconino,  
1212 Cedar Mesa, and White Rim sandstones (cool shades) belong to a regional blanket of eolian  
1213 strata that was derived largely from the Appalachian and/or Ouachita orogen, where strata of



1214 the Castle Valley and Cutler formations (warm shades) include greater proportions of detritus  
1215 derived from local basement sources.

1216 **Figure 12.** Sketch map of relevant tectonic features in southwestern Laurentia during Late  
1217 Triassic time [adapted from Figure 42 of Dickinson (2018)].

1218 **Figure 13.** Plot showing interpreted maximum depositional ages (and  $2\sigma$  uncertainties) for each  
1219 sample, as determined by the four methods described above and reported in DR Table 6.  
1220 Preferred ages (vertical red lines) are the average of the ages calculated by these four methods.  
1221 CA-TIMS and ID-TIMS ages are shown in approximate stratigraphic position (as shown by Kent  
1222 et al., 2019), with outcrop samples in gray symbols and core samples using black symbols.  
1223 Smaller symbols represent ID-TIMS ages or CA-TIMS ages based on a single age or of uncertain  
1224 reliability. Stratigraphic units are keyed to dominant rock type, with brown = mudstone and  
1225 siltstone, yellow = sandstone, pink = bentonite. Average grain size of each sample is shown with  
1226 bars on left (from Appendix 1 and DR Table 1). PDP curves to right show 2.0 Ga to 240 Ma ages,  
1227 as plotted on Figure 7. Also shown are age models of Kent et al. (2019) and Rasmussen et al.  
1228 (2019). Vertical red bands show interpreted ages of main clusters of maximum depositional  
1229 ages.

1230 Curves across top of diagram show the distribution of ages from (1) fore-arc strata of the  
1231 Barranca and El Antimonio Groups in Sonora (Gonzalez-Leon et al., 2009; Gehrels and Pecha,  
1232 2014) and the Great Valley Group in California (DeGraaff-Surpless et al., 2002; Surpless et al.,  
1233 2006; Wright and Wyld, 2007), (2) Permian-Triassic igneous rocks in California (Chen and  
1234 Moore, 2982; Miller et al., 1995; Tobisch et al., 2000; Barth and Wooden, 2006, 2011, 2013;  
1235 Saleeby and Dunne, 2015), and (3) strata of the Chinle Formation in other parts of the Colorado  
1236 Plateau (Dickinson and Gehrels, 2008; Riggs et al., 2012; Marsh et al., 2019). Diamond-shaped  
1237 symbols beneath curves represent individual ages.

1238 **Figure 14.** Depositional model of strata of the Chinle Formation encountered in the CPCP core.  
1239 Each time slice contains information about the dominant grain size of the host sedimentary  
1240 rock, the abundance of syn-depositional-age zircon grains that are interpreted to be air-fall in  
1241 origin, and the abundance of recycled zircon grains that pre-date deposition.



Figure 1 (NAmap)

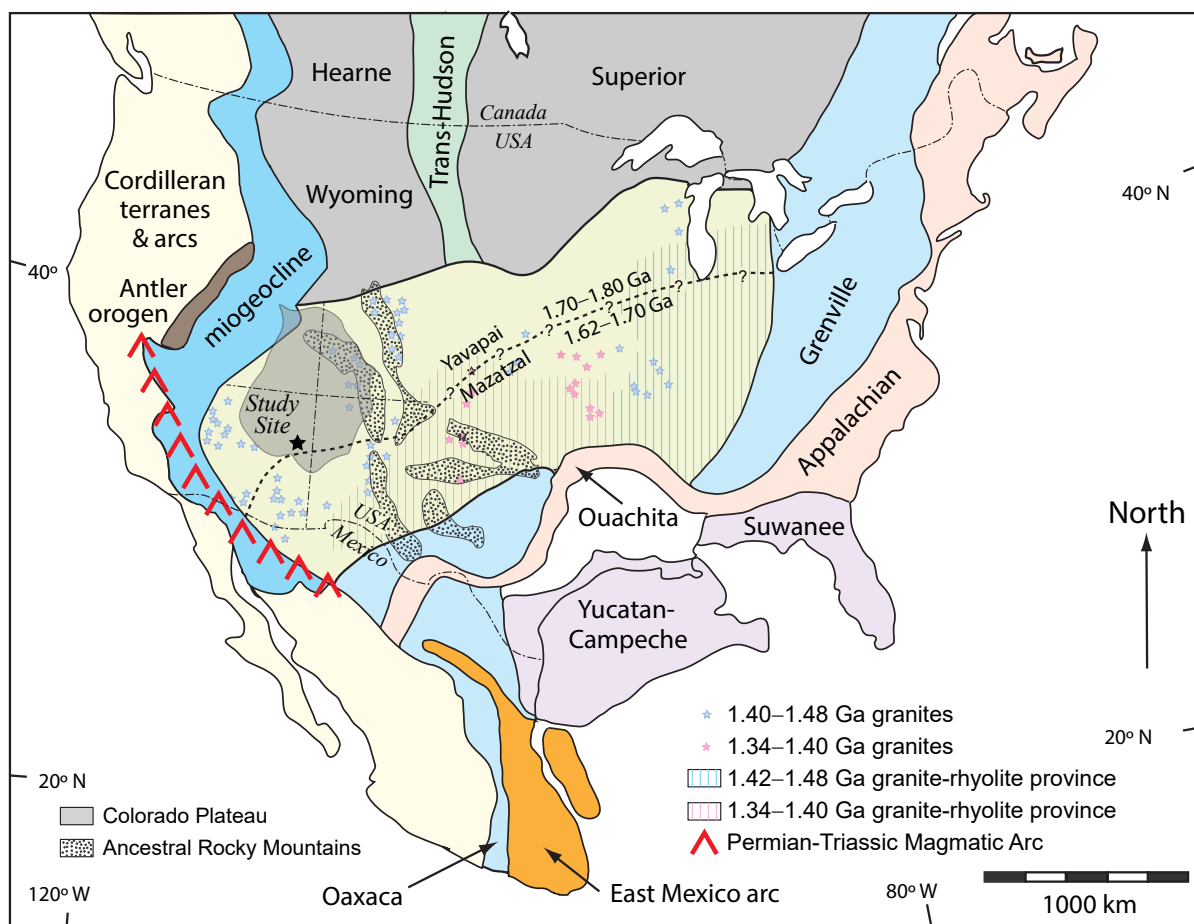




Figure 2 (Strat Column)

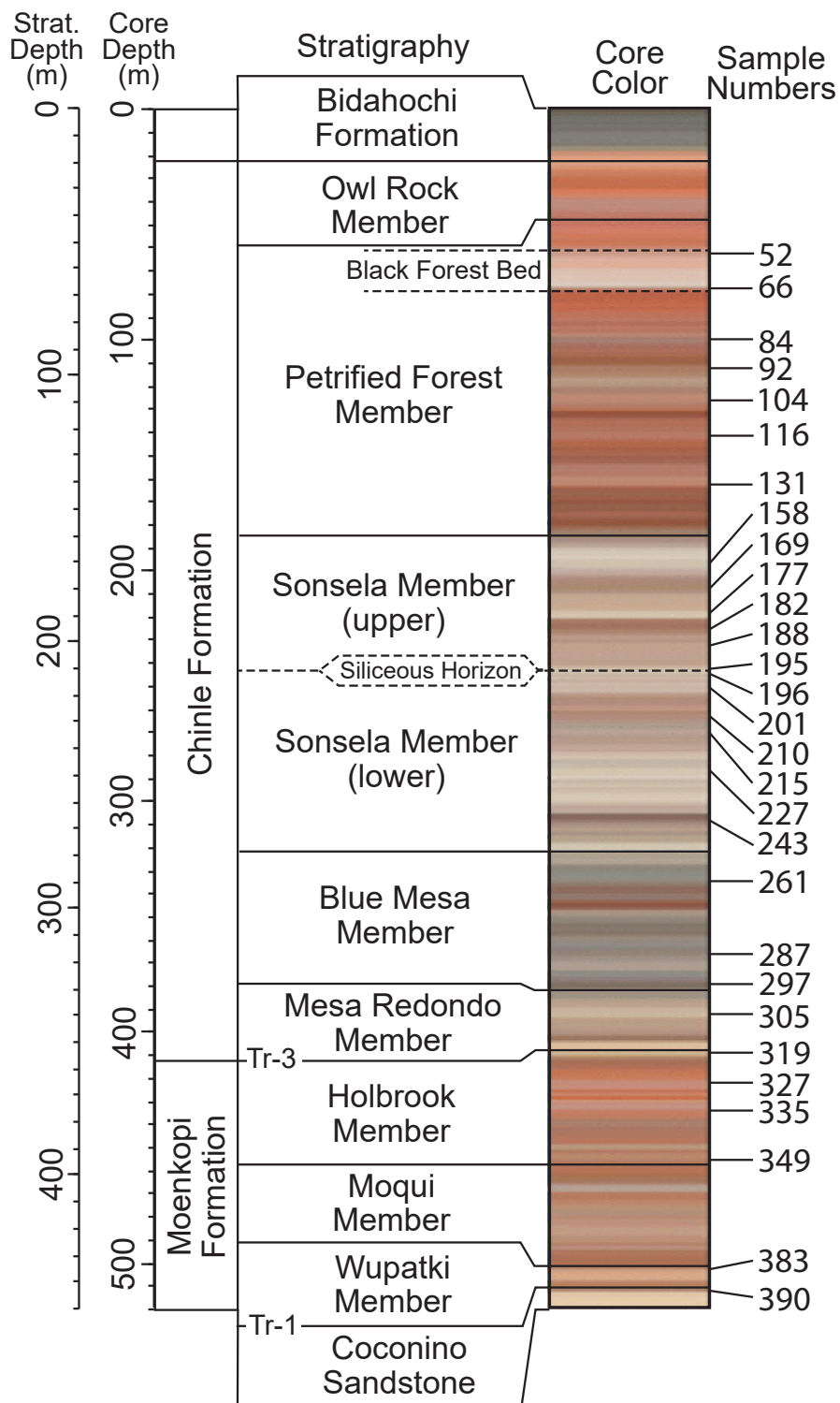




Figure 3 (App-Ouach-Bsmt-EMArc-CordArc PDP)

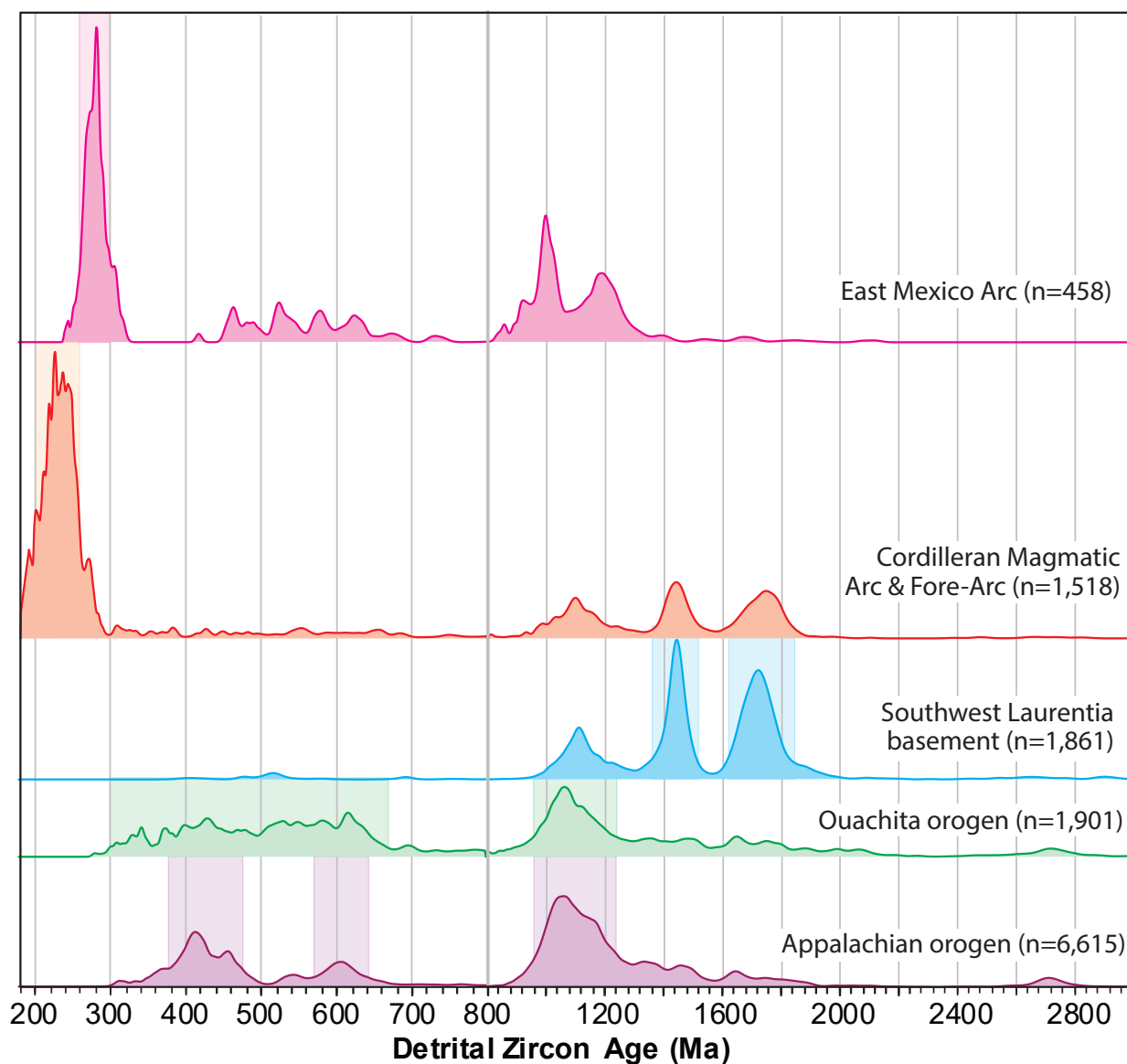




Figure 4 (Standard Ages)

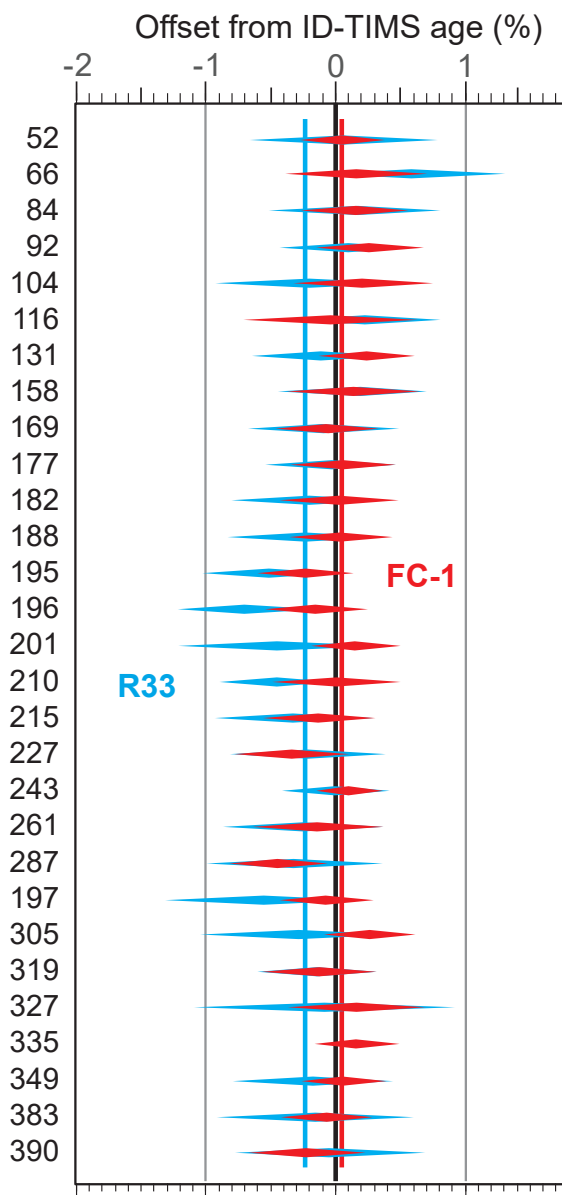




Figure 5 (Coconino PDP)

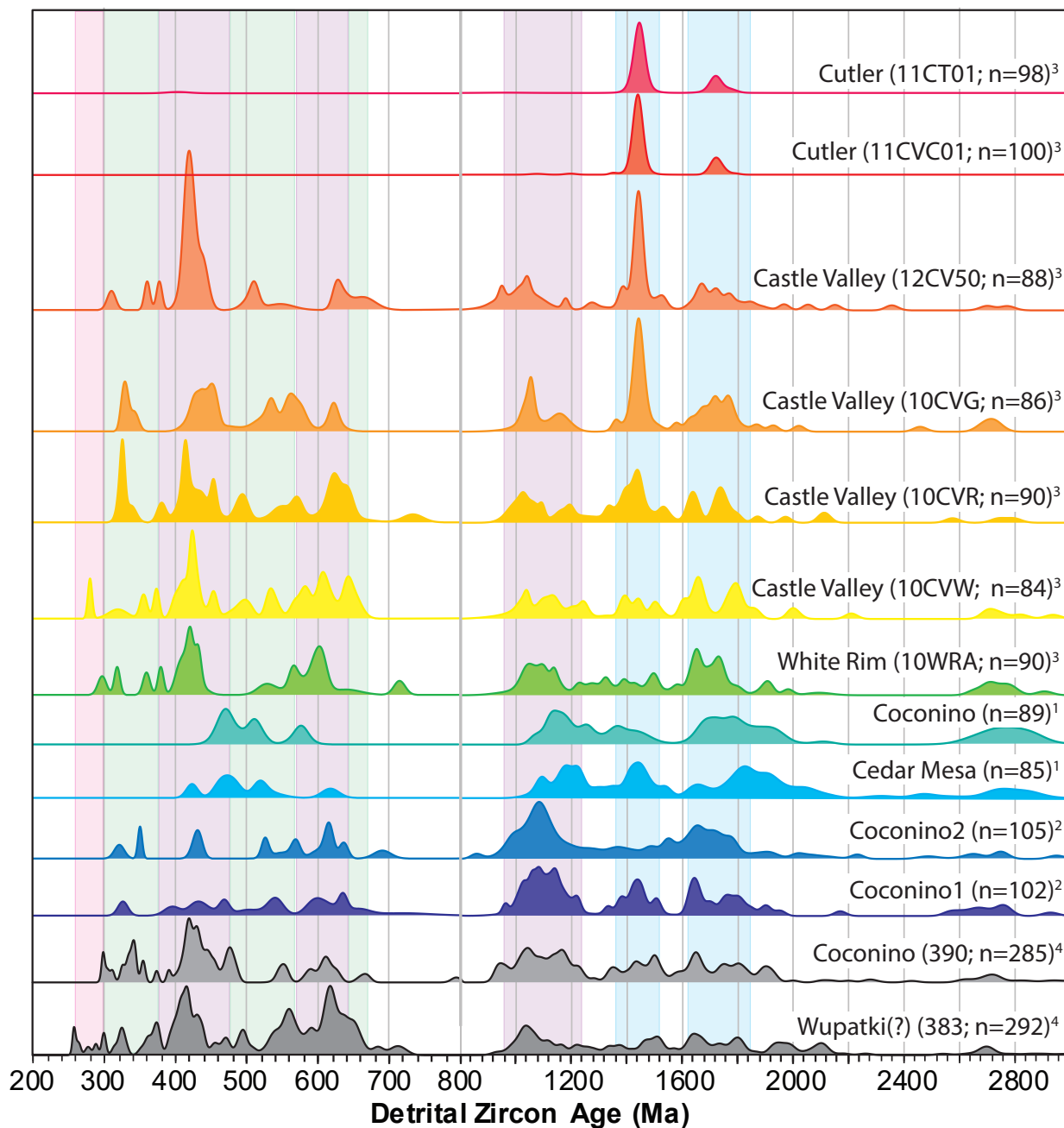






Figure 6 (Moenkopi PDP)

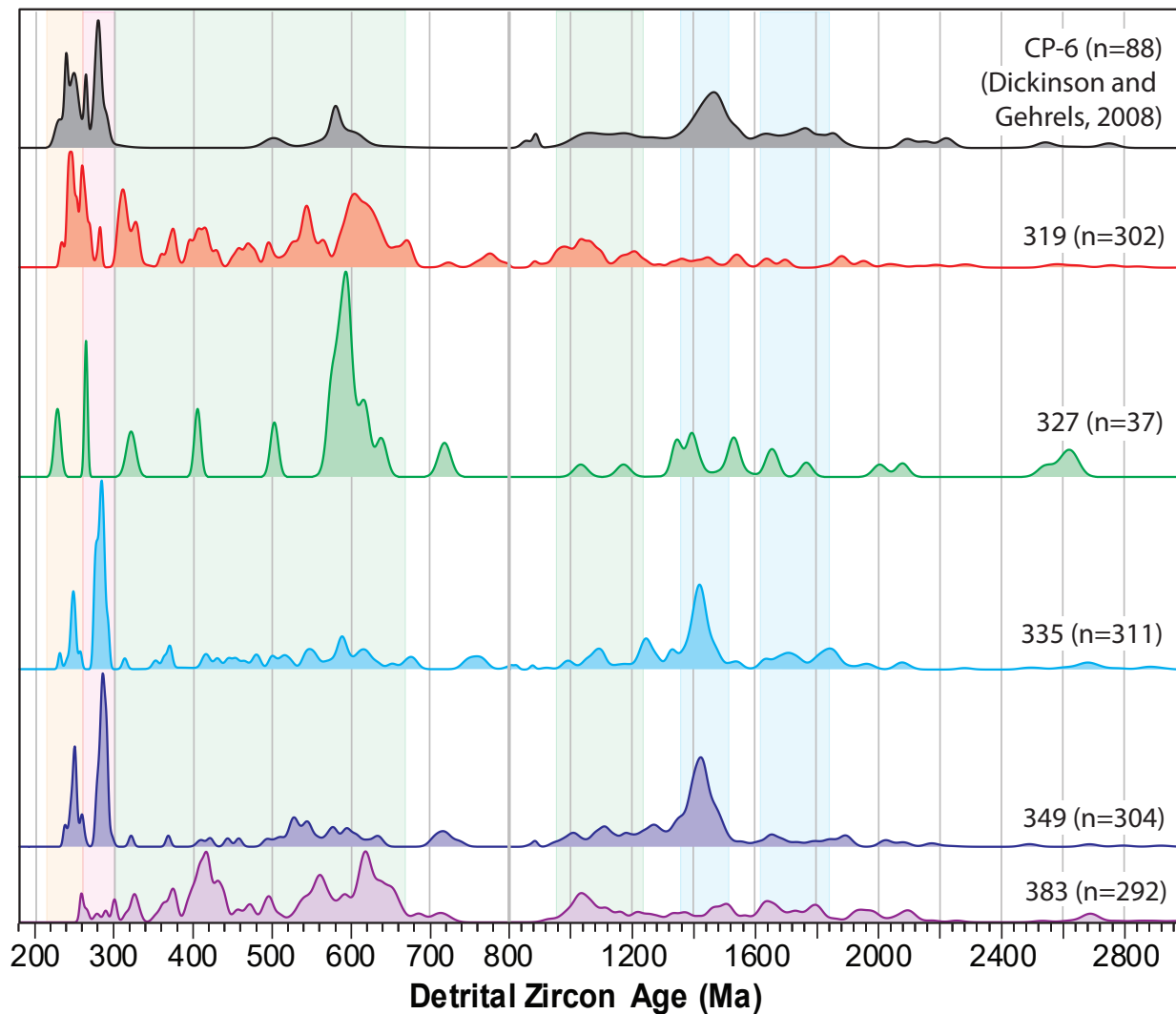




Figure 7 (Chinle PDP)

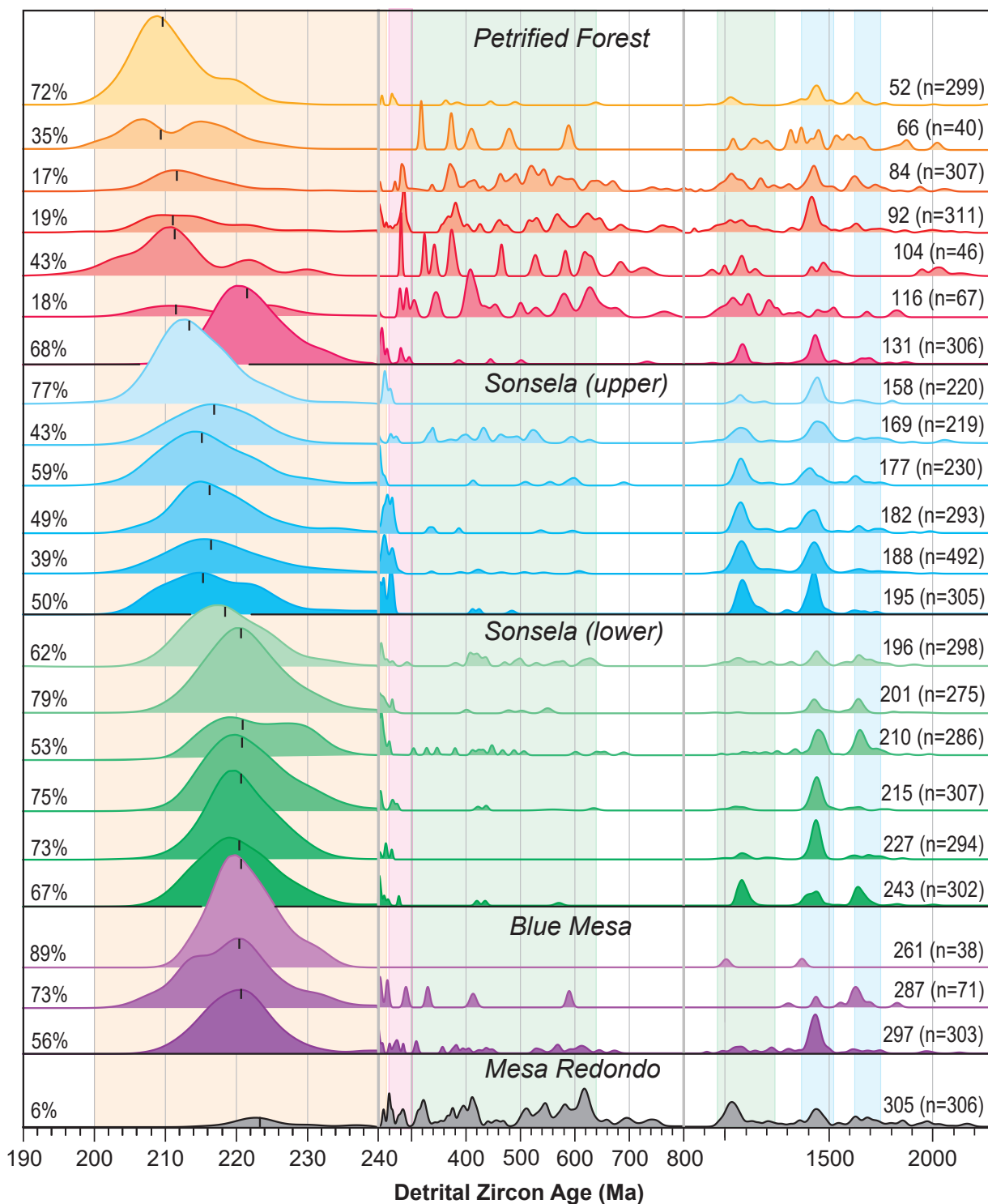




Figure 8 (Coco-Moen-Chin PDP)

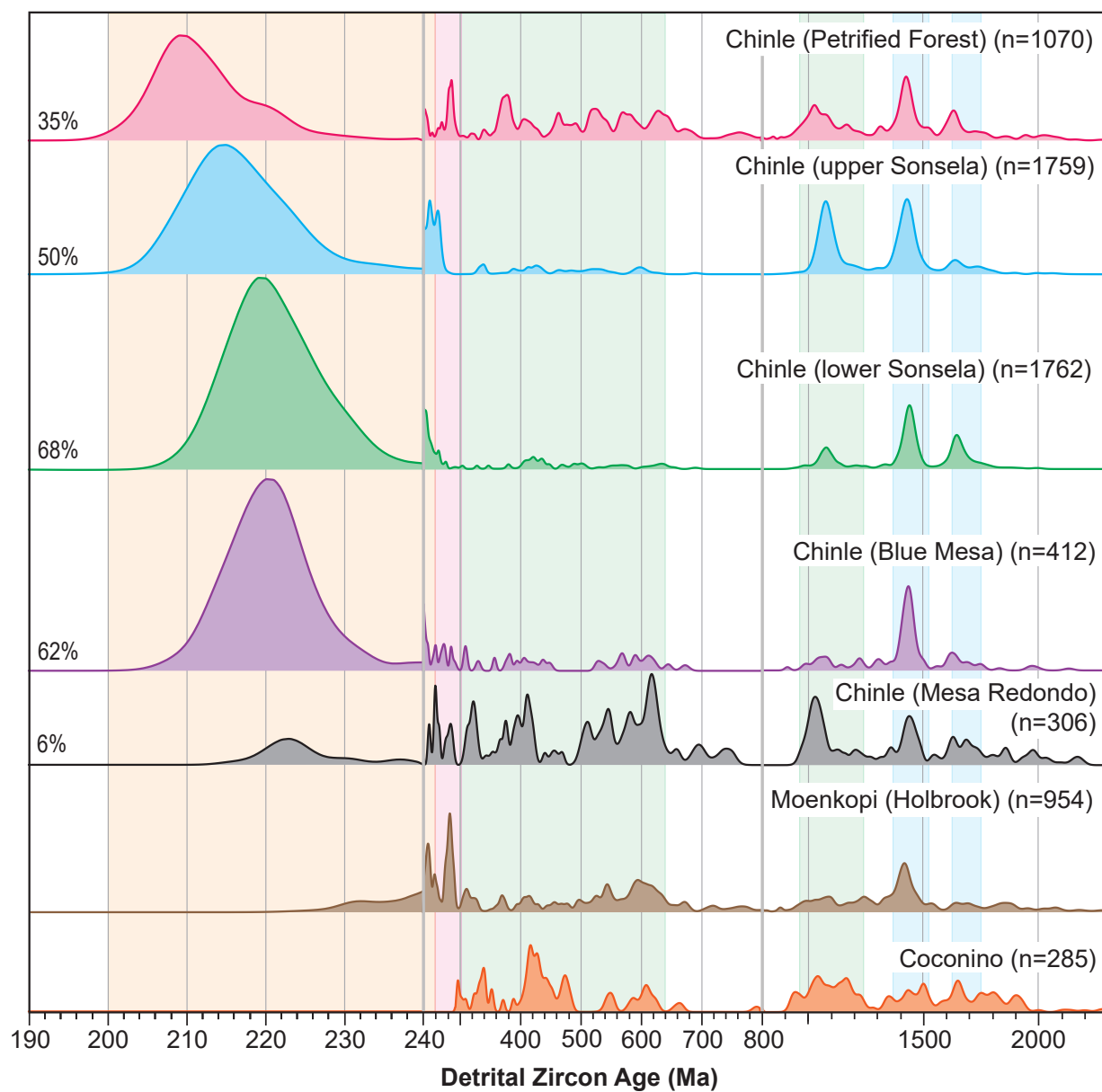




Figure 9 (MDS Plots)

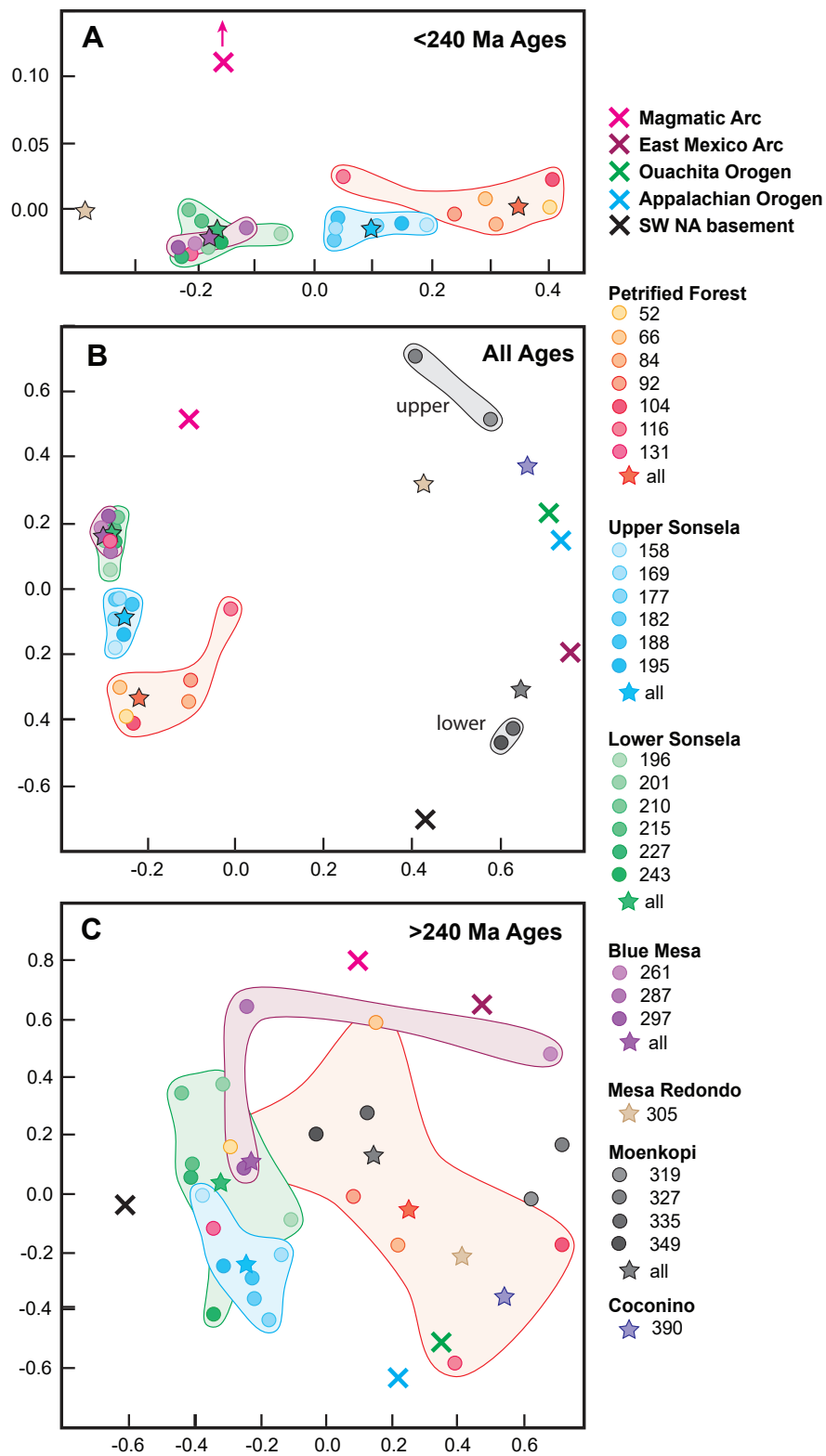




Figure 10 (Uconc-UTh plot)

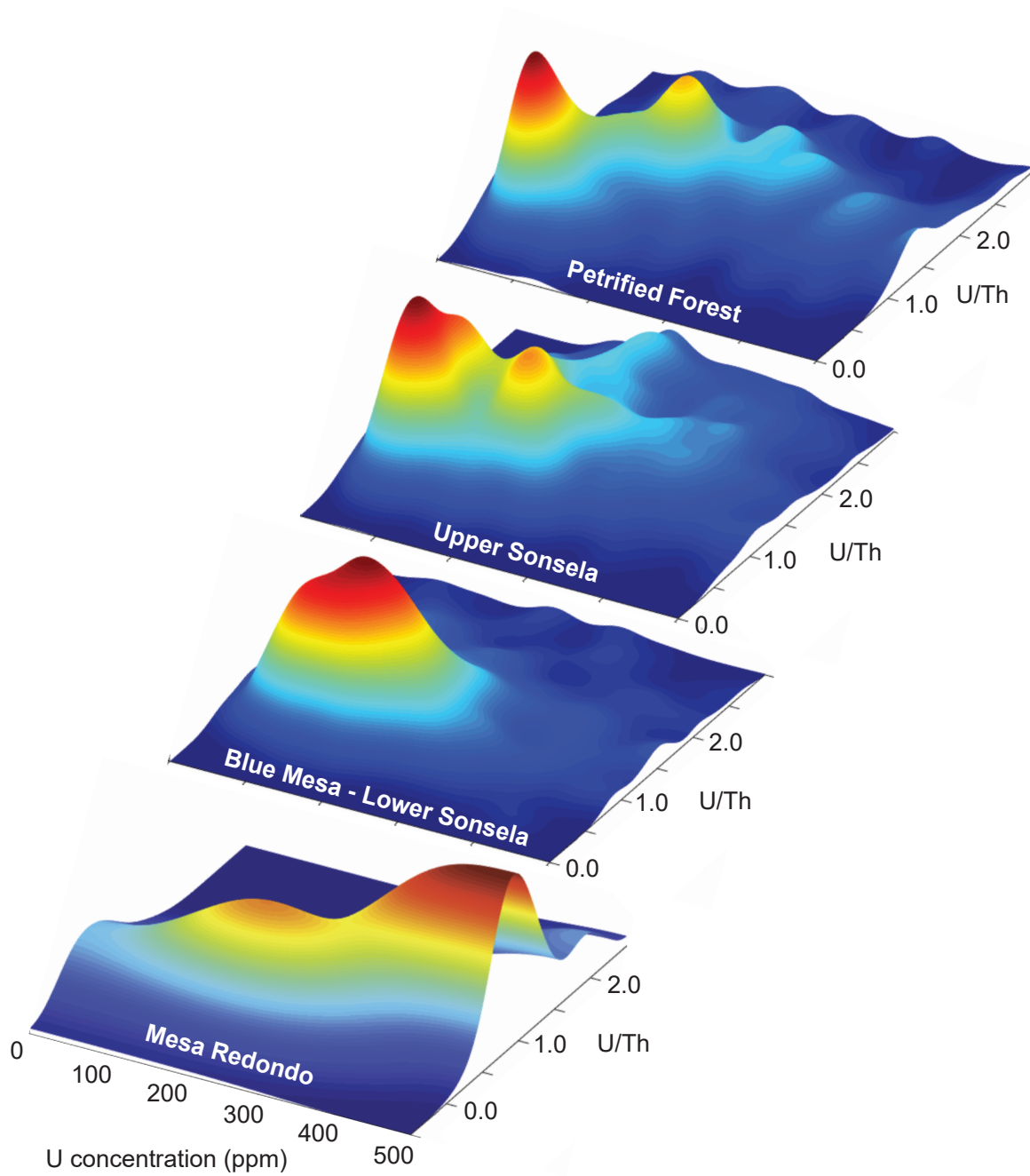




Figure 11 (AOB CO MDS plot)

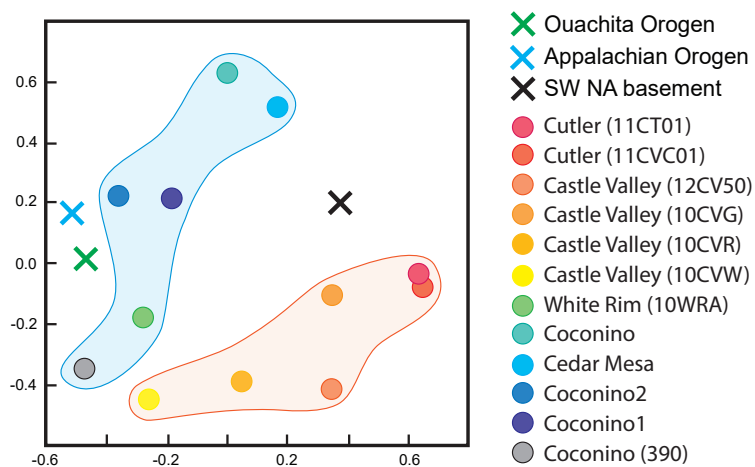




Figure 12 (Triassic Paleogeography)

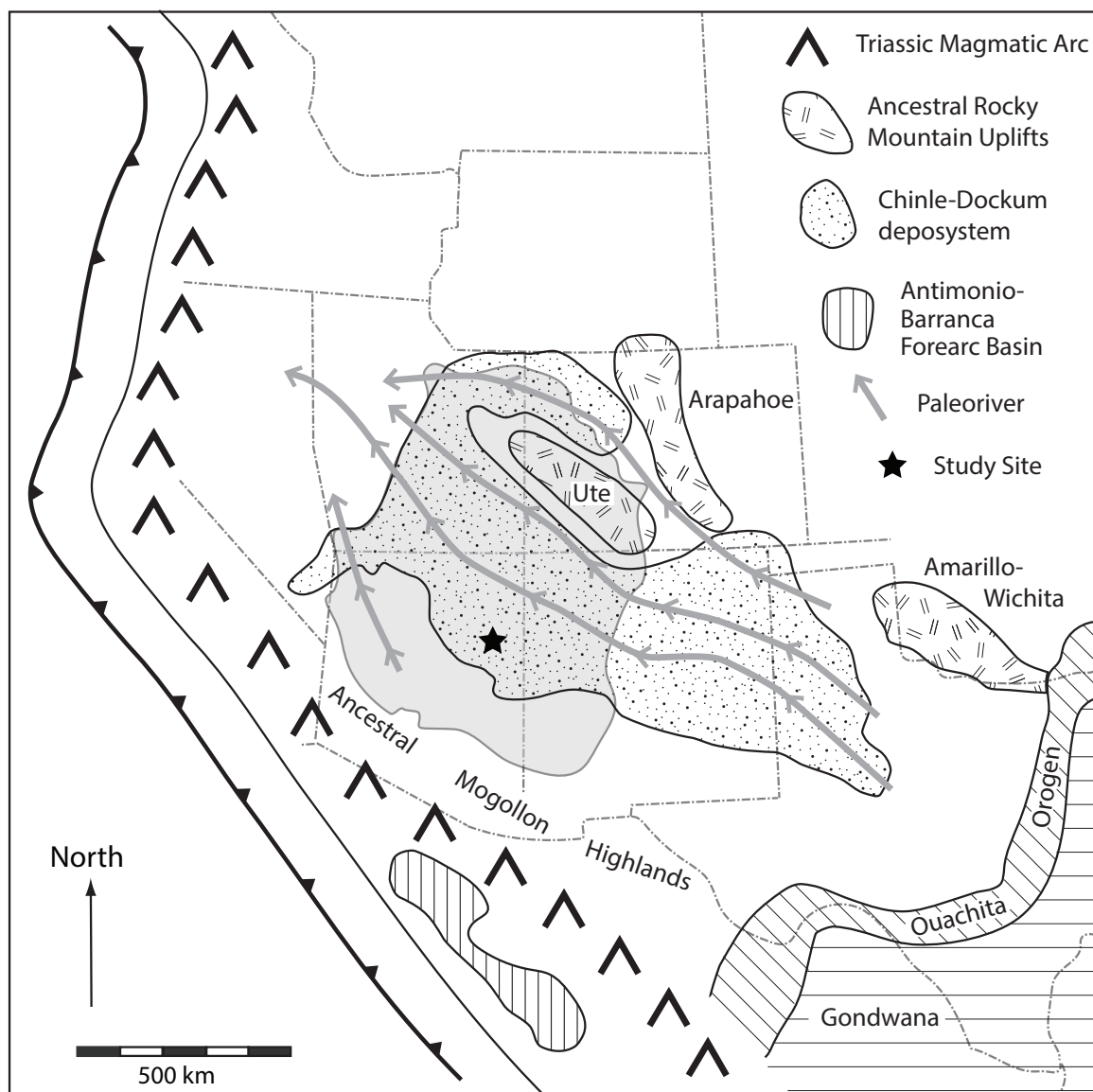






Figure 13 (DZ MDA plot)

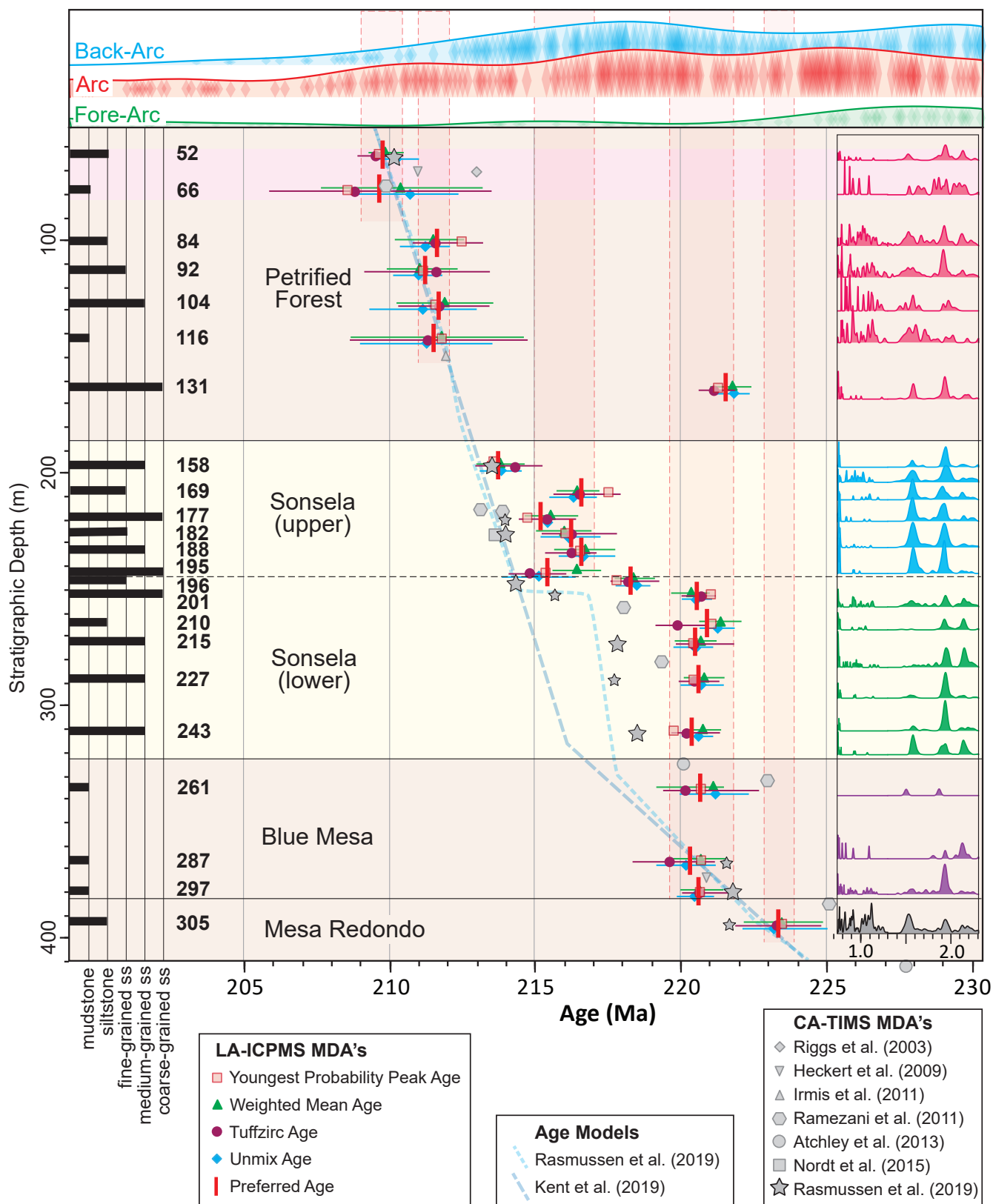
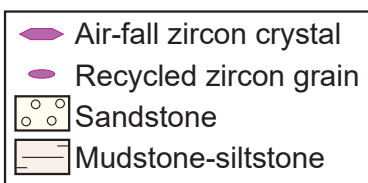
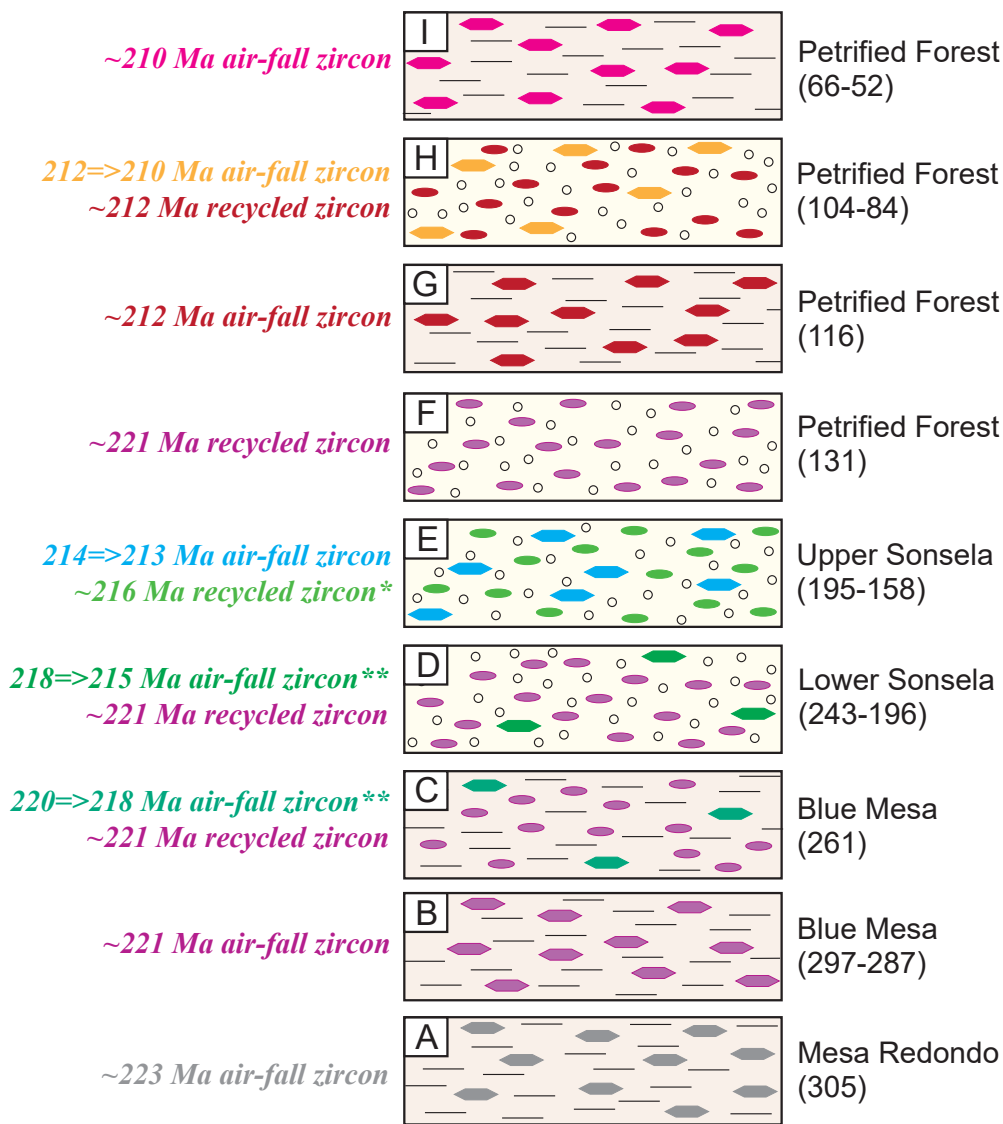




Figure 14 (Chinle Strat)

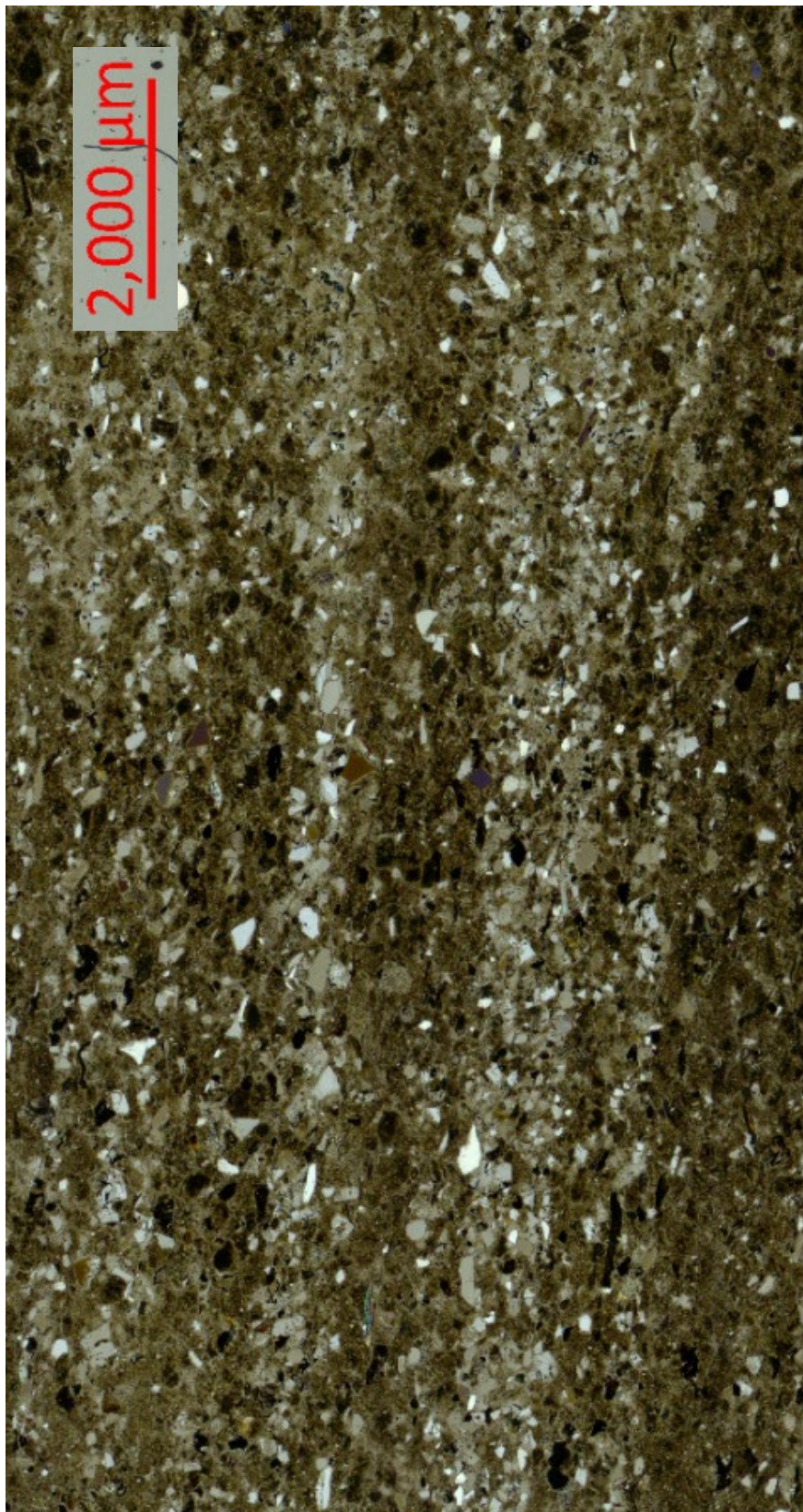


*\*Uncertain source for ~216 Ma recycled grains in upper Sonsela*

*\*\*Low abundance of 220-215 Ma air-fall grains in lower Sonsela*

Appendix 1 (Sample Images)

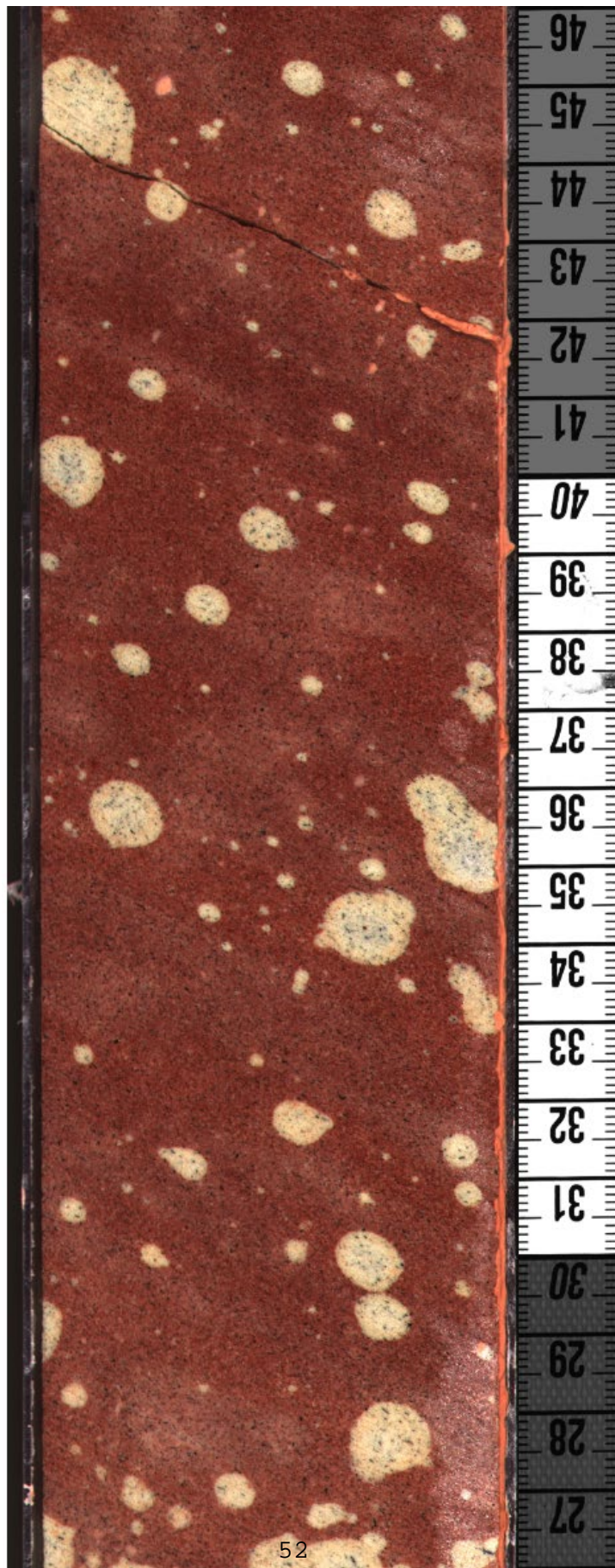
Sample 52-2





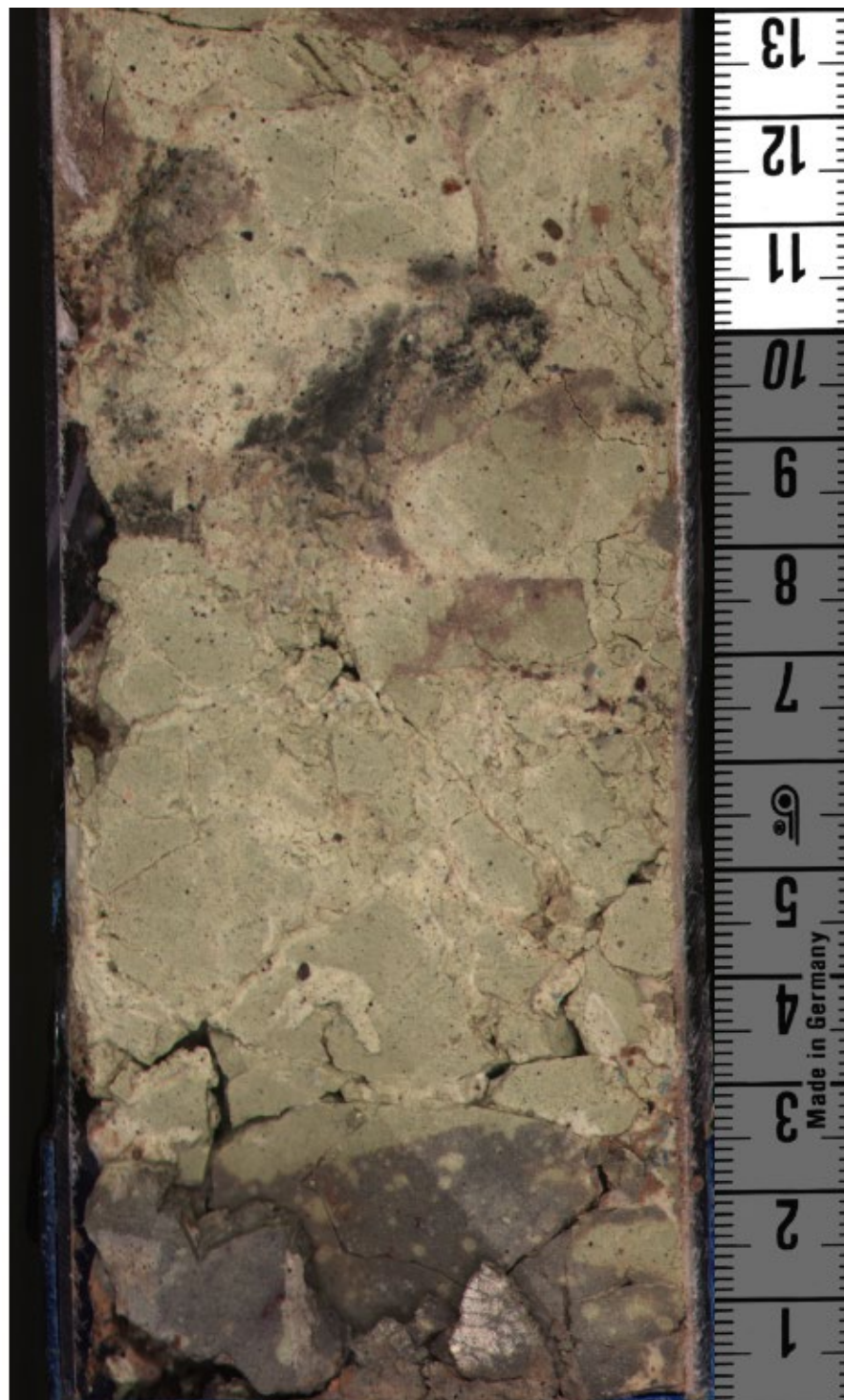


Sample 52-2





Sample 66-1  
(no thin section image available)







Sample 84-2  
(no thin section image available)







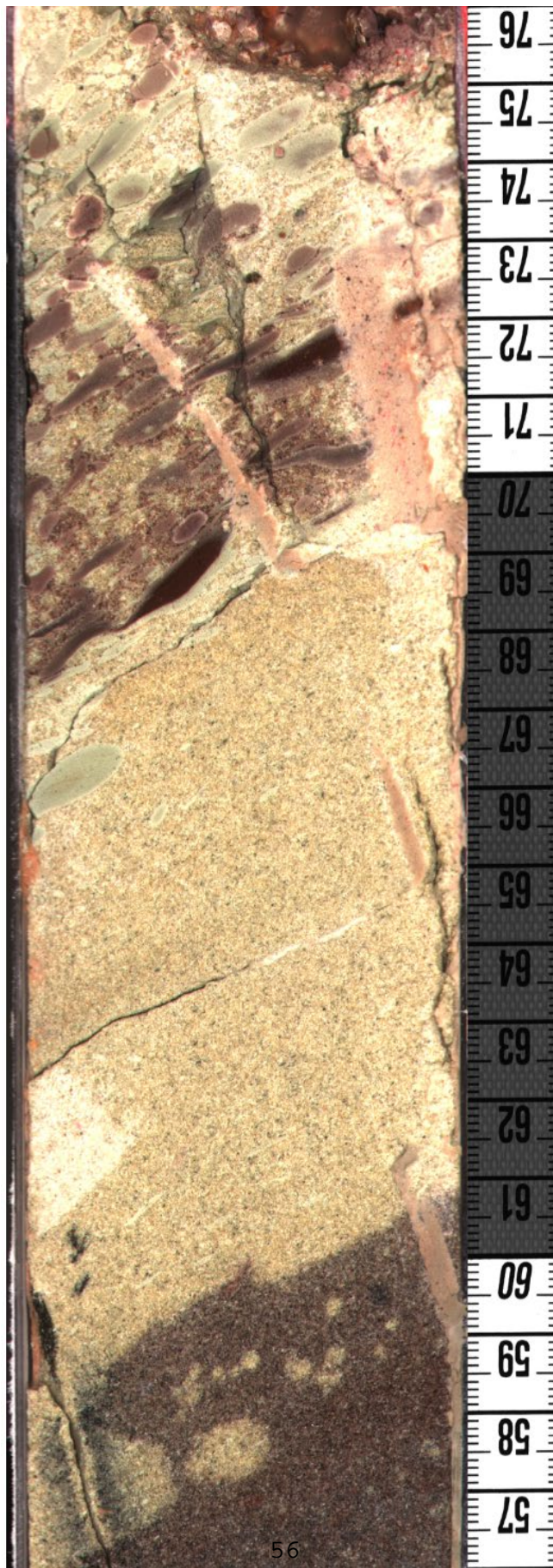
Sample 92-2







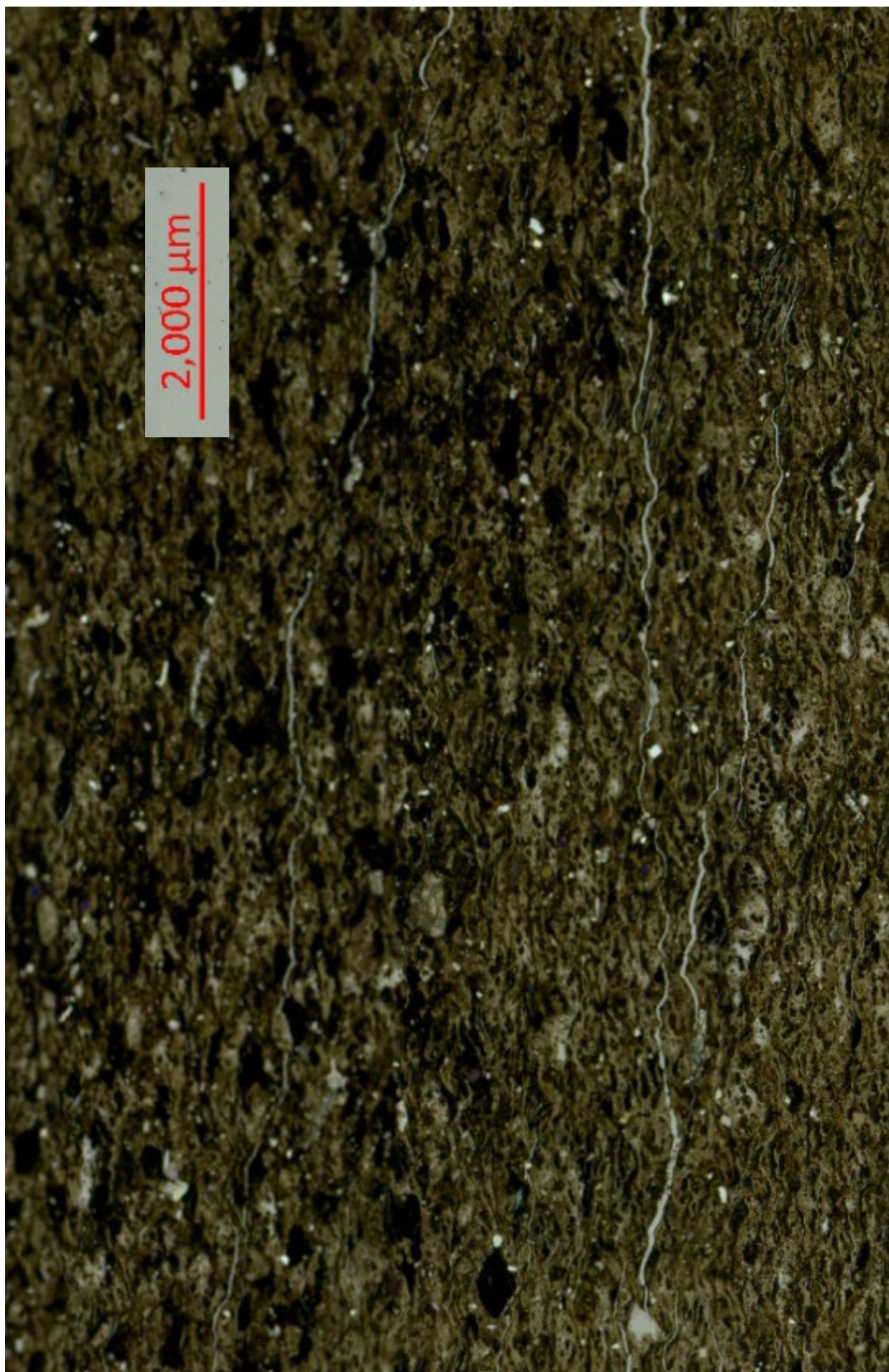
Sample 92-2







Sample 104-3





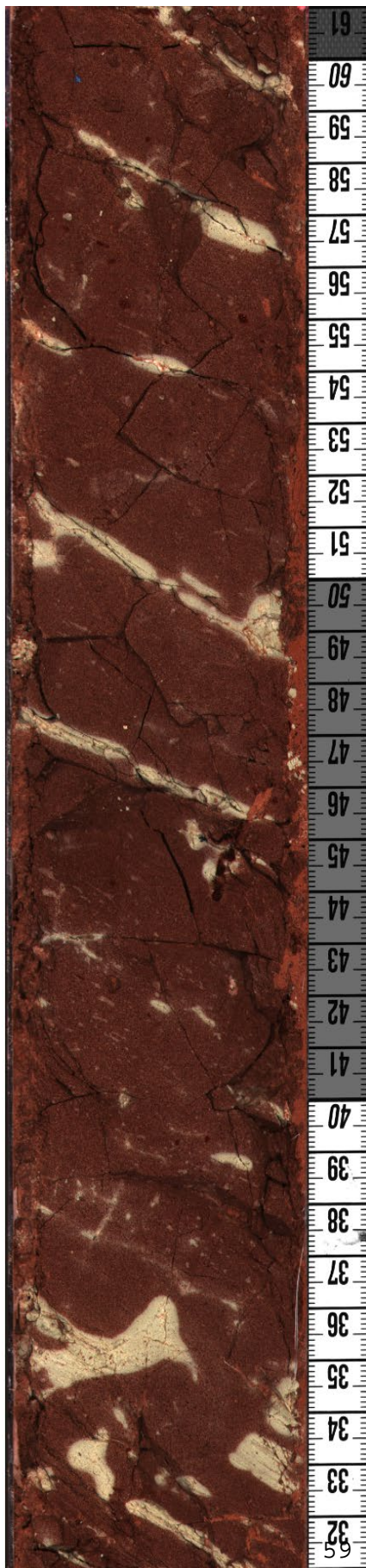


Sample 104-3





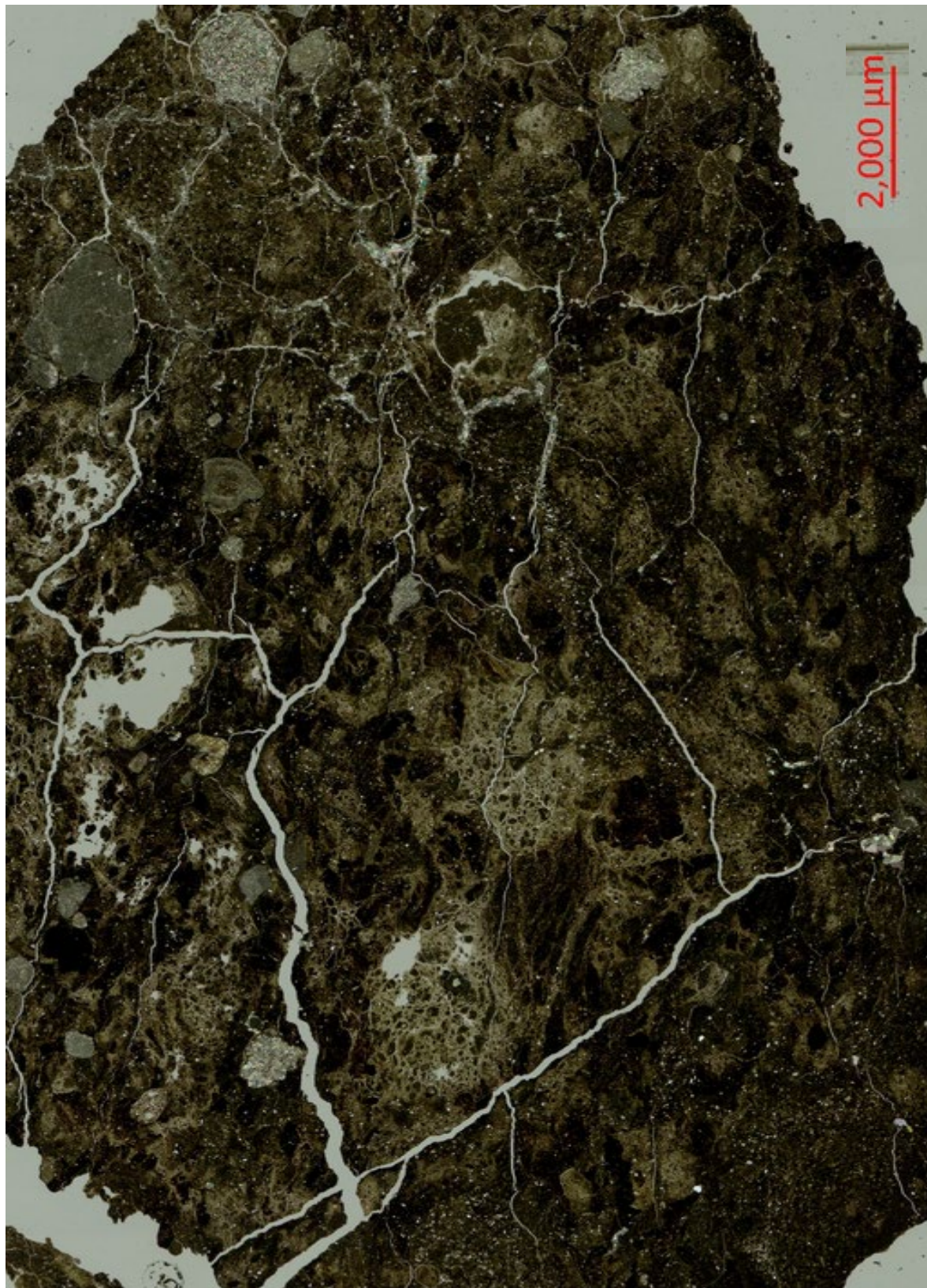
Sample 116-1  
(no thin section image available)







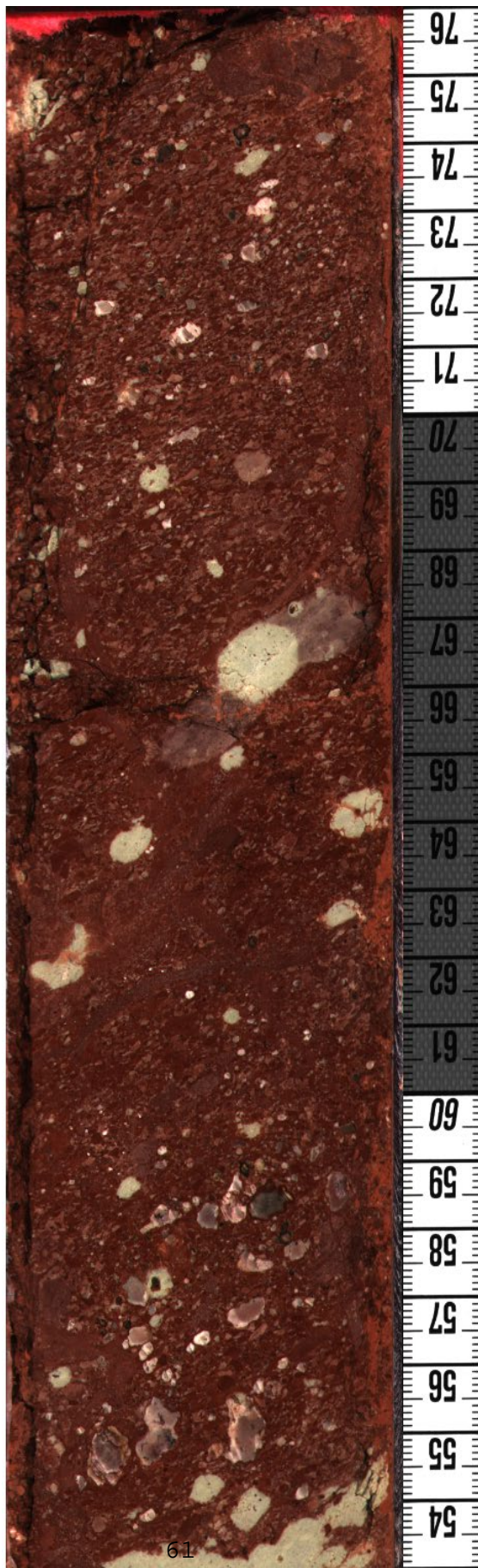
Sample 131-2







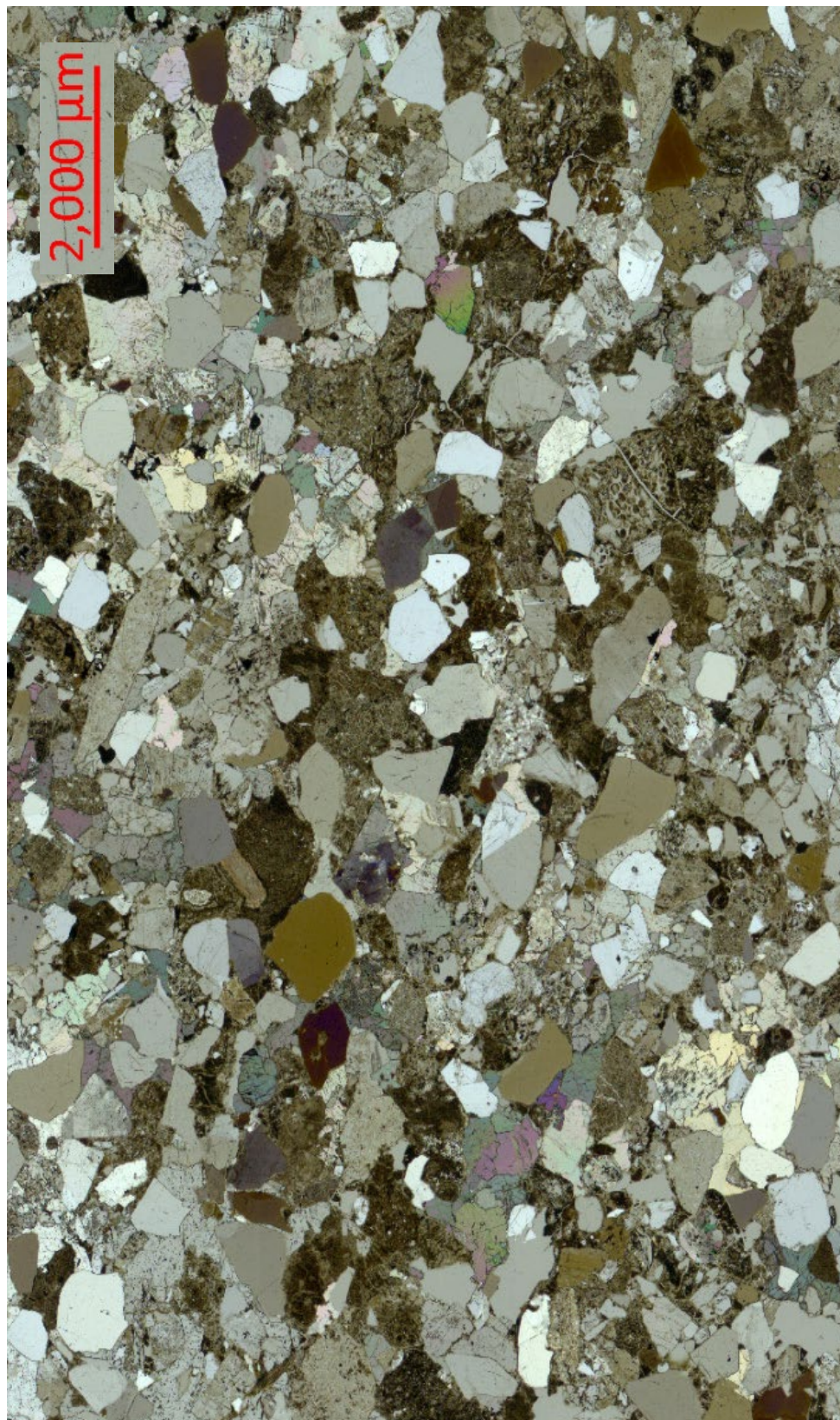
Sample 131-2







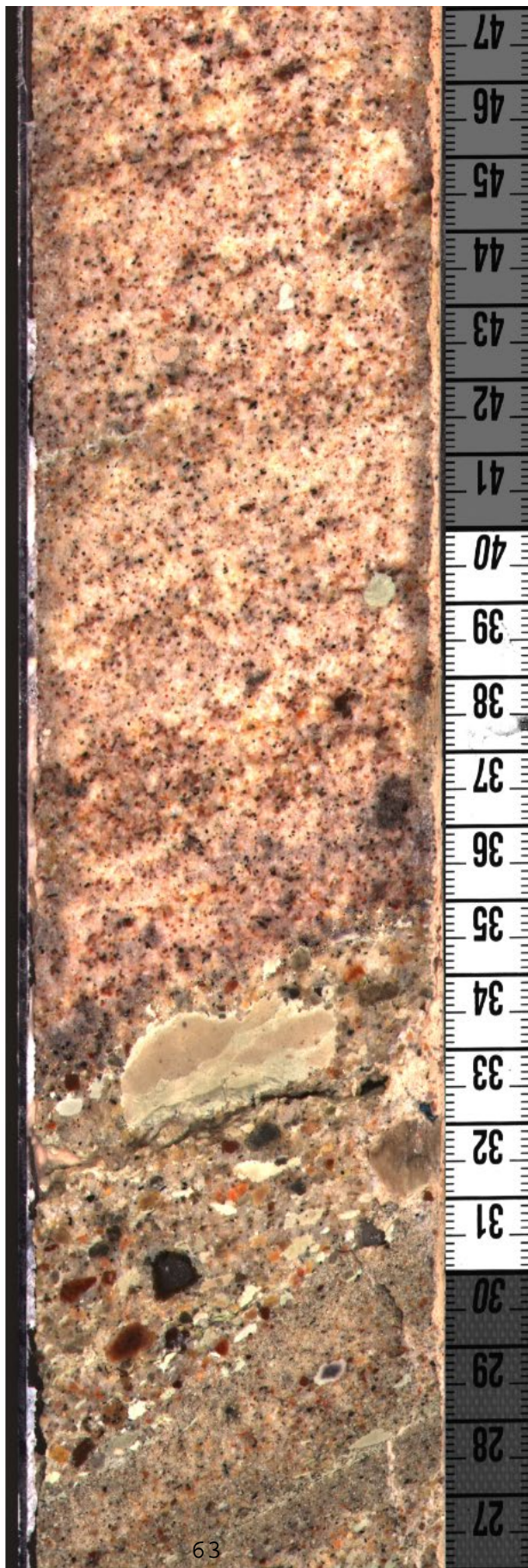
Sample 158-2







Sample 158-2





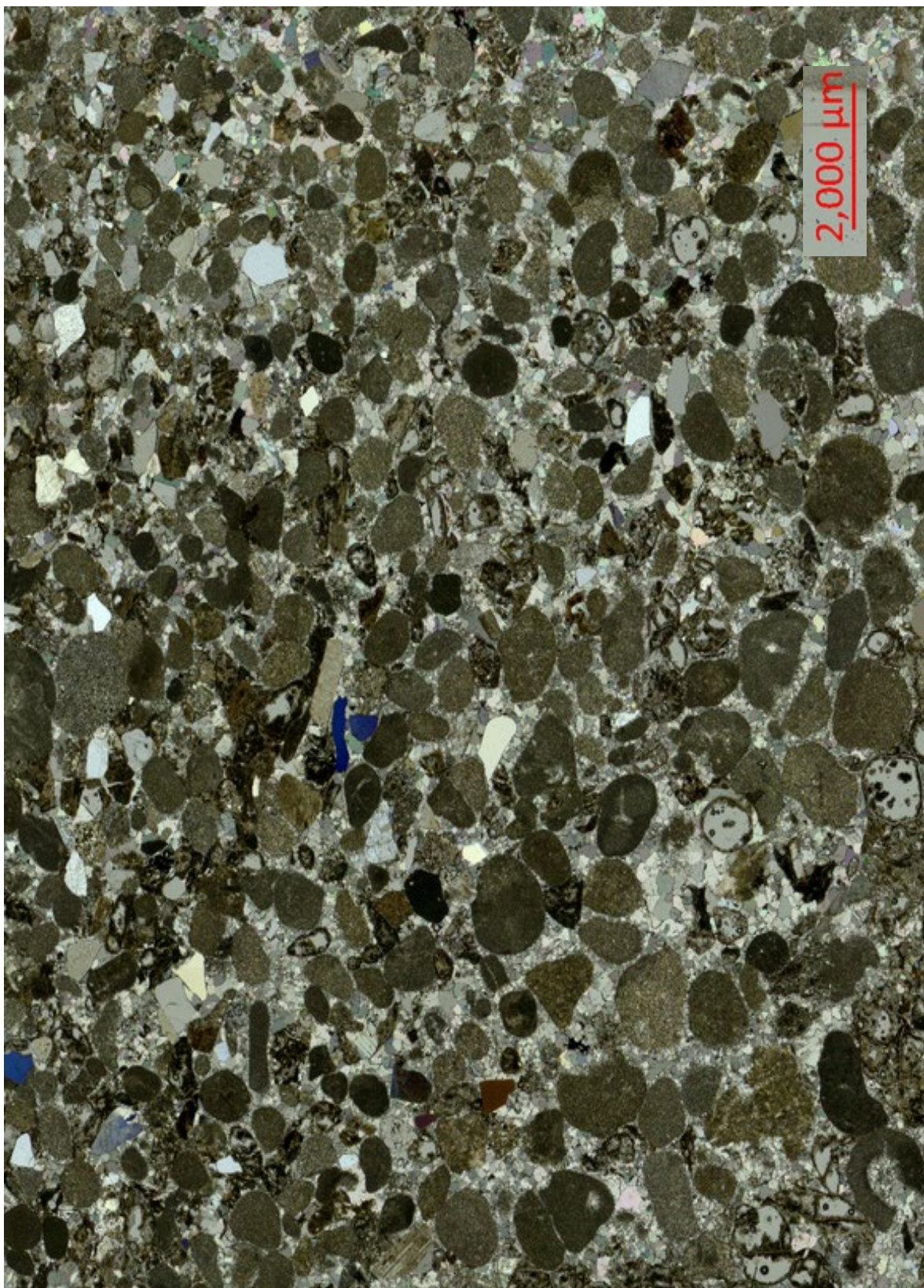
Sample 169-1  
(no thin section image available)







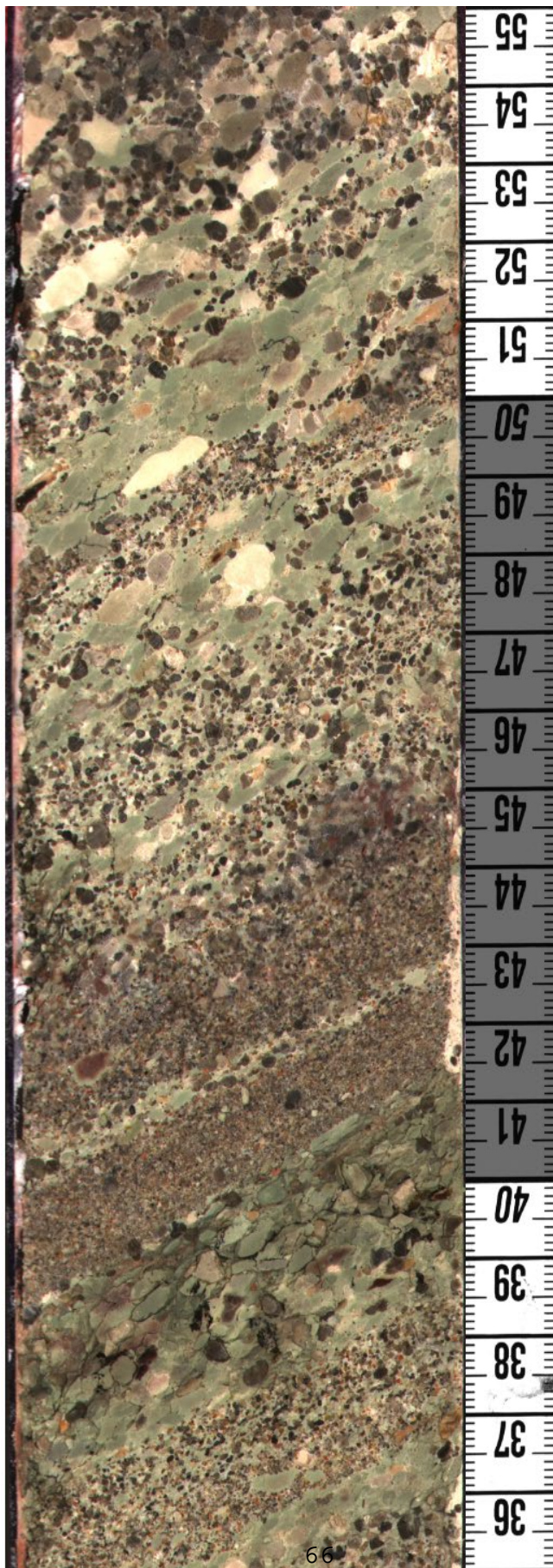
Sample 177-1







Sample 177-1





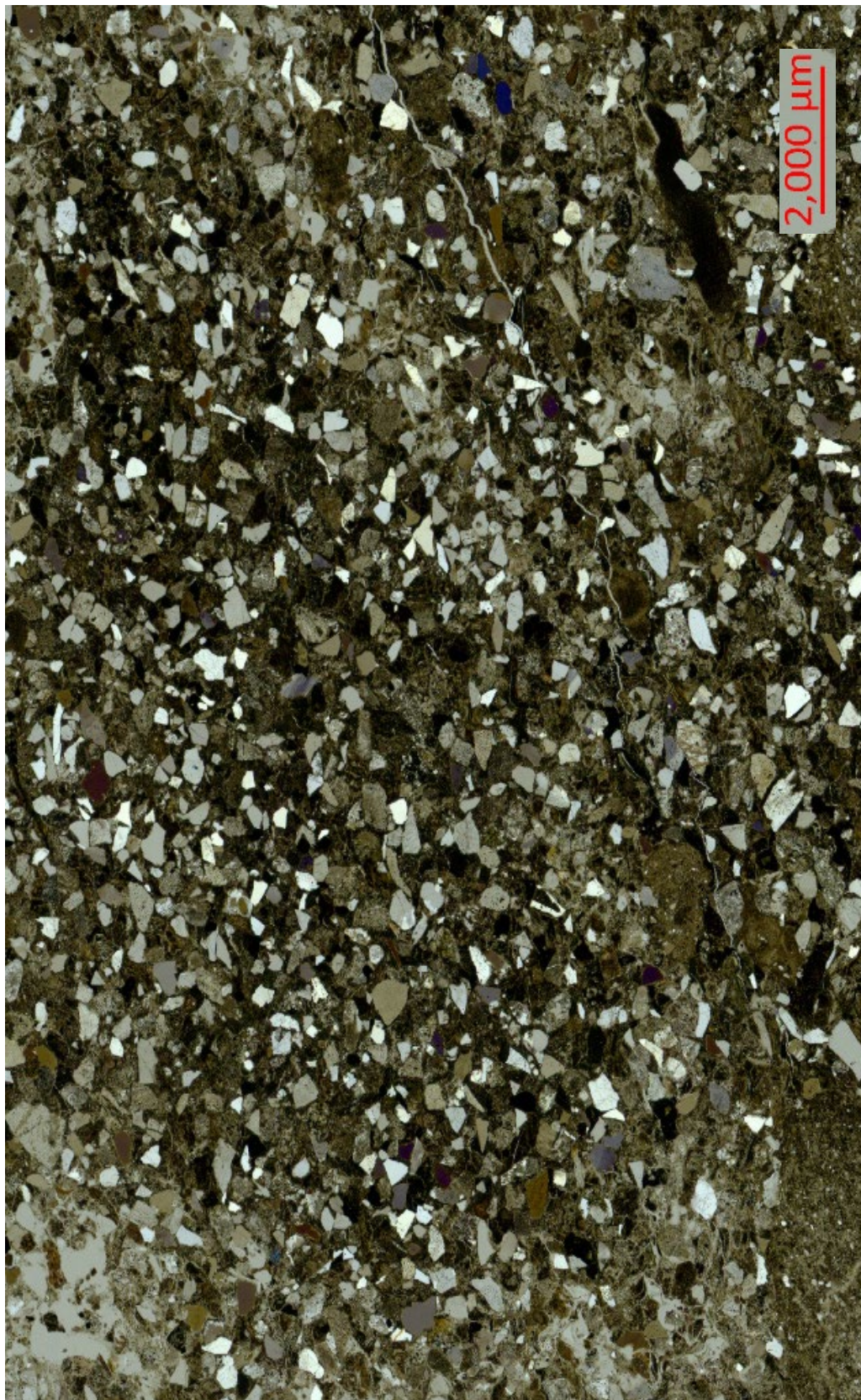
Sample 182-1  
(no thin section image available)







Sample 188-2







Sample 188-2







Sample 195-2







Sample 195-2







Sample 196-3







Sample 196-3







Sample 201-1







Sample 201-1





Sample 210-1  
(no thin section image available)







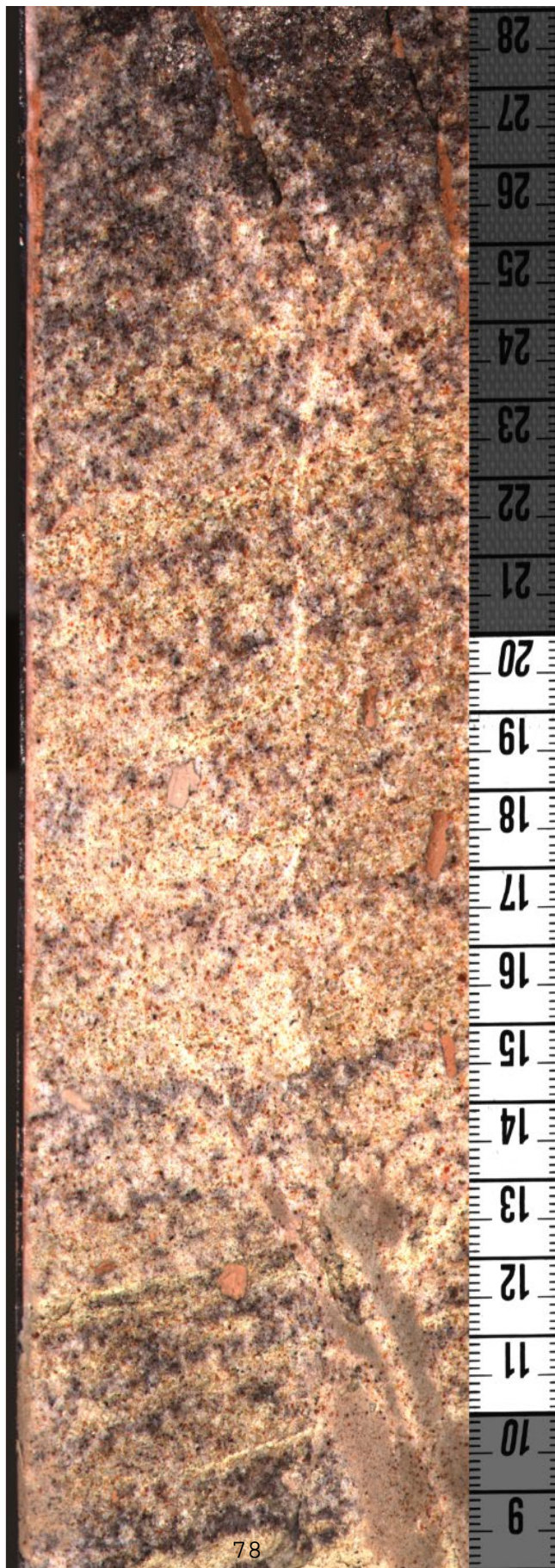
Sample 215-2







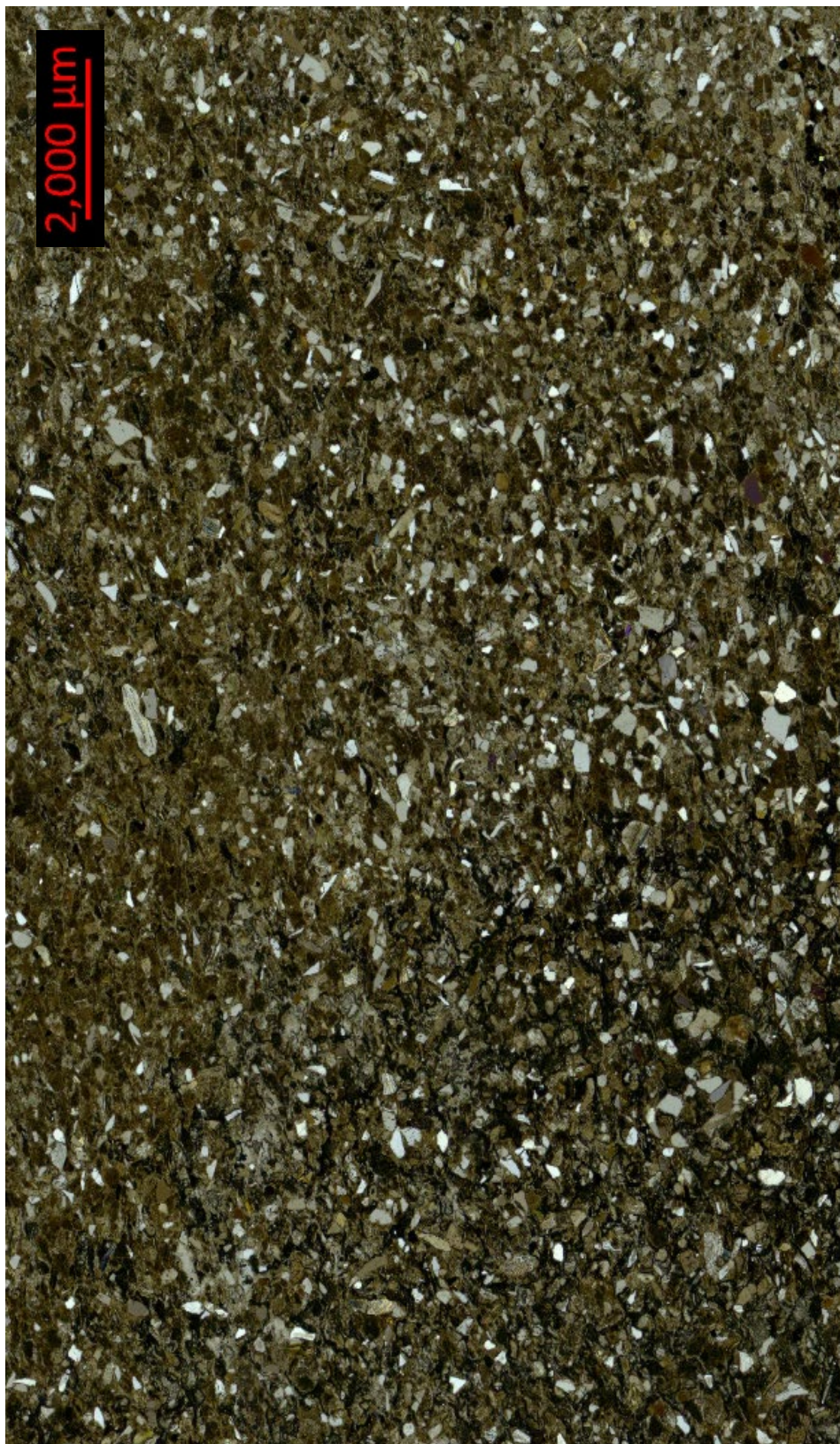
Sample 215-2







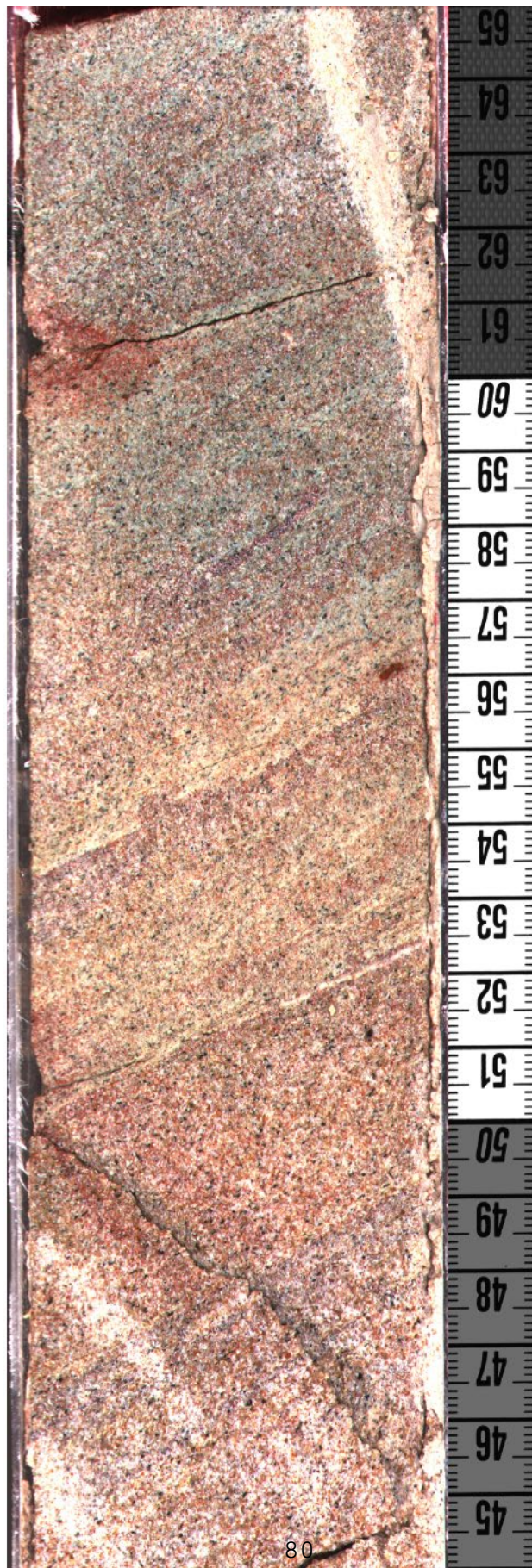
Sample 227-3







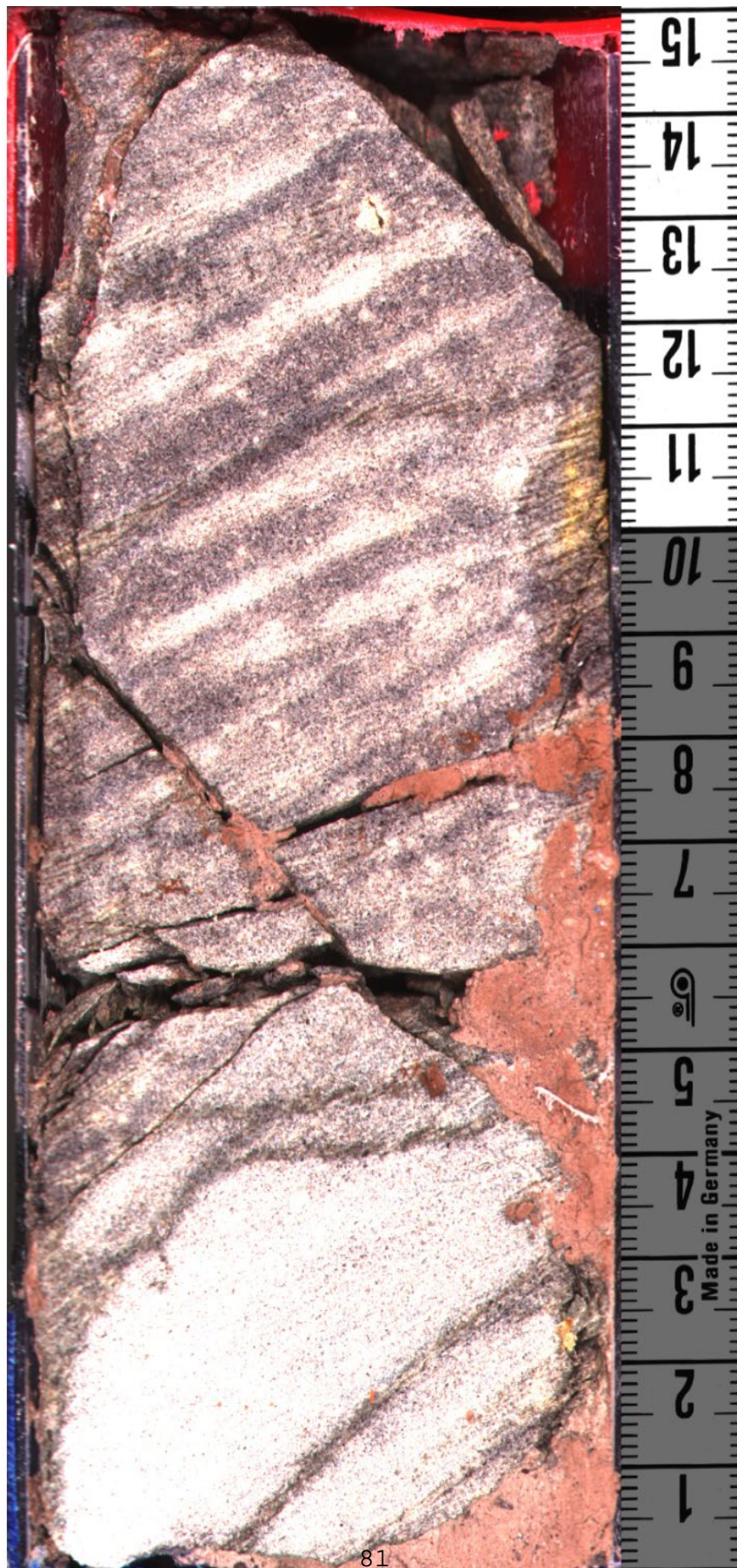
Sample 227-3





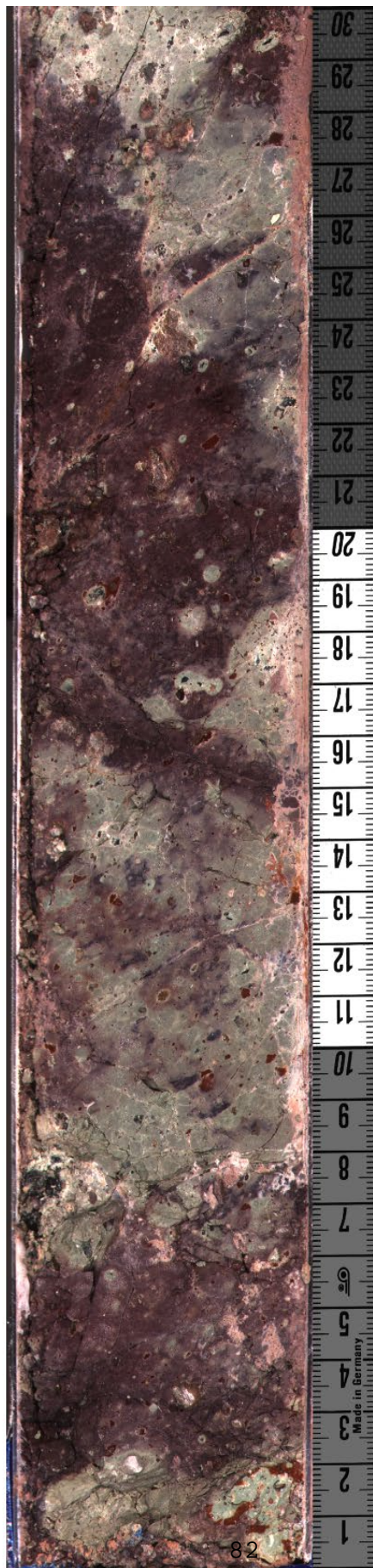


Sample 243-3  
(no thin section image available)





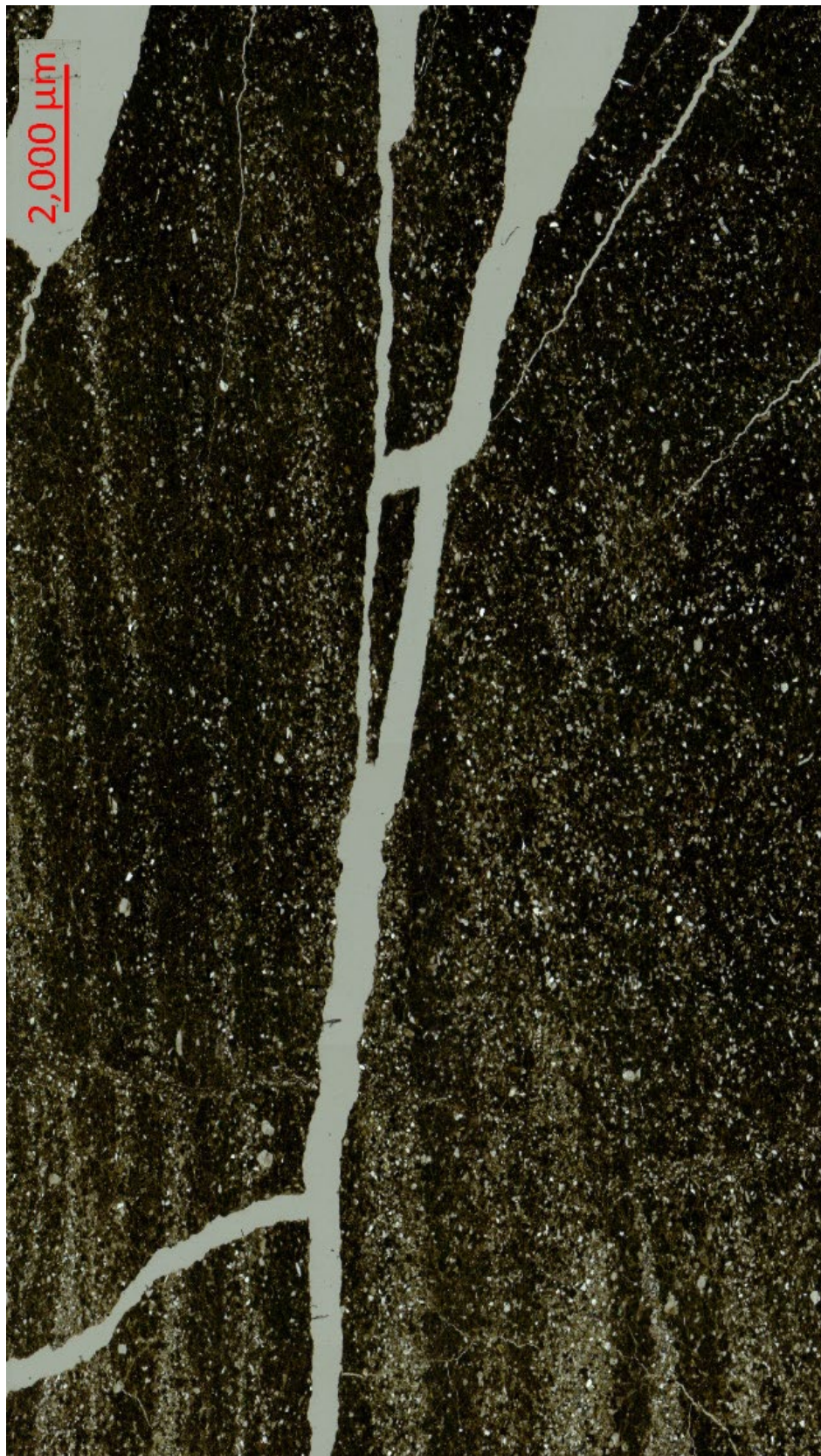
Sample 261-1  
(no thin section image available)







Sample 287-2







Sample 287-2







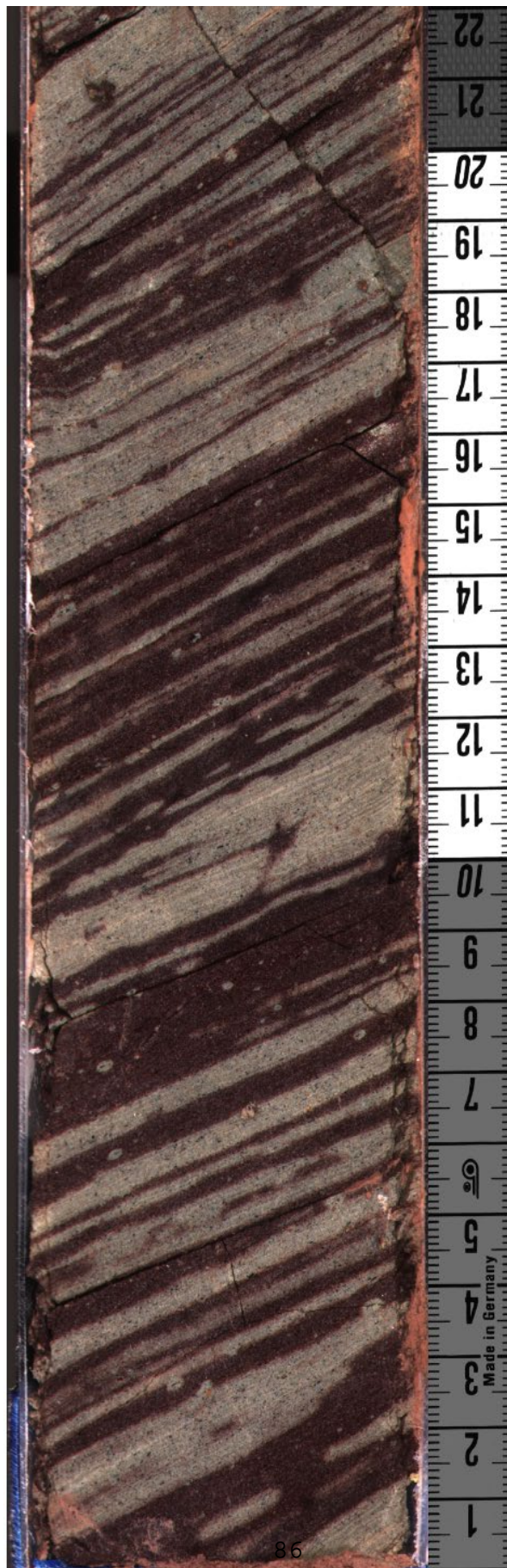
Sample 297-2







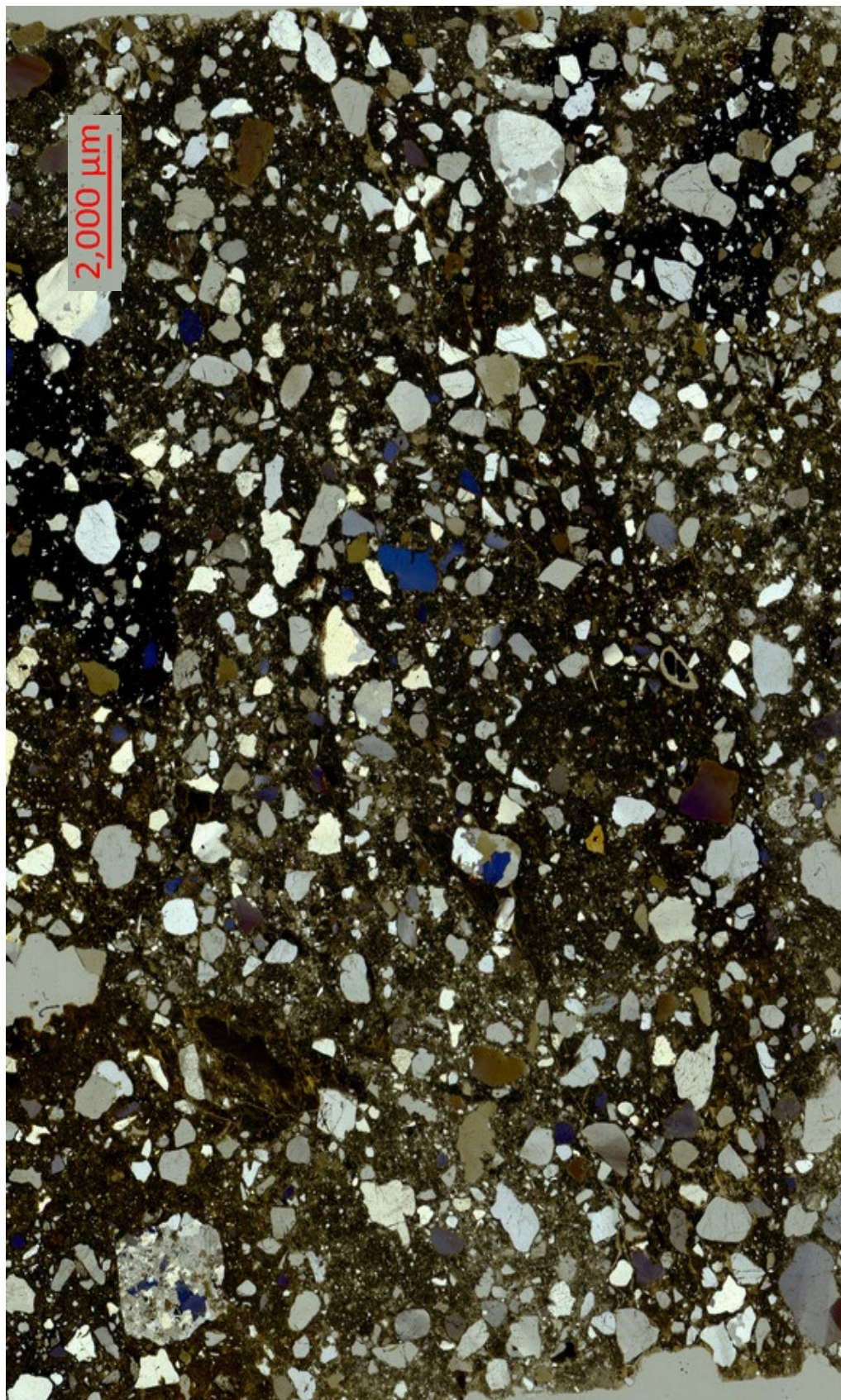
Sample 297-2







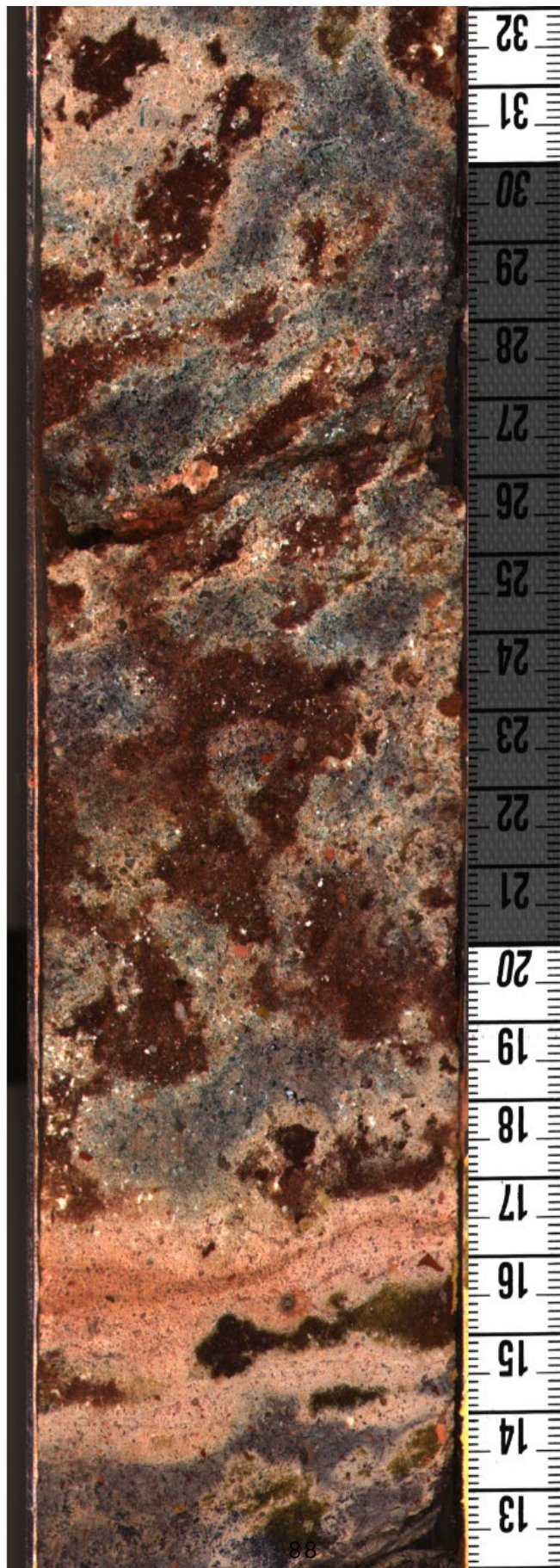
Sample 305-2







Sample 305-2







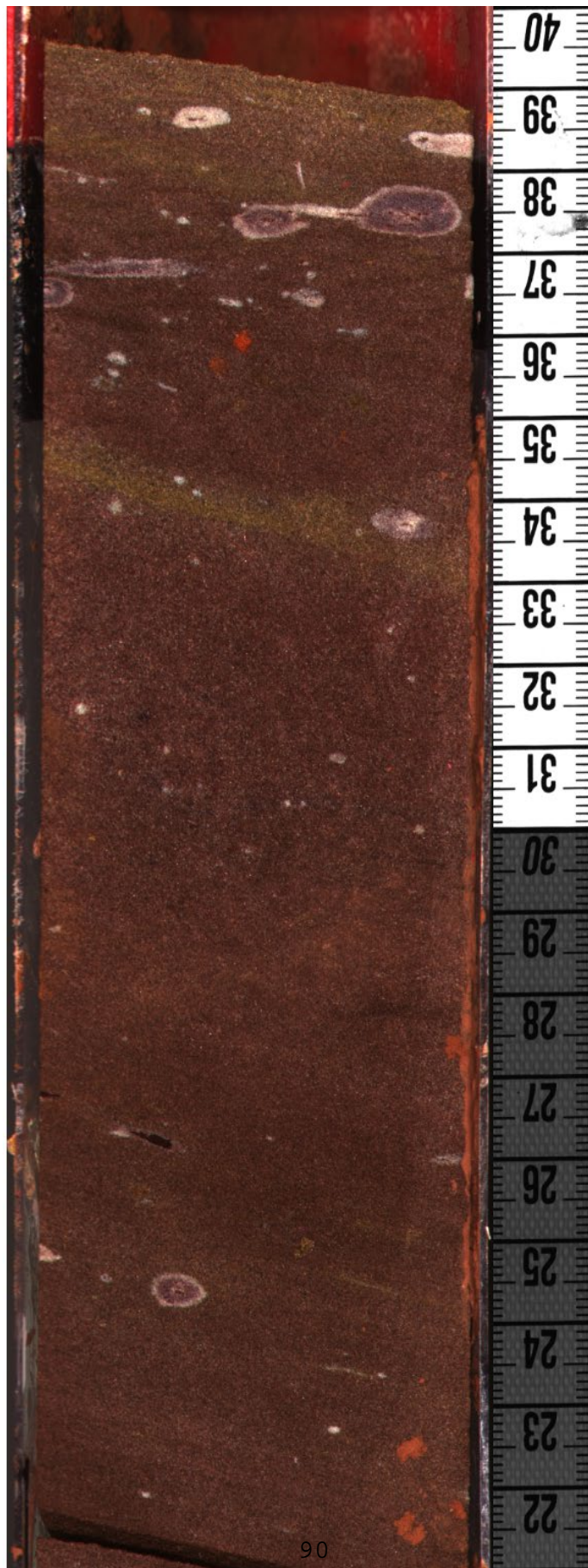
Sample 319-2





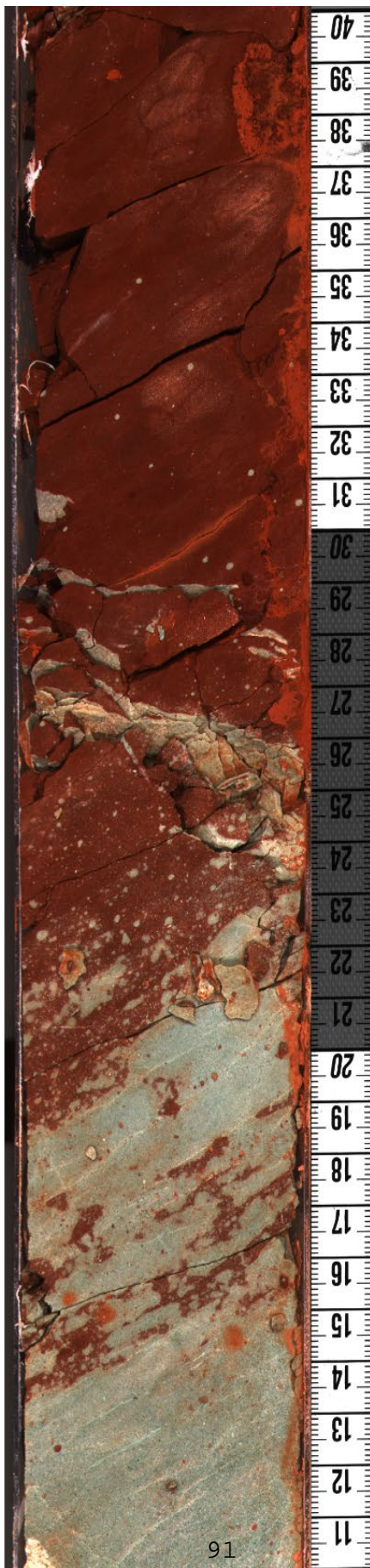


Sample 319-2





Sample 327-2  
(no thin section image available)





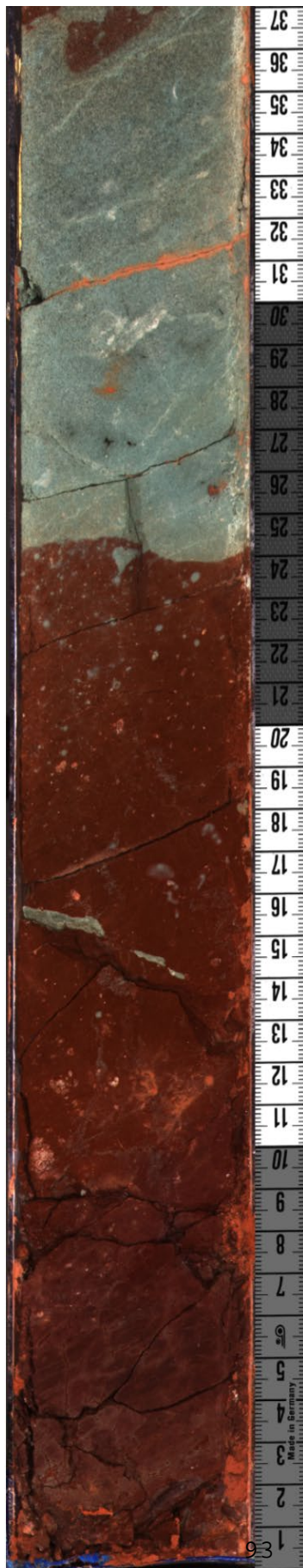


Sample 335-1





Sample 335-1







Sample 349-3







Sample 349-3







Sample 383-2







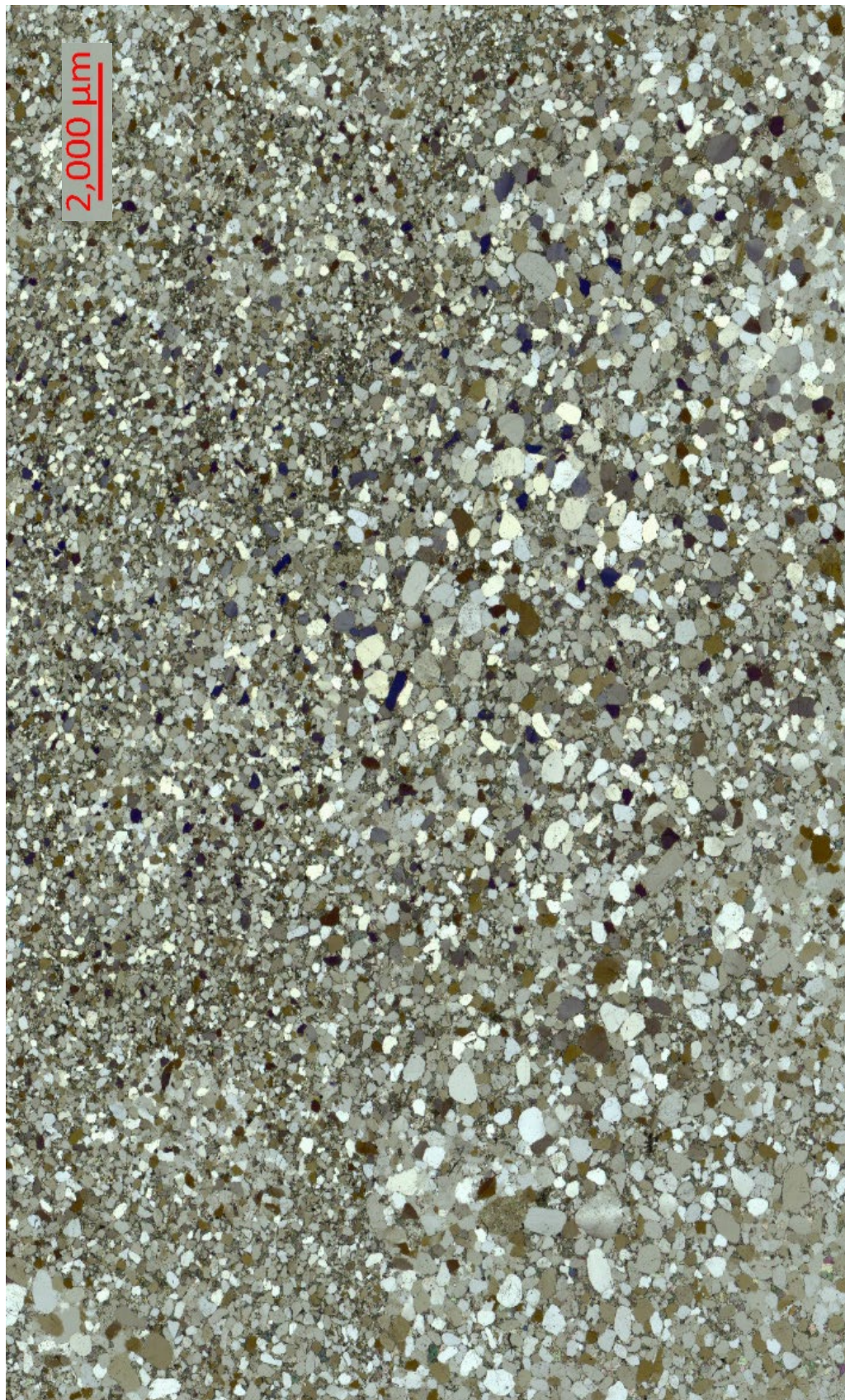
Sample 383-2







Sample 390-1







Sample 390-1







### Appendix 2 (CA-TIMS vs LA-ICPMS ages)

